Universidade de São Paulo

Instituto de Biociências

Departamento de Genética e Biologia Evolutiva

Camila de Freitas Almeida

Regeneração muscular na miopatia centronuclear associada a mutações no gene *DNM2*

Skeletal muscle regeneration in *DNM2*-related centronuclear myopathy

São Paulo

2019

Camila de Freitas Almeida

Regeneração muscular na miopatia centronuclear associada a mutações no gene *DNM2*

Skeletal muscle regeneration in *DNM2*-related centronuclear myopathy

Versão original

Tese apresentada ao Instituto de Biociências da Universidade de São Paulo, para a obtenção do Título de Doutor em Ciências, na área de Biologia Genética

Orientadora: Profa. Dra. Mariz Vainzof

São Paulo

2019

Ficha catalográfica elaborada pelo Serviço de Biblioteca do Instituto de Biociências da USP, com os dados fornecidos pelo autor no formulário:

http://www.ib.usp.br/biblioteca/ficha-catalografica/ficha.php

Almeida, Camila de Freitas
Regeneração muscular na miopatia centronuclear associada a mutações no gene DNM2 / Camila de Freitas Almeida; orientadora Mariz Vainzof. -- São Paulo, 2019.

155 f.

Tese (Doutorado) - Instituto de Biociências da Universidade de São Paulo, Departamento de Genética e Biologia Evolutiva.

1. Miopatia centronuclear. 2. Dinamina 2. 3. Regeneração muscular. 4. Células-satélite. I. Vainzof, Mariz, orient. II. Título.

Bibliotecária responsável pela estrutura da catalogação da publicação:
Elisabete da Cruz Neves – CRB – 8/6228

Comissão Julgadora:

Prof(a). Dr(a).

Prof(a). Dr(a).

Prof(a). Dr(a).

Prof(a). Dr(a).

Prof(a). Dr(a).

Orientador(a)

To Nilma

And to all strong women in my life

Scientia Vinces

(Vencerás pela Ciência – lema da Universidade de São Paulo)

Acknowledgments

Agradeço à minha mãe e ao meu pai por todo o esforço empregado para que eu conseguisse ingressar na universidade, concluir minha graduação e continuar meus estudos na pós-graduação, indo muito além do que as nossas condições normalmente possibilitariam. Sem vocês, eu jamais teria realizado a minha vontade de ser pesquisadora, ainda mais em um país no qual o acesso ao ensino superior de qualidade é restrito às elites.

I'm very grateful to Mariz Vainzof, my supervisor since I was an undergrad student, for trusting me to conduct this research, to have guided my first steps in the scientific world, to have opened so many doors for my future, to have taught me that the most valuable quality of a researcher is her credibility. I admire your trajectory and I'm proud to have been part of your team. I hope I had fulfilled your expectations of me. You'll be my mentor for life.

My sincere thanks to Marc Bitoun who embarked with us in this project and welcomed me in his lab during my one-year doctoral stage in Paris. The value of my period in your lab goes beyond the data generated from the experiments. With you, I learned that better than have the right answer, is to ask the right questions. You are an example for me as a team leader, of scientific rigor, objectiveness, and kindness. Thank you for your patience with my numberless mails and for helping me to always see the glass as half full.

To all my present (and past) colleagues that I had the opportunity to work with along all these long 11 years at LabProt. You've been my second family; people with whom I spent more time than anybody else during all these years. To the actual team: Leticia, Léo, Lucas, Antonio, and Felipe, thank you all for supporting and cheering me in these ~~terrible~~ final months. And of course, for the hilarious afternoons at our office. Lê, you are more than the lab technician and you know that. You're my cherished friend, who took care of me and have supported me in the most difficult times inside and outside the lab. Stephanie, as we saw in that meme: fri**end**ship can **end**, girl/boyfri**end** can **end**, only lab partner has no **end**! You were the best lab partner I could ever have had and that I still have somehow, even if you're so far away. More than and above that, you are of course my life friend. Thank you for supporting and encouraging me during this journey. Antonio and Léo, thank you for saving me with last-minute experiments. You're awesome. Lucas, thank you for all the statistical discussions and fun time.

Mon séjour à Paris ne serait pas le même sans les collègues sympas du Labo 103. Merci à : Bernard pour tes blagues (un peu noires parfois) ; Corine pour ta gentillesse et les délicieuses gâches pour le goûter ; Agathe pour l'aide au labo et les croissants (oui, oui, on mangeait tout le temps) ;

Margot pour tes bêtises d'après 18h (les chansons et les bruits de pigeon inclus) ; Anaïs pour ta bonne humeur tous les jours. Merci, Karishma pour ta joie de vivre et pour avoir parlé « franglais » avec moi, tu m'as fait sentir comme si j'étais chez moi. Et un merci spécial à toi, Éline, très aimable et attentionnée ; tu m'as beaucoup aidé pendant mon séjour et même après mon retour. Karishma et Éline, je ne vais jamais oublier votre entreprise dans la « mission échantillons » et la compagnie jusqu'à l'aéroport.

I could not forget to thank all the members of Team 2 and the people from the *Institut de Myologie*. Bruno Cadot, thanks for the assistance with cell tracking experiments and the microscope. Delphine, thank you for all the discussions later in the afternoon and also by many emails exchanged even after my return. Damilly, thank you for making the first weeks smoother and all the talks about our challenges as post-grads.

At last, but not the least, a big thanks to my lovely boyfriend Wesley, who has been by my side for a long time and knows better than anyone what I've been through. Thank you for supporting me, trusting me and not let me collapse. This path would have been harder without you.

Finally, I acknowledge the University of São Paulo and the Biosciences Institute that provided me the conditions for my intellectual and professional development. And all the members of the Human Genome and Stem Cell Research Center.

Agradeço à *Fundação de Amparo à Pesquisa do Estado de São Paulo,* FAPESP, pelos auxílios financeiros concedidos nos processos números 2015/18914-4 (Bolsa no país) e 2017/07376-7 (Bolsa do estágio no exterior). As opiniões, hipóteses e conclusões ou recomendações expressas neste material são de responsabilidade dos autores e não necessariamente refletem a visão da FAPESP.

Agradeço também às agências federais CNPq e CAPES pelo financiamento da infraestrutura do laboratório.

Author's Note

This thesis is subdivided into chapters, in accordance with the guidelines proposed by the Biosciences Institute of the University of São Paulo. Text formatting is in conformity to *Associação Brasileira de Normas Técnicas* (ABNT NBR 6023), except chapter 4, which was written following the instructions of the periodic journals where it was submitted for publication. The first chapter is a general introduction, where I present the theoretical scaffold on which my Ph.D. project was elaborated, followed by the objectives.

In the third chapter, I describe the general methodology, in which I tried to include the essential information to permit anyone to reproduce the experiments here presented. Chapters 4, 5 and 6 are written in the format of manuscripts. Finally, a general discussion and conclusions are presented in chapter 7.

Table of contents

List of illustrations

Resumo

ALMEIDA, Camila de Freitas. **Regeneração muscular na miopatia centronuclear associada a mutações no gene *DNM2***. 2019. 155p. Tese de Doutorado em Ciências (Biologia - Genética) - Instituto de Biociências, Universidade de São Paulo, São Paulo, 2019.

O músculo esquelético possui grande capacidade regenerativa após sofrer lesões, por causa da presença das chamadas células-satélite, que permanecem no tecido em estado quiescente, mas que, na presença de uma lesão, são capazes de proliferar e formar e/ou reparar miofibras. As células-satélite são importantes para o crescimento e manutenção do músculo adulto. Porém, em diversas doenças neuromusculares, a quantidade, a função e a capacidade proliferativa destas células podem estar comprometidas.

As miopatias centronucleares (CNM) são um grupo de doenças musculares caracterizadas por fraqueza muscular generalizada e o posicionamento dos núcleos na porção central da miofibra. A forma autossômica dominante (AD-CNM) é causada por mutações no gene *DNM2.* A proteína dinamina 2 é expressa ubiquamente e está envolvida no remodelamento de membranas, no tráfego intracelular e na dinâmica do citoesqueleto. Consequentemente, os mecanismos fisiopatológicos também são diversos e não completamente compreendidos, principalmente o fato de ser uma doença músculo-específica.

Nesta tese de doutorado, buscamos investigar as células-satélite no contexto da miopatia centronuclear. Para isto, utilizamos o camundongo modelo KI-*Dnm2*^{R465W}, portador da mutação mais frequente em pacientes humanos. Como na miopatia centronuclear não há um processo degenerativo em atividade, induzimos nos camundongos a lesão muscular por choque elétrico, em protocolo desenvolvido nesta tese, comparativamente a injeção de cardiotoxina. Verificamos que o número de células satélite no músculo gastrocnêmio do camundongo KI-*Dnm2*^{R465W} é reduzido em relação aos animais selvagens. Em consequência disto, o potencial regenerativo do animal mutante é reduzido e o músculo não se recupera completamente.

Investigamos também os efeitos funcionais de duas mutações, p.R465W e p.E650K, em mioblastos imortalizados. Examinamos o potencial miogênico *in vitro*, a propriedade migratória e a capacidade de endocitose. Verificamos que o potencial miogênico destas células é afetado pelas mutações, porém de maneiras distintas. Mostramos também que ambas as mutações impactam negativamente na capacidade migratória dos mioblastos, o que em parte justifica as alterações no potencial miogênico dos mesmos. Por fim, verificamos que a capacidade endocítica em mioblastos é alterada a depender da mutação, o que indiretamente também pode afetar a capacidade de diferenciação miogênica.

Palavras-chave: miopatia centronuclear; dinamina 2; regeneração muscular; células-satélite.

Abstract

ALMEIDA, Camila de Freitas. **Skeletal muscle regeneration in *DNM2*-related centronuclear myopathy**. 2019. 155p. Ph.D. thesis in Sciences (Biology - Genetics) – Biosciences Institute, University of São Paulo, São Paulo, 2019.

The skeletal muscle has a remarkable regenerative capacity upon injury, due to the presence of the satellite cells, which remain quiescent in the tissue, but, when required, they are able to proliferate and form and/or repair myofibers. Moreover, satellite cells are important to muscle growth and maintenance. However, in many neuromuscular disorders, the amount, function, and proliferative capacity of these cells are impaired.

Centronuclear myopathies (CNM) are a group of muscle diseases characterized by generalized muscle weakness and myofibers with central nuclei. The autosomal dominant form (AD-CNM) is caused by mutations in the *DNM2* gene. Dynamin 2 protein is ubiquitously expressed and is involved in membrane remodeling, intracellular trafficking, and cytoskeleton dynamics. Therefore, the pathophysiological mechanisms are equally diverse e not completely understood, mainly the fact to be a muscle-specific disease.

In the present Ph.D. thesis, we sought to investigate the satellite cells in the context of centronuclear myopathy. For this, we used the mouse model KI-*Dnm2*^{R465W}, bearing the most frequent mutation found in human patients. Since in centronuclear myopathy there is no evident degenerative process ongoing, we induced muscle lesion by electrical shock, a protocol developed for this thesis, comparatively to cardiotoxin injection. We verified that the number of satellite cells in gastrocnemius muscle is reduced in the KI-*Dnm2*^{R465W} mouse in relation to wild-type animals. As a result, the regenerative potential of the mutant mouse is decreased and the muscle is not able to fully recover.

In addition, we investigated the functional consequences of two mutations, p.R465W and p.E650K, in immortalized myoblasts. We examined the myogenic potential in vitro, the migratory property, and the endocytosis capacity. We found that both mutations impact on the myogenic potential, but in different ways. We also show that both mutations impair the migratory capacity of myoblasts that justify, in parts, the alterations in their myogenic potential. Finally, we verified that the endocytosis capacity is affected in a mutation-dependent manner, which may also indirectly disturb the myogenic differentiation efficiency.

Keywords: centronuclear myopathy; dynamin 2; muscle regeneration; satellite cells.

I. Chapter 1 - Introduction

I.1. The skeletal muscle tissue

I.1.1. Function and structure

Humans have approximately 600 muscles in their bodies, accounting for 40 % of total body mass in adult. There are three main muscle types: cardiac, smooth and skeletal muscle. Striated skeletal muscle is the most common and contributes for many and diverse mechanical and metabolic activities, providing body sustenance, force generation and movement (FRONTERA; OCHALA, 2015).

The skeletal muscle is organized in a very ordered and hierarchical architecture. It is composed by bundles of myofibers (or muscle fibers) associated with connective tissue. Muscle fibers are post-mitotic and multinucleated cells, delimited by the sarcolemma - the plasma membrane - surrounded by a layer of connective tissue named endomysium. A group of muscle fibers is aligned to each other and packed by a layer of connective tissue, the perimysium. Finally, these bundles of myofibers are wrapped by the epimysium, forming the muscle (Figure 1).

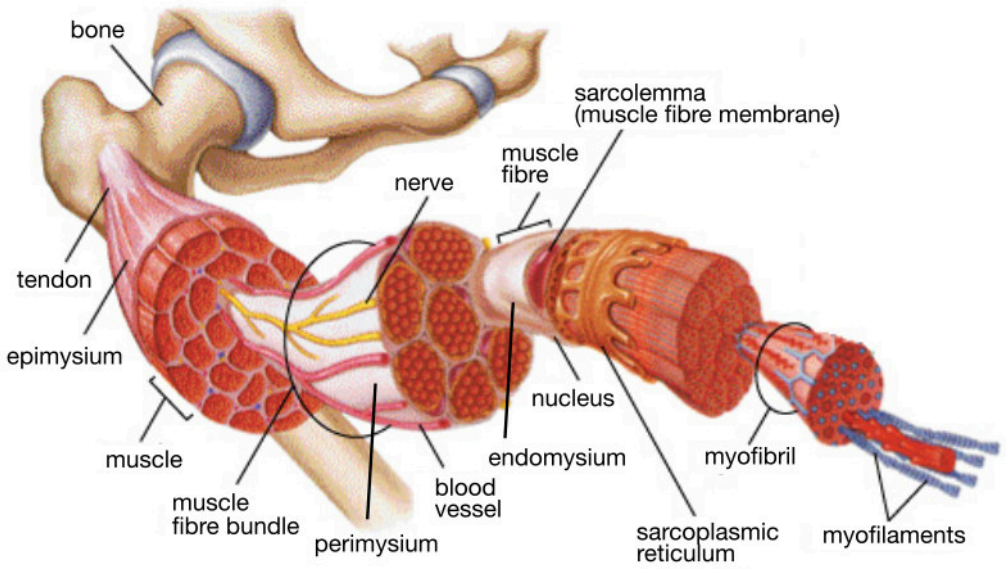

Figure 1 Skeletal muscle structure

The skeletal muscle is formed by bundles of myofibers, held together by layers of connective tissue and permeated with nerves and blood vessels. Nuclei are located at myofibers' periphery. The sarcoplasm is filled with myofilaments of contractile proteins. Adapted from *The Muscular System Manual: The Skeletal Muscles of the Human Body,* 3rd ed. Joseph E. Muscolino. Elsevier Health Sciences.

The intracellular organization of muscle cells is also unique. The sarcoplasm is filled with filaments of contractile proteins, the myofibrils, composed mainly by actin and myosin proteins. The myofilaments are formed by repeated segments of thick filaments of myosin and thin filaments of actin, named sarcomere, the muscle contractile unit. The sarcomere is the segment delimited by two Z-lines where actin thin filaments anchor. It contains an A-band (the superposition of actin and myosin) that separates two I-bands which are composed by actin. The H-band is formed only by myosin thick filaments (CLARK et al., 2002) (Figure 2).

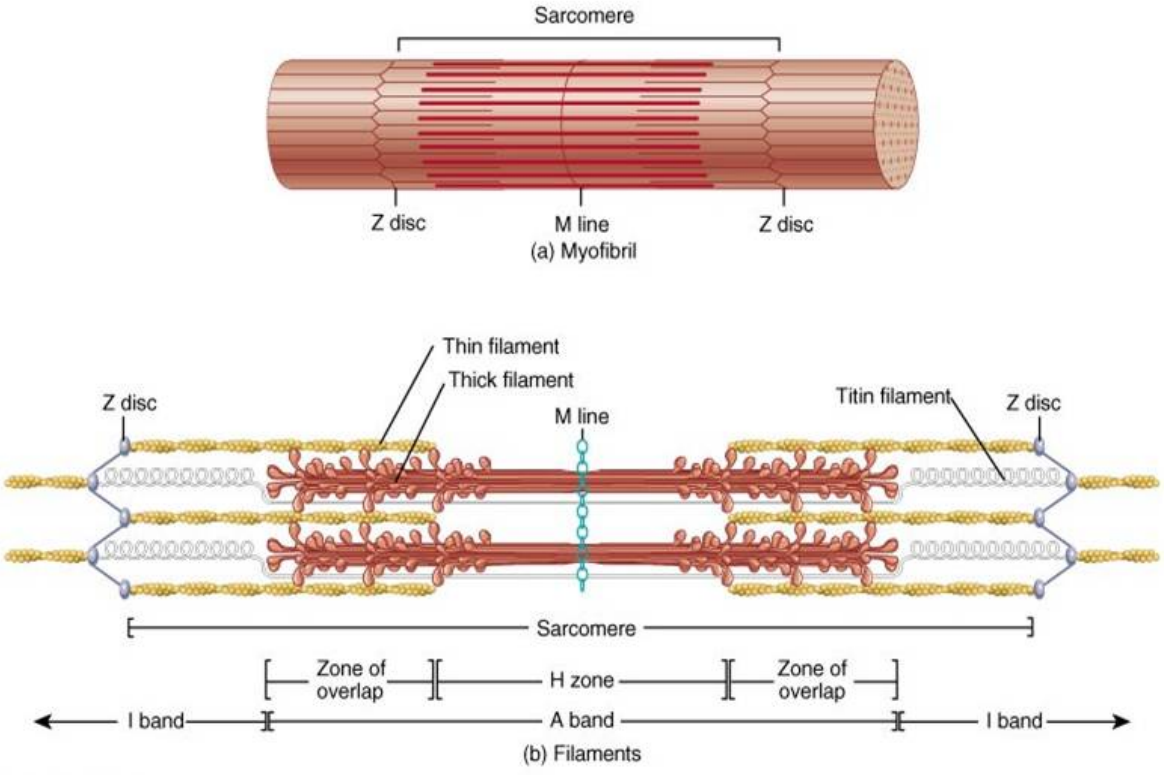

Figure 2 The sarcomere

Sarcomeres are formed of actin and myosin filaments that slide over each other during muscle contraction. Extracted from Tortora & Derrickson *Introduction to the human body 10th edition*

The sarcoplasmic reticulum (SR) surrounds the myofibrils and it exerts functions of transport and storage, regulating the flux of ions Ca^{2+} which are required for muscle contraction. Transversal invaginations of plasma membrane form a muscle-specific structure named T-tubule which together with the sarcoplasmic reticulum form the triad. This triad is essential for excitation-contraction coupling (ECC), the communication between the nervous system and calcium release. The action potential propagates through the T-tubule and reaches calcium channels on the SR promoting calcium release from SR and initiation of muscle

contraction (Figure 3). During contraction, the myosin filaments change conformationally through ATP hydrolysis, and slide over actin filaments, shortening the sarcomere and consequently the whole muscle fiber (FRONTERA; OCHALA, 2015).

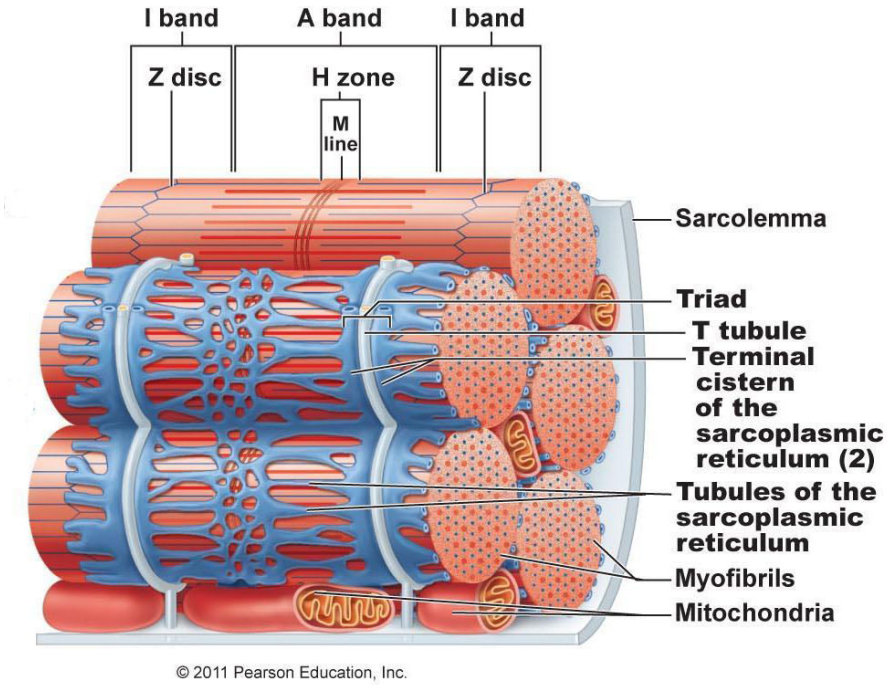

Figure 3 Transversal (T)-tubule and triad
Sarcolemma invaginations form the T-tubules which together with the sarcoplasmic reticulum form the triad. Extracted from Human anatomy and physiology 9e Elaine Marieb Katja Hoenh.

The muscle plasma membrane is also very specialized and it is the location of many muscle-specific protein complexes responsible for the connection between the intracellular cytoskeleton and the extracellular matrix (ERVASTI, 1993) required to stabilize the fiber and force transmission during contraction. Among these protein complexes, the dystrophin-glycoprotein complex (DGC) is composed of several proteins, including β-dystroglycan that is anchored to the plasma membrane and interacts with dystrophin in the cytoplasm and with the extracellular α-dystroglycan. Dystrophin interacts with the cytoskeletal actin and α-dystroglycan, and, finally attaches the whole complex to the extracellular laminin (IBRAGHIMOV-BESKROVNAYA et al., 1992; YOSHIDA; OZAWA, 1990).

I.1.2. Myogenesis and regulatory factors

Skeletal muscle development can be divided as follows: cell fate determination (myoblasts formation); myoblasts proliferation; alignment and fusion of myoblasts; myotube formation; myotube maturation and fiber formation (Figure 4).

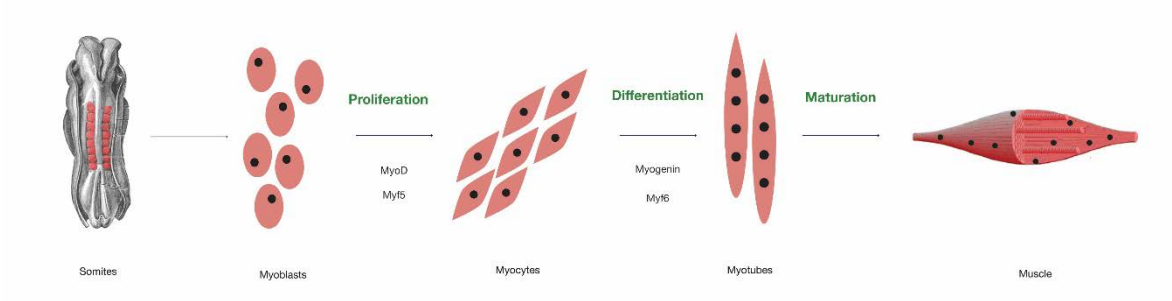

Figure 4 Skeletal muscle development

Skeletal muscle originates from somites. Myoblasts proliferate and express MYF5 and MYOD, then they start to differentiate and fuse; myogenin and MYF6 control the terminal differentiation.

Each step of muscle development is highly controlled by regulatory factors that act in a precise spatiotemporal order (PARKER; SEALE; RUDNICKI, 2003) (Figure 5). The myogenic precursors that give rise to muscles from trunk and limbs derive from somites, transient spheres of paraxial mesoderm flanking the neural tube and notochord in the embryo. Head and neck muscles have their origin in the anterior paraxial mesoderm, which does not form somites (BUCKINGHAM, 2017; CHAL; POURQUIÉ, 2017). During early steps of embryogenesis, the transcription factor PAX3 is responsible for the determination of cell fate, survival, self-renew and migration of muscle progenitor cells (BUCKINGHAM, 2017; HUTCHESON et al., 2009; MAGLI et al., 2013). Under the influence of the signaling factors SHH, WNT and BMP secreted by the notochord and neural tube, the somites transit into sclerotome (precursor of tendons, ribs and vertebral column) and dermomyotome from which cells delaminate and give rise to the dermis and myotome. It is at this point that the expression of myogenic regulatory factors (MRFs) is first detected (OTT et al., 1991). PAX3 is also directly or indirectly involved in the activation of the MRFs MYF5, MYOD, MRF4 (or MYF6) and MYOG (myogenin), which are the coordinators of the myogenic program, determining cell fate and regulating the terminal differentiation of committed cells (ASFOUR; ALLOUH; SAID, 2018; ZAMMIT, 2017). Then, myogenesis progresses through different sets of proliferation and differentiation, known as primary and secondary myogenesis.

In the primary myogenesis, the myofibers arise from PAX3+ progenitors in the dermomyotome (HORST et al., 2006; HUTCHESON et al., 2009), forming the templates for future myofibers. In secondary myogenesis, there is a downregulation of PAX3 and myogenic progenitors start to upregulate MRFs and express PAX7, which is a PAX3 orthologue, more active during post-natal growth and regeneration. The PAX7+ cells either fuse with each other or fuse to the preexisting myofibers, sustaining muscle growth in the fetal period (CHAL; POURQUIÉ, 2017; ONTELL; KOZEKA, 1984).

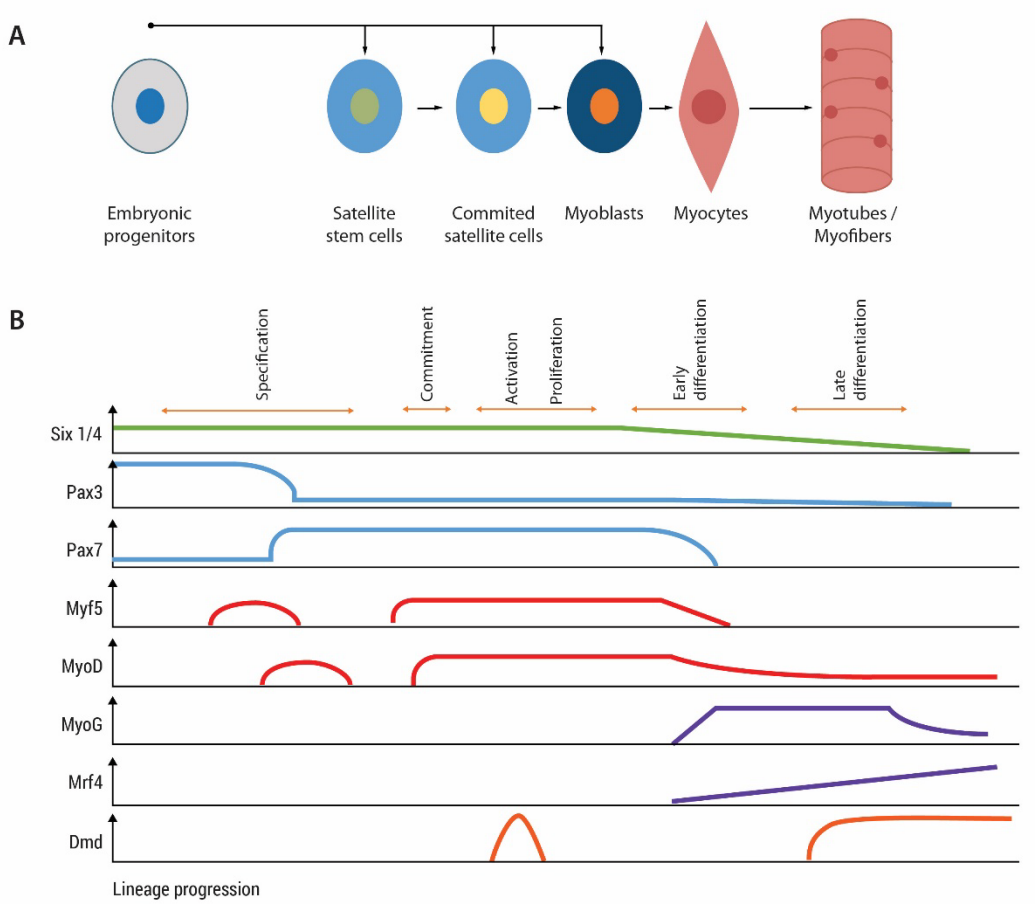

Figure 5 Cellular and molecular hierarchy of muscle development

(A) During development, an embryonic progenitor directly originates satellite stem cells, committed satellite cells, and myoblasts, which afterwards form a mature fiber. Some of them remain as satellite cells. In adult myogenesis, satellite cells can form myoblasts that will go through a similar process observed in development. (B) Expression of transcription factors involved in myogenesis. Extracted from Almeida et al, 2016.

The MRFs consist of the four muscle-specific transcription factors MYF5, MYOD, MYOG and Myogenic Regulatory Factor 4 (MRF4 or MYF6). They act in distinct phases of muscle development, regulating proliferation, cell cycle arrest and activation of muscle-specific genes for sarcomere assembly and terminal differentiation (ASFOUR; ALLOUH; SAID, 2018; HERNÁNDEZ-HERNÁNDEZ et al., 2017; ZAMMIT, 2017). The MRFs share a common protein

structure composed of three domains: an N-terminal cysteine/histidine-rich domain, a central region with a basic helix-loop-helix (bHLH) motif and a C-terminal serine/threonine-rich domain (OLSON, 1990). The bHLH domain leads DNA binding to the E-box consensus sequence CANNTG, found in promoter and enhancer sequences of many muscle-specific genes (BERKES; TAPSCOTT, 2005).

MYF5, MYOD, and MYF6 have overlapping functions as shown by distinct gene inactivation studies, that demonstrated that muscle formation is possible even in the absence of one of them. In *Myod*$^{-/-}$ mice, an elevation of *Myf5* expression compensates the role of *Myod*, forming apparently normal musculature (RUDNICKI et al., 1992). A similar situation is observed in *Myf5*-null mice (BRAUN et al., 1992). Mice mutant for *Myf6* develops a normal musculature with upregulation of myogenin expression, demonstrating that MYF6 acts as a negative regulator of myogenin (PATAPOUTIAN et al., 1995; ZHANG; BEHRINGER; OLSON, 1995).

In opposition, in myogenin-null mice, myogenesis fails, with the presence of only a few myofibers and predominance of undifferentiated myoblasts (HASTY et al., 1993; NABESHIMA et al., 1993; RAWLS et al., 1995), showing that myogenin is indispensable for late steps in embryogenesis, especially for the expression of myosin heavy chain and actin. Mice lacking both *Myf5* and *MyoD* have a complete absence of muscle formation, although *Myf6* being able to specify the myotome in early development, indicating that *Myf6* is also capable to initiate myogenesis (KASSAR-DUCHOSSOY et al., 2004; RUDNICKI et al., 1993). Double-mutant mice for *MyoD* and *Myf6* have a muscle phenotype similar to myogenin-null ones, despite normal expression of myogenin, suggesting that *MyoD* and *Myf6* have a redundant function and myogenin alone is insufficient for normal myogenesis (RAWLS et al., 1995).

Taken together, all these studies establish *MyoD* and *Myf5* important for myogenic determination, while myogenin and *Myf6* are more engaged with terminal muscle differentiation. The correct balance in the expression of all these four genes is required for complete and normal muscle formation.

I.1.3. Muscle regeneration and Satellite cells

Although being a post-mitotic tissue, skeletal muscle has a remarkable capacity to regenerate upon injury. This regenerative potential is mainly due to the presence of muscle-resident stem cells, named satellite cells. Satellite cells were described for the first time more than 50 years ago, in a seminal work by Mauro, residing between the plasma membrane and the basal lamina (MAURO, 1961).

Skeletal muscle repair can be divided into three phases: 1) degeneration/inflammation, defined by rupture and necrosis of myofibers and invasion of inflammatory cells; 2) repair phase, in which dead cells are phagocyted and new fibers and scar tissue start to be produced; 3) remodeling phase, when muscles fibers are reorganized, scar tissue is remodeled and muscle function is restored (TURNER; BADYLAK, 2012). The whole process is completed within weeks (Figure 6).

Muscle regeneration is triggered by the presence of myonecrosis that is characterized by segmented sarcoplasm about 24 hours post-injury. The lesion destroys the plasma membrane integrity, increasing ions calcium influx, activating autodigestion mechanisms (HUARD; LI; FU, 2002). Concomitantly, there is the infiltration of inflammatory cells, which exert many functions in all phases of regeneration (Figure 6) (GROUNDS, 2014).

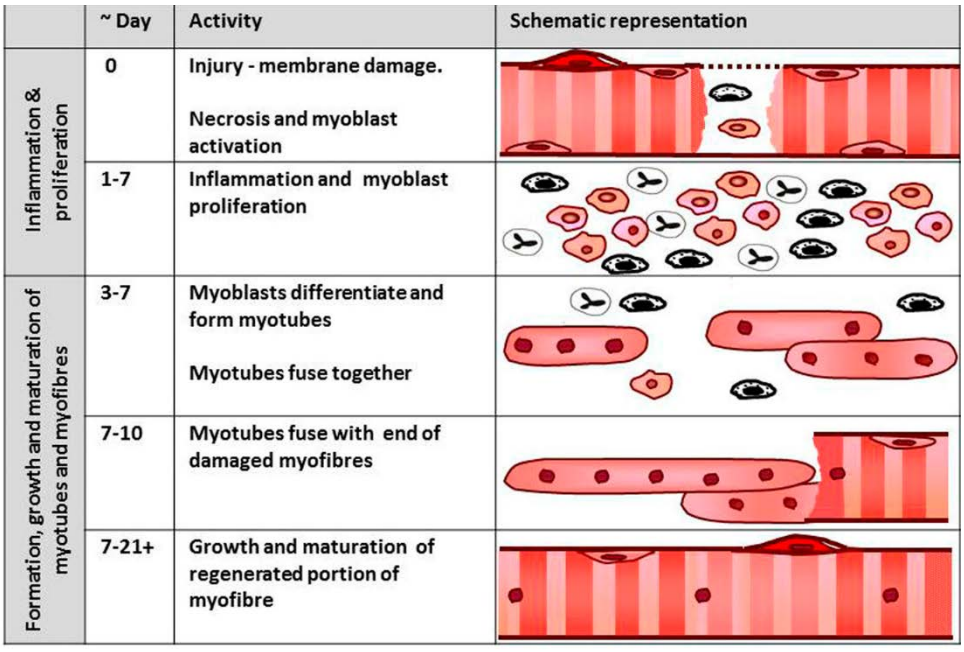

Figure 6 Cellular events in response to muscle injury
The injury is featured by membrane fragmentation. Within one day of damage, the first inflammatory cells appear. Myoblast proliferation starts at day one and continues up to day seven. Differentiation and fusion occur from days 3 to 10. Afterwards, inflammation decreases and the new myofibers maturate. Regenerated myofibers have their nuclei positioned at the central portion. Modified from Grounds, 2014.

Degeneration and inflammation develop within the first days after injury. The front of inflammatory cells includes macrophages, neutrophils, mast cells, and lymphocytes. They secrete enzymes and cytokines promoters of inflammation, but also other molecules that will work both on tissue cleaning from cellular debris and activation of muscle precursor cells and hence myogenesis (BRUNELLI; ROVERE-QUERINI, 2008; HUARD; LI; FU, 2002; KHARRAZ et al., 2013).

The muscular regeneration itself starts generally after the third day and requires the action of the satellite cells (SCs), the muscle stem cells, although other cell types can also contribute (PARKER; SEALE; RUDNICKI, 2003). Satellite cells originate during development as reservoir cells and are responsible for post-natal growth, maintenance, and repair of injuries caused both by exercise and disease (ALMEIDA et al., 2016). These cells represent from 3% to 11% of the total number of myonuclei in adult muscle, varying from species to species. Neonate mice have about 32% of nuclei of SCs, but this number drops to 5% in adult mice (ALLBROOK; HAN; HELLMUTH, 2007; BISCHOFF; HEINTZ, 1994).

SCs are recognized by their location and, more specifically, by the expression of many molecular markers, especially the transcription factor PAX7, the canonical satellite cell regulator (SEALE et al., 2000). Experiments in which Pax7-expressing cells were conditionally ablated in adult tissue showed impaired muscle regeneration after acute injury, highlighting the absolute necessity of these cells for muscle repair (LEPPER; PARTRIDGE; FAN, 2011; SAMBASIVAN et al., 2011).

In uninjured muscle, satellite cells stay in a quiescent state, characterized by inhibited cell division and undifferentiated morphology, controlled by several transcriptional, signaling and epigenetic pathways. Quiescent stem cells are marked by the presence of PAX7 and absence of MYOD and other markers related to cell proliferation (YOSHIDA et al., 1998; ZAMMIT et al., 2004). Generally, all the mechanisms are devoted to sustain PAX7 expression and repress MRFs expression.

NOTCH signaling pathway plays a major role in promoting SC quiescence, demonstrated by different works (BJORNSON et al., 2012; BUAS; KADESCH, 2010; CONBOY; RANDO, 2002; JIANG et al., 2014; MOURIKIS et al., 2012). Upon satellite cell activation, NOTCH rapidly declines. Experimental abrogation of NOTCH signaling leads SCs to differentiate,

without passing through proliferation and thereby leading to stem cell pool depletion. This result also demonstrates the role of NOTCH for self-renew (MOURIKIS et al., 2012). Ectopic expression of members of the NOTCH pathway showed an upregulation of PAX7, which in turn suppresses MYOD (WEN et al., 2012), thus reinforcing the role of NOTCH for the stability of quiescence. In its turn, NOTCH is regulated by the FOXO3 transcription factor, which stimulates NOTCH receptors expression, helping the maintenance of quiescence (GOPINATH et al., 2014).

In spite of all these mechanisms to keep satellite cells in a quiescent state in adult muscle, when required, they are promptly activated and start to proliferate in order to repair injured fibers and/or form new myofibers. The subsequent cellular and molecular steps are coordinated by transcription factors analogously to embryonic development, only with some specific differences (Figure 5) (GROUNDS, 2014; RUDNICKI et al., 2008).

The activation of SCs is a transient process: the damaged fibers as well as the inflammatory cells release growth factors, like fibroblast growth factor (FGF), tumor necrosis factor-α (TNF-α) and hepatocyte growth factor (HGF), known to activate signaling pathways related to cell cycle (LI, 2003; TATSUMI et al., 1998; YABLONKA-REUVENI; SEGER; RIVERA, 1999). The entry on S phase is stimulated by FGF2, through the stimulation of ERK1/2 pathway (JONES et al., 2001).

The rapid activation of SCs suggests that these cells are somewhat primed to respond as quickly as possible. MYOD and MYF5 are the first and most important regulators of SCs proliferation and differentiation once they are activated. Therefore, their expression must be actively repressed during quiescence, whereas quickly upregulated following activation. In fact, many mechanisms have been uncovered in this sense.

Although MYOD protein is undetectable in quiescent satellite cells, yet PAX7 and FOXO3 induce its mRNA expression. Then, its translation is somehow repressed. In practice, TTP (tristetraprolin), an mRNA destabilizing protein, drives *Myod* transcripts to mRNA decay (HAUSBURG et al., 2015). In addition, p38α and p38β MAPK, which are essential for SCs awakening, induce MYOD protein translation by inhibiting TTP and allowing cell cycle entry (JONES et al., 2005). By this, TTP ensures that MYOD is stable only when the satellite cell is activated.

Similarly, *Myf5* is also subjected to transcriptional and post-transcriptional control. The microRNA miRNA-31 was shown to sequestrate *Myf5* mRNA into cytoplasmic granules in quiescent SCs. Upon activation, these granules disassemble and *Myf5* mRNA is immediately available for strong protein expression (CRIST; MONTARRAS; BUCKINGHAM, 2012). *Myf5* gene transcription is regulated by CARM1 (a methyltransferase), which methylates PAX7 and leads it to associate with HMT (histone methyltransferase) complex and then induce *Myf5* transcription in activated SCs (KAWABE et al., 2012; MCKINNELL et al., 2008).

Following activation, SCs proliferates intensely to give rise to the new cells that will repair the lesion. Most of the satellite cells are a short-term repopulating cell (KUANG et al., 2007), while a subset is capable of long-term self-renew (GUREVICH et al., 2016; KUANG et al., 2007; ROCHETEAU et al., 2012). So, in order to maintain the stem cell pool, it is necessary that a fraction of cells return to the quiescent state and ensure a sufficient number of cells for future lesions. This is accomplished by some mechanisms discussed below.

Satellite cells can undergo either symmetric or asymmetric division. In asymmetrical divisions that occur in an apical-basal orientation, one cell daughter will commit to the muscle program (the one closer to the myofiber) and the other will remain quiescent (the one closer to the basal lamina). This asymmetry is achieved by the distribution of different factors between daughter cells. PAX7+ cells that never expressed MYF5 contributes to the stem cell reservoir, while PAX7+/MYF5+ cells preferentially differentiate (KUANG et al., 2007). PAX7+/MYOD- cells are self-renewing, PAX7+/MYOD+ cells are proliferative, while PAX7-/MYOD+ ones are committed to myogenic differentiation (HALEVY et al., 2004; OLGUIN; OLWIN, 2004; ZAMMIT et al., 2004). The same is valid for MYOG: PAX7-/MYOG+ cells progress through myogenic differentiation and PAX7+/MYOG- cells are destined to self-renew (YENNEK et al., 2014).

Still, self-renew can also occur by symmetrical divisions: *Wnt7a* drives symmetrical division of satellite cells in regenerating muscle, stimulating the expansion of both cells contributing to muscle repair and self-renew (LE GRAND et al., 2009).

Besides MRFs, other proteins are involved in satellite cell fate determination. Sprouty1 (SPRY1) is a marker of quiescent satellite cells (FUKADA et al., 2007) and its disruption in PAX7+ satellite cells impairs their return to quiescence and consequently, hampers the

reestablishment of the SC pool after injury by 50%. During the proliferation phase, *Spry1* expression is reduced, but those cells meant to go back to quiescence, reacquire *Spry1* expression and inhibit cell cycle (SHEA et al., 2010). With aging, DNA methylation suppresses *Spry1*, thereby reducing the ability to return to quiescence and to the stem cell pool in aged muscles (BIGOT et al., 2015).

It was found that dystrophin, a protein generally expressed in mature myofibers, participates in cell polarity definition and that dystrophin deficiency leads to a loss in the number of asymmetrical divisions and ultimately, to a reduced stem cell pool and poor regeneration (DUMONT et al., 2015). More recently, epidermal growth factor receptor (EGFR) and aurora kinase A (Aurka) were identified as regulators of asymmetrical divisions. EGF treatment of dystrophin-deficient mouse rescued the SC polarity and enhanced regeneration, helping to restore muscle strength (WANG et al., 2019).

I.1.3.1. Induced lesion approaches

Generally, the degenerative and regenerative phases following an injury are very similar among the different types of muscle and various causes of the lesion, but the extension and dynamic of each phase can vary according to the type of muscle, the source of lesion or the animal model (IRINTCHEV; WERNIG, 1987; LEFAUCHEUR; SÉBILLE, 1995; MITCHELL; MCGEACHIE; GROUNDS, 1992; PAVLATH et al., 1998).

Currently, there are many available techniques to induce muscle degeneration in animal models to the study of muscle regeneration in healthy and diseased conditions. They are divided into three classes of agents: myotoxins, such as cardiotoxin (CTX), notexin (NTX); chemicals, like barium chloride ($BaCl_2$); and physical, like denervation, transplantation, irradiation, crush and freeze injury. Generally, all these injury models induce a phase of intense necrosis followed by muscle regeneration and tissue remodeling. Many studies take advantage of these models to drive general conclusions about muscle regeneration.

However, each model has its particularities and may impact the muscle differently, inducing a different regeneration process too. In *Myf5*-null mice injured by freeze injury and cardiotoxin injection, both methods helped to identify a perturbed regeneration in this mouse

model. Nonetheless, one specific role of *Myf5* was identified only in the freeze-injury model. Although the loss of satellite cells at the damaged area by freeze-injury was comparable to CTX injection, in the latter the satellite cells were more evenly distributed. So, in the freeze injury model, the cells contributing to regeneration must come from long distances, which showed to be more difficult in the absence of *Myf5* (GAYRAUD-MOREL et al., 2007), underscoring the need to carefully take in account the method of lesion employed.

Cardiotoxin injection is the most popular method, probably because of the easiness to employ this method, reproducibility, consistency and perhaps tradition in literature, although all its biological properties are unknown. CTX is a protein kinase C-specific inhibitor isolated from snake venom; it appears to provoke the depolarization and contraction of muscle fibers, disrupting the membrane and to lyse different types of cell. But there are probably potential side effects of this toxin still to be determined (CHARGÉ; RUDNICKI, 2004).

By comparing four different lesion methodologies (freeze, NTX, CTX, and $BaCl_2$), a study found that despite causing similar necrosis and complete recovery one month after, significant differences were detected between them. For example, the injection of CTX, NTX, and $BaCl_2$ stimulated monophasic necrosis, followed by regeneration, while the freeze-injury model presented an asynchronous regeneration, with all regeneration phases present at the same time (HARDY et al., 2016).

Satellite cells population was also differently affected. In freeze injury, they observed a loss of 95% of satellite cells, while in the other methods, about 60% of the cells survived 18 hours after injection. Three months post-injury, in the freeze and $BaCl_2$ models the SCs numbers returned to normal counts, in contrast to myotoxins models, in which the number of SCs increased substantially (HARDY et al., 2016). Therefore, despite in all models, the muscle regeneration is successful, the time course can vary significantly and this must be considered in the experimental design.

I.2. Neuromuscular disorders

The term *neuromuscular disorders* encompasses a vast group of disorders affecting primarily the peripheral nerves and/or the muscle fibers. They are divided into groups and subgroups: spinal amyotrophies, neuropathies, congenital muscular dystrophies (several subtypes), progressive muscular dystrophies (many forms), myotonic dystrophy, metabolic myopathies, congenital myopathies and others (LAING, 2012; REED, 2002). A complete list of all the genes identified in neuromuscular disorders can be found at http://www.musclegenetable.fr/.

This present work was done on a congenital myopathy, so the next sessions are dedicated to this topic.

I.2.1. Congenital myopathies

The congenital myopathies comprise a group of genetic skeletal muscle disorders, typically present at birth or in early childhood and characterized by hypotonia and skeletal muscle weakness with stable or slowly progressive clinical course. Late onset or adult forms were also identified. The clinical presentation is heterogeneous and not certainly benign, including severe forms and even fatal ones. Five major categories are recognized: nemaline myopathy, core myopathies, myosin storage myopathy, congenital fiber disproportion and centronuclear myopathies (NORTH et al., 2014).

Traditionally, the congenital myopathies have been identified by specific histological findings on muscle biopsy (NORTH et al., 2014; REED, 2002). The genetics includes X-linked and autosomal inheritance, both dominant and recessive, involving many different genes. The same gene can be related to different forms, as well as one form can be caused by multiple genes.

In nemaline myopathy, the most common histological finding is the presence of rods, structures formed mainly by alpha-actinin and desmin. Seven genes were associated with this form and they code for components of thin filaments of the sarcomere. Thus, the mutations lead to a loss in force generation during contraction (LAING, 2012; NANCE et al., 2012).

Central core myopathies are characterized by the presence of areas without oxidative and glycolytic activity, reflecting the absence of mitochondria, and central foci of abnormal

myofibrils. Several genes were associated with these diseases, but the most frequent ones are *RYR1* and *SEPN1* (NANCE et al., 2012; NORTH et al., 2014; REED, 2002).

Myosin storage myopathy is characterized by the accumulation of ATPase and hyaline bodies in type I muscle fibers (DYE et al., 2006). In congenital fiber-type disproportion myopathy, there is a relative type 1 fiber hypotrophy compared to type 2 fibers (KISSIEDU; PRAYSON, 2016).

The centronuclear myopathies will be detailed in the next topic.

I.2.1.1. Centronuclear myopathies

Congenital myopathies with central nuclei or centronuclear myopathies (CNM) are classically identified by histological findings on muscle biopsies, mainly by the presence of many muscle fibers with nuclei arranged in rows in the central portion of the fiber without evident signs of degeneration or regeneration and in absence of other histopathological features of congenital myopathies (ROMERO, 2010).

The clinical presentation is very heterogeneous: patients present from severe hypotonia at birth to mild late-onset muscle weakness. The first group of patients with moderate and mild forms were identified in the 60s, and after, the severe cases of male newborns, with X-linked inheritance (ROMERO; BITOUN, 2011).

Three main forms are identified according to the inheritance pattern: recessive X-linked caused by mutations in *MTM1* (myotubularin) (XL-MTM) (LAPORTE et al., 1996; THOMAS; WALLGREN-PETTERSSON, 1996); autosomal recessive caused by *BIN1* (amphiphysin) mutations (AR-CNM) (NICOT et al., 2007); and autosomal dominant form due to *DNM2* (dynamin 2) mutations (AD-CNM) (BITOUN et al., 2005) and *BIN1* (BÖHM et al., 2014). *RYR1* mutations (mainly autosomal recessive) are also found (BEVILACQUA et al., 2011; WILMSHURST et al., 2010). Very rare cases were linked to *CCDC78* (MAJCZENKO et al., 2012) and *MTMR14* (TOSCH et al., 2006) are associated with late-onset autosomal dominant mutations. More recently, the genes *TTN* (CARMIGNAC et al., 2007; CEYHAN-BIRSOY et al., 2013) and *SPEG* (AGRAWAL et al., 2014) were found mutated in recessive cases.

Epidemiological data about CNM is limited, but the estimated incidence of all CNM forms is of 24 per one million births. Most of the cases are of XL-MTM (69.7%), and the remaining 30.3% is distributed among the other genes: 8.3% DNM2, 8.3% RYR1, 2.8% BIN1 and 11% of unknown genetic origin. Based on survival curves, the estimated prevalence is of 45% for XL-MTM and 55% for all no-XL-MTM forms (data calculated for the United States, Europe, Japan, and Australia). Translating into numbers, it means that currently exist approximately 4600 CNM patients in these regions (VANDERSMISSEN et al., 2018).

i. X-linked myotubular myopathy (XL-MTM)

X-linked myotubular myopathy is caused by *MTM1* mutations and affects mainly male newborns (LAPORTE et al., 1996), but there is an increasing number of female carriers manifesting symptoms reported on literature (SAVARESE et al., 2016). The term myotubular was coined because of the resemblance of myofibers with immature myotubes present during development (SHER et al., 1967; SPIRO, 1966). This also raised the hypothesis that these fibers never completed the maturation process, but this was never proved (ROMERO, 2010) since *Mtm1* knock-out mice have a normal muscle development and maturation (BUJ-BELLO et al., 2002).

Affected males usually present severe symptoms: hypotonia at birth, external ophthalmoplegia, generalized muscle weakness, and respiratory failure, leading to death in the first year of life. They require ventilatory support and a feeding tube. Individuals presenting milder symptoms and receiving intense medical care can survive until adolescence (JUNGBLUTH; WALLGREN-PETTERSSON; LAPORTE, 2008; ROMERO; BITOUN, 2011).

In the muscle biopsy, it is observed a high number of small fibers, large central nuclei, and predominance of type I fibers (Figure 7A and B). Central areas stain darker for periodic acid Schiff (PAS) and reduced staining for myofibrillar ATPase reaction. The reaction for oxidative enzymes activity shows increased activity in the central region of fibers, surrounded by a pale halo at the periphery (ROMERO, 2010; ROMERO; BITOUN, 2011; SEWRY; WALLGREN-PETTERSSON, 2017) (Figure 7C).

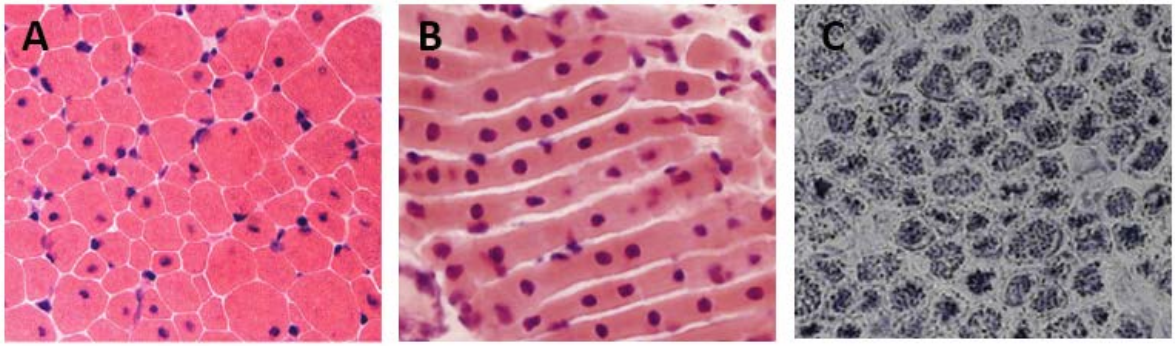

Figure 7 XL-MTM histopathology

Hematoxylin and eosin staining in (A) transversal section and (B) longitudinal section, showing central nuclei and small size fibers. (C) Oxidative enzymes staining highlights fibers with a dark central region, frequently surrounded by a pale peripheric halo. Modified from Romero, 2010 and Sewry and Wallgren-Petterson, 2017.

MTM1 gene has 15 exons and more than 300 mutations were already described, leading to absence or reduced activity of the protein (BIANCALANA et al., 2003; HERMAN et al., 2002; LAPORTE et al., 2000; TSAI et al., 2005). *MTM1* gene codes for myotubularin, a phosphoinositide phosphatase involved in phosphoinositides metabolism and trafficking (BLONDEAU et al., 2000).

Myotubularin acts in a broad range of cellular processes, particularly membrane trafficking. MTM1 dephosphorylates PI3P and PI3,5P2 and produces PI and PI5P, important second messengers in membrane trafficking and endocytosis. It was suggested that PI3P may play a role during myogenesis and cell differentiation (TAYLOR; MAEHAMA; DIXON, 2002).

Myotubularin has also been involved in endosomal trafficking (TSUJITA et al., 2004), excitation-contraction coupling (AL-QUSAIRI et al., 2009), in functions at the neuromuscular junction (DOWLING et al., 2012), autophagy (FETALVERO et al., 2013), cytoskeletal organization (HNIA et al., 2011) and satellite cell proliferation and survival (LAWLOR et al., 2012). The depletion of *Mtm1* expression in the muscles of adult mice causes a phenotype of myotubular myopathy, showing that myotubularin is also necessary for proper muscle function in adult muscle and not only for development (JOUBERT et al., 2013). This diversity of functions of myotubularin could be an explanation for the gravity of the disease.

ii. Autosomal recessive centronuclear myopathy (AR-CNM)

The classical autosomal recessive form of CNM is due to *BIN1* mutations. *RYR1, TTN, CCDC78, MTMR14* and *SPEG* mutations cause a CNM-like phenotype. Cases related to

mutations in these genes are sparse, except for *RYR1* mutations which are more frequently identified in CNM-like patients.

BIN1 codes for amphiphysin 2, a ubiquitous protein, mostly expressed in brain and muscles. Only a few cases have been described with recessive *BIN1* mutations (CLAEYS et al., 2010; NICOT et al., 2007). The clinical features can be positioned as intermediaries between XL-MTM and AD-CNM forms (ROMERO, 2010). Patients present delayed motor milestones, difficulties to run, walk and climb stairs. Muscular atrophy, diffuse weakness, ptosis, facial diplegia, and ophthalmoplegia are common features (ROMERO; BITOUN, 2011). Muscle biopsies show a predominance of centronuclear small type I fibers. By oxidative histochemical staining, its observable fibers with a central clear zone with a dark surround (ROMERO, 2010; ROMERO; BITOUN, 2011) (Figure 8). Amphiphysin 2 plays a role in T-tubule organization and in muscle maturation and mutations disrupt these properties (COWLING et al., 2017; NICOT et al., 2007).

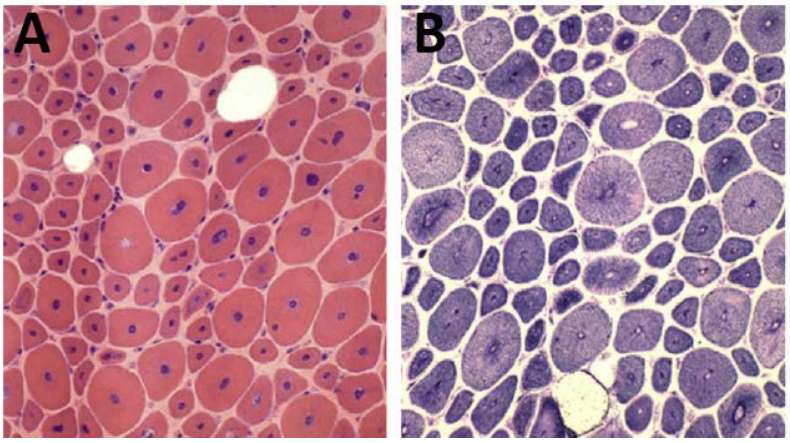

Figure 8 AR-CNM histopathology
(A) Hematoxylin and eosin staining in transversal section showing central nuclei, small rounded fibers and accumulation of endomysial tissue. (B) Oxidative enzymes staining reveals a central zone with dark border corresponding to the nuclear area. Modified from Romero, 2010.

iii. Autosomal dominant centronuclear myopathy (AD-CNM)

The clinical spectrum in the autosomal dominant form of centronuclear myopathy is wide. It varies from severe sporadic forms manifesting from birth (BITOUN et al., 2007), to mild forms with childhood and adolescence-onset (BITOUN et al., 2005), but the most frequent are the late-onset forms. AD-CNM phenotype can include delayed motor milestones,

facial and muscular weakness, ptosis and ophthalmoplegia (FISCHER et al., 2006; HANISCH et al., 2011). Muscle weakness progresses slowly and for most patients; cardiac and respiratory functions are normal. Loss of ambulation may occur only after the fifth decade of life (FISCHER et al., 2006).

In severe cases of neonatal onset CNM, the patients present generalized weakness, hypotonia, facial weakness with open mouth, ptosis and ophthalmoplegia (BITOUN et al., 2007), the progression is also slow (MELBERG et al., 2010; SUSMAN et al., 2010), but it can be fatal (JUNGBLUTH et al., 2010). A strength improvement can occur during childhood (SUSMAN et al., 2010); however, some children develop respiratory problems later (BITOUN et al., 2007; MELBERG et al., 2010).

The most prominent histological features are the central location of many nuclei, no signs of degeneration/regeneration, predominance of type I small fibers, hypotrophy of slow muscle fibers, slight deposition of endomysial connective tissue, and the radial distribution of sarcoplasmic strains from the central nuclei, identified by nicotinamide adenosine dinucleotide-tetrazolium reductase staining (NADH-TR) (JEANNET et al., 2004; SEWRY; WALLGREN-PETTERSSON, 2017) (Figure 9).

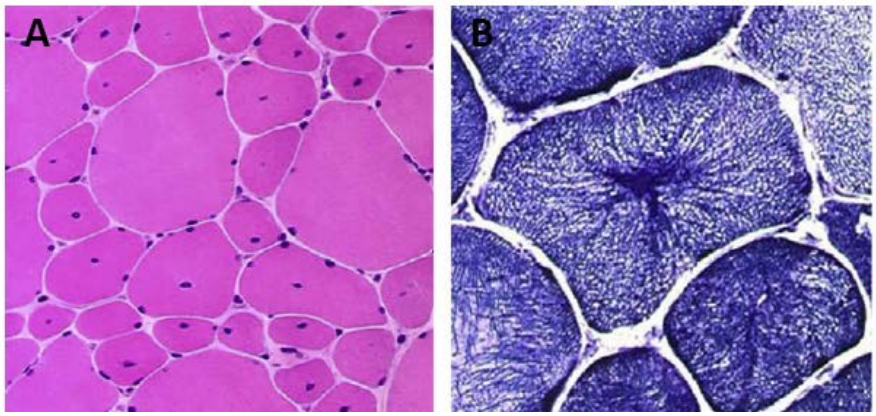

Figure 9 AD-CNM histopathology

(A) Hematoxylin and eosin staining in transversal section showing central nuclei in small fibers (B) Oxidative enzymes staining shows radial sarcoplasmic strands. Modified from Romero, 2010.

To date, 28 mutations were found in the *DNM2* gene as causative of AD-CNM (Figure 10). In addition, one mutation (p.Phe379Val) was found in homozygous state, causing a lethal congenital syndrome (KOUTSOPOULOS et al., 2013). A set of ten mutations located in the

middle domain cause Charcot-Marie Tooth (CMT) neuropathy that affects motor and sensory nerves, which the main feature is impaired myelination of neurons (SIDIROPOULOS et al., 2012). Hereditary spastic paraplegia is a third phenotype related to *DNM2* mutation (SAMBUUGHIN et al., 2015). There is no overlap between AD-CNM and CMT mutations.

Genotype-phenotype correlations are not clear, except for de novo mutations on the C-terminal portion of the PH domain: all are associated with severe neonatal phenotypes (BITOUN et al., 2007). For some mutations, a classification into three distinct classes was proposed: p.Ala618Thr and p.Ser619Trp/Leu are linked to the severe and neonatal onset phenotype; p.Glu368Lys is associated with intermediate clinical manifestation; and p.Arg369Trp, p.Arg465Trp, p.Arg522His/Cys and p.Arg523Gly mutations are present in patients with milder clinical manifestations (BÖHM et al., 2012).

For a long time, mutations only in *DNM2* were found in AD-CNM. However, surprisingly in 2014, Böhm et al. identified five new heterozygous mutations in *BIN1* in five families with AD-CNM, in which no *DNM2* mutation had been found (BÖHM et al., 2014).

The subjacent pathological mechanisms of AD-CNM and CNMs, in general, are not completely understood, but some studies have been contributing to relevant conclusions about the molecular basis of this disease. In the next session, dynamin 2 features and the pathophysiological mechanisms proposed for the CNMs will be detailed.

I.2.2. Dynamin 2 and Pathophysiological mechanisms in CNM

i. The protein dynamin 2 and its functions

Human *DNM2* gene is located on chromosome 19, has 114 kb, divided into 22 exons and produces, by alternative splicing, four main isoforms. The *DNM2* transcript is ubiquitously expressed, but it is more abundant in the brain and skeletal muscle (DIATLOFF-ZITO et al., 1995; DURIEUX et al., 2010a).

The dynamin superfamily embodies an assortment of multi-domain large GTPases, which exert a broad range of cellular functions, mainly vesicle formation and trafficking. Dynamin 2 is one of the three classical dynamins and is formed by five distinct domains. The

N-terminal GTPase domain makes the hydrolysis of GTP (CHEN et al., 2004), while the middle domain (MD) participates in DNM2 self-assembly and in conformational change induced by GTP hydrolysis (SMIRNOVA et al., 1999). The pleckstrin homology (PH) domain binds to phosphoinositides at the plasma membrane, directing dynamin to the membrane (KLEIN et al., 1998). The GTPase Enhancing Domain (GED) is proposed to participate in DNM2 self-oligomerization (SEVER; MUHLBERG; SCHMID, 1999). Finally, the proline-rich domain (PRD) interacts with the SH3 domains of the many proteins with which DNM2 interplays (HEYMANN; HINSHAW, 2009) (Figure 10).

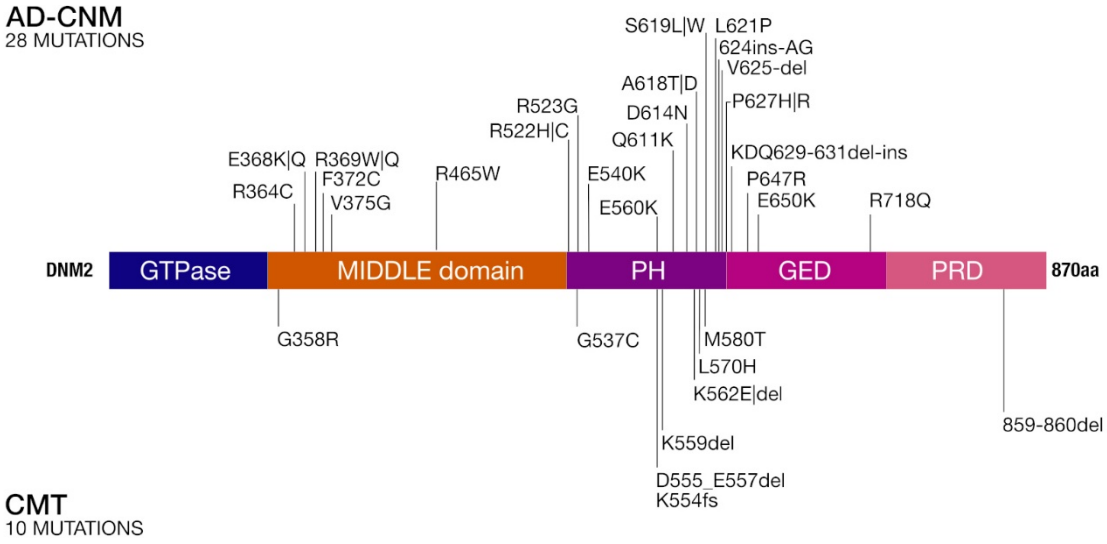

Figure 10 Dynamin 2 structure and mutations.

Dynamin 2 is formed by five conserved structural domains: an N-terminal GTPase, a middle domain, a pleckstrin homology domain that binds phosphoinisitides at the membrane, a GTPase effector (GED) domain that promotes the self-assembly and GTP hydrolysis, and a proline-rich domain (PRD) that binds to several SH3-domain containing proteins. To date, 28 mutations were reported as causative of CNM and 10 mutations are the cause of CMT.

The first property of dynamins to be discovered was its ability to promote membrane fission (ANTONNY et al., 2016). This was first observed in *Drosophila shibire* mutants in which dynamin mutation led to the accumulation of vesicles bound to the plasma membrane (VAN DER BLIEK; MEYEROWRTZ, 1991). Subsequently, dynamin 2 was proved to be a facilitator of clathrin-coated vesicles budding and thus in clathrin-mediated endocytosis and vesicle trafficking in general (METTLEN et al., 2009). DNM2 oligomerizes into helical polymers around

the neck of the nascent vesicle, and by GTP hydrolysis changes its conformation, constricting the plasma membrane and scissoring it (Figure 11).

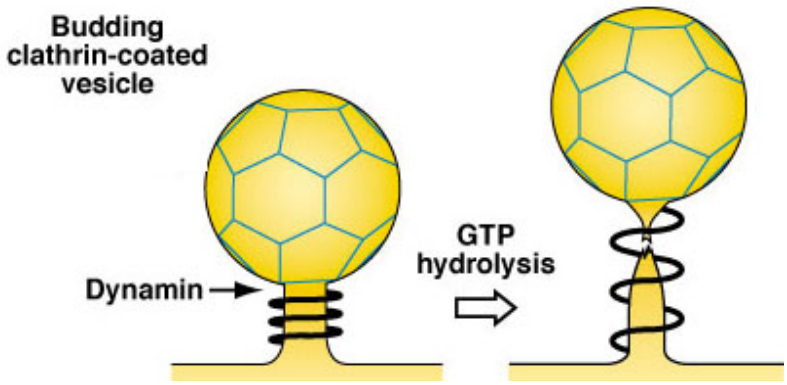

Figure 11 Dynamin 2 in endocytosis
Dynamin 2 is a facilitator of clathrin-coated vesicles budding. It oligomerizes into helical polymers around the neck of the nascent vesicle, and by GTP hydrolysis changes it conformation, constricting the plasma membrane and scissoring it.

DNM2 also plays a role in clathrin-independent endocytosis, intracellular trafficking of membranes, exocytosis, actin and microtubule dynamics, the cohesion of the MTOC (MicroTubule Organizing Centre), and apoptosis (DURIEUX et al., 2010a).

In figure 12 are represented the diverse cellular compartments in which DNM2 had been found playing a role (Figure 12). This gives an idea about the complexity that might be involved in the pathophysiological mechanisms underlying the dominant centronuclear myopathy and why there is still a lot to unravel about the functions of dynamin 2 for all tissues, especially for the skeletal muscle.

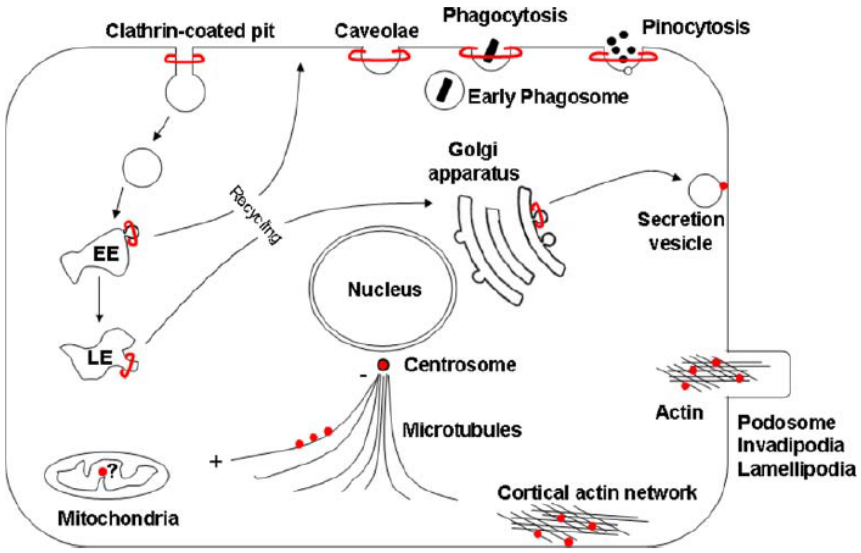

Figure 12 DNM2 functions
The multiple cellular localizations reported for DNM2 are represented in red.EE: early endosome; LE: late endosome. Extracted from Durieux et al, 2010.

The specific roles of dynamin in skeletal muscle are not yet determined, but the localization of DNM2 in muscle cells can give some clues. DNM2 localizes at the plasma membrane, the I-band, and the perinuclear regions. It also partially co-localizes with the microtubule network, at the neuromuscular junction and nearby sarcomeric Z-disks close to triads (COWLING et al., 2011; DURIEUX et al., 2010b) where it participates in T-tubule organization (TINELLI; PEREIRA; SUTER, 2013).

In the next session, the muscle-specific roles of dynamin 2 that have been revealed from studies of DNM2 mutants will be exposed.

ii. Pathophysiological hypotheses

The heterogeneity seen in the genetics, histopathology and clinical features in CNMs is also reflected in the variety of hypotheses raised to explain the development of these disorders. The three main proteins implicated in the CNMs – myotubularin, dynamin 2 and amphiphysin 2 – are involved in membrane remodeling and trafficking issues, which are relevant to cellular processes like endocytosis, intracellular vesicle trafficking, and autophagy. The impairment of these functions would consist of a major mechanism common to all the CNMs (COWLING et al., 2012), besides more specific mechanisms restrained to each form.

Studies performed in different animal models for centronuclear myopathies have suggested several pathogenic mechanisms, including triad abnormalities (AL-QUSAIRI et al., 2009; DOWLING et al., 2009; TOUSSAINT et al., 2011), calcium homeostasis deregulation (FRAYSSE; GUICHENEY; BITOUN, 2016; KUTCHUKIAN et al., 2017), defects in neuromuscular junction (DOWLING et al., 2012; GIBBS et al., 2013; ROBB et al., 2011), clathrin-mediated endocytosis impairment (BITOUN et al., 2009), actin kinetics impairment (GONZÁLEZ-JAMETT et al., 2017) mitochondria and desmin cytoskeleton alterations (FRANCK et al., 2019; HNIA et al., 2011), and satellite cells defects (LAWLOR et al., 2012).

The localization of DNM2 is altered in mutant DNM2 models, with cytosolic accumulation in vitro (JAMES et al., 2014; KENNISTON; LEMMON, 2010; KIERDASZUK et al., 2013; KOUTSOPOULOS et al., 2011; LIU; LUKIYANCHUK; SCHMID, 2011) and in vivo (CHIN et al., 2015; DURIEUX et al., 2010b; GONZÁLEZ-JAMETT et al., 2017). In fibroblasts and muscle from CNM-DNM2 patients, there is a normal expression of both mRNA and protein of the mutated and wild-type dynamin 2 (BITOUN et al., 2005, 2009; ECHANIZ-LAGUNA et al., 2007; KIERDASZUK et al., 2013; KOUTSOPOULOS et al., 2013) that favors for a dominant-negative effect of the heterozygous mutations, resulting in loss of function. Nonetheless, some studies point out that several DNM2 mutations increase oligomer stability and GTPase activity (KENNISTON; LEMMON, 2010; WANG et al., 2010). Furthermore, overexpression of wild-type or mutant-DNM2 leads to a CNM-like phenotype in mice and alterations in T-tubules in Drosophila (CHIN et al., 2015; COWLING et al., 2011; LIU et al., 2011). Therefore, some authors hypothesize that DNM2 mutations imply a gain of function effect. Nevertheless, the debate is ongoing and it is still not possible to draw unambiguous conclusions.

Both BIN1 and DNM2 participate together in the endocytic process, suggesting endocytosis impairment as a pathogenic consequence in autosomal CNM. Indeed, the impairment in clathrin-mediated endocytosis was reported in patient-derived fibroblasts with DNM2 mutations (BITOUN et al., 2009; KOUTSOPOULOS et al., 2011), however, this was not yet demonstrated in human myoblasts. In opposition, other studies did not confirm these observations (LIU; LUKIYANCHUK; SCHMID, 2011; SIDIROPOULOS et al., 2012). And it still obscures how the impairment of endocytosis has a muscle-specific impact since it is a ubiquitous cellular process. The impact of DNM2 mutations on other membrane trafficking processes, like in the endosomal pathway and exocytosis have not been explored either.

On fibroblasts transfected with DNM2 mutants, it was observed a decrease on activation of MAPK ERK1/2 pathway by EGF stimulation (BITOUN et al., 2009), a process known to be dependent on endocytosis and DNM2 (ANDRESEN et al., 2002; KRANENBURG; VERLAAN; MOOLENAAR, 1999). The same was not true for CNM patient-derived fibroblasts, but this needs to be clarified on muscle cells (BITOUN et al., 2009).

Alterations in the autophagy pathway have also been associated as a mechanism shared by CNMs (AL-QUSAIRI et al., 2013; FETALVERO et al., 2013). Autophagy is important to the degradation of defective proteins and organelles, infection defense and adaptation to changes in metabolism (MIZUSHIMA, 2007; SANDRI et al., 2013). Autophagy is particularly important for neurons and muscles, since their high energy demand, and, together with the ubiquitin-proteasome system, autophagy acts in the pathogenesis of muscle atrophy (SANDRI et al., 2013). Autophagy pathway involves several steps, carefully regulated, starting with autophagosome assembly, which fuses with lysosomes, resulting in the final degradative structures, the autolysosomes (MIZUSHIMA, 2007). Autophagy has emerged as an important primary and secondary mechanism for many neuromuscular diseases, including the CNMs (MERLINI; NISHINO, 2014).

Considering the links between endocytic and autophagic pathways, it was also expected to find alterations of autophagy in CNM-DNM. In fact, in the heterozygous mouse model for CNM-DNM2, it was demonstrated an upregulation of genes related to ubiquitin-proteasome and autophagy pathways (DURIEUX et al., 2010b). The homozygous animals showed an even pronounced phenotype regarding the autophagy, manifesting increased glycogen storage, hepatomegaly, hypoglycemia and early death (DURIEUX et al., 2012).

Dynamins have a critical role in actin network by elongating (GU et al., 2010), remodeling (MOOREN et al., 2009) and stabilizing (YAMADA et al., 2013) actin filaments. Dynamin 2 has emerged as a player in actin network remodeling because of its oligomerization and GTPase properties and its interactions with actin-related proteins. There are three actin isoforms in skeletal muscle: alpha-actin in the composition of the sarcomere, and beta- and gamma-actins present in other cytoskeletal elements that regulate trafficking and stabilization of plasma membrane proteins (KEE; GUNNING; HARDEMAN, 2009). Both dynamin 2 and gamma-actin localize in areas of intense membrane remodeling and trafficking (COWLING et

al., 2011; DURIEUX et al., 2010b; PAPPONEN et al., 2009). Additionally, mice lacking gamma-actin in muscles develop a CNM-like phenotype, suggesting a link between actin and centronuclear myopathy pathogenesis (SONNEMANN et al., 2006).

Recently, it was shown that DNM2 mutations expressed in human-derived myoblasts suppress *de novo* actin polymerization and insulin-induced insertion of GLUT4 – a glucose receptor – into the plasma membrane and its endocytosis. Moreover, myofibers isolated from the knock-in mouse model of CNM-DNM2 exhibit the same effects seen on human transfected myoblasts. Taken together, these findings confirm a prominent role of DNM2 in actin cytoskeleton dynamics and consolidate one more layer for the understanding of CNM pathophysiology (GONZÁLEZ-JAMETT et al., 2017).

The middle domain of DNM2 is essential for its centrosomal localization and binding to gamma-tubulin (THOMPSON et al., 2004) and it is where most of the mutations concentrate in. DNM2 mutants have abnormal centrosomal labeling in fibroblasts, so the mutations could be hindering its proper localization to the main MTOC or its interaction with gamma-tubulin (BITOUN et al., 2005).

In addition, microtubule and actin networks play a central role in nuclear positioning in muscle cells (MORRIS, 2003). Nuclear positioning in skeletal muscle is a sophisticated process; during fiber maturation, nuclei must be precisely moved, distributed and organized at the fiber's periphery (BRUUSGAARD et al., 2003; CADOT; GACHE; GOMES, 2015). In skeletal muscle, the number of nuclei determines the final fiber's size and each nucleus controls the transcription of a determined volume of cytoplasm, named as the myonuclear domain (LANDING; DIXON; WELLS, 1974; WHITE et al., 2010). Although the central position of nuclei is a hallmark of the CNM, this has not been much explored in the literature. In recent work, the morphometry, number, and positioning of the nuclei were investigated in the tibialis anterior muscle of KI-*Dnm2* mice. They found a lower number of nuclei per unit of fiber length that can explain the hypotrophy seen in the heterozygous mice, but at a specific age (3 weeks). The lack of nuclei accretion with growing was attributed to a reduced number of satellite cells on TA muscle (FONGY et al., 2019). Furthermore, the spatial organization of myonuclei is affected, like the nuclear orientations and distance between neighbor nuclei, and the authors raised the possibility of an altered anchoring at the periphery, but this needs to be further

addressed, taking into account the effects of DNM2 mutations on microtubule and actin networks. Finally, it is underscored the need to further explore the consequences of satellite cell's deficiency in this context (FONGY et al., 2019).

The role of satellite cells during development and skeletal muscle regeneration is established and consolidated as a consensus, in opposition to their participation in adult muscle maintenance and hypertrophy that is a target of controversy. For muscular dystrophies, muscle disorders in which there is chronic degeneration, the role of satellite cells both for disease progression and the potential therapeutic target is outstanding. Considering the centronuclear myopathies, the number of investigations aiming at the study of these cells is limited.

The mouse model for XL-MTM showed a reduced satellite cell number as evidenced by reduced PAX7 expression and number of myogenic cells isolated from muscle and quantified by flow cytometry. Furthermore, with aging, the number of SCs declined. In vitro and in vivo studies demonstrated a reduced proliferative capacity and increased susceptibility to apoptosis, probably triggered by altered Ca^{2+} homeostasis due to MTM1 deficiency (LAWLOR et al., 2012). In addition, depletion of MTM1 from mouse muscle postnatally led to a 90% reduction in the number of SCs (JOUBERT et al., 2013). These studies argue for the exhaustion of the SC population contributing to disease progression in XL-MTM.

As the muscle fiber is a syncytium, cell fusion is an essential step for muscle formation, in which actin cytoskeleton passes through an intense remodeling. By targeting *Dnm2* with siRNA, Leikina et al. showed inhibited syncytium formation by C2C12 mouse myoblasts (LEIKINA et al., 2013). Using a knock-out conditional mouse model, Shin et al. ablated the expression of DNM2 in myoblasts and observed impaired myotube formation. They also targeted clathrin-mediated endocytosis by using a siRNA against clathrin and the number of myotubes formed was reduced (SHIN et al., 2014). Thus, dynamin and CME showed to be important for myoblast fusion.

Excitation-contraction coupling is central for muscle functioning through the regulation of Ca^{2+} flux in the sarcoplasmic reticulum. For this, an adequate T-tubule structure is crucial. It is already documented the participation of MTM1 (AL-QUSAIRI et al., 2009; DOWLING et al., 2009), BIN1 (LEE, 2002; RAZZAQ, 2001; TOUSSAINT et al., 2011) and DNM2

(CHIN et al., 2015; GIBBS et al., 2014) proteins in T-tubule biogenesis and maintenance; thus the ECC impairment could be a pathological mechanism shared by all the CNMs and with a clear and direct explanation for the muscle weakness suffered by the patients.

The over-expression of mutant R465W-DNM2 in the muscles of adult mice induced a CNM-like phenotype, accompanied by T-tubule disorganization, suggesting a role for DNM2 in adult muscle maintenance (COWLING et al., 2011). Afterward, another group reported hyperactivity of other DNM2 mutants resulting in T-tubule fragmentation in mice and fly muscles and consequently disturbing ECC (CHIN et al., 2015).

The knock-in mouse model for CNM-DNM2 showed an elevated cytosolic Ca^{2+} concentration, signaling for perturbed calcium homeostasis (DURIEUX et al., 2010b). Later, Ca^{2+} signaling and ECC dysfunctions were described in this same mouse model and correlated with muscle weakness (FRAYSSE; GUICHENEY; BITOUN, 2016; KUTCHUKIAN et al., 2017).

Papers published in the last years are delineating a scenario in which a close interaction and interdependence between MTM1, BIN and DNM2 are increasingly central for a range of cellular process for proper muscle function. And in this scenario, DNM2 is emerging as a key player, giving insights for a comprehensive understanding of CNM pathogenesis and providing venues for the development of therapeutic strategies.

DNM2 was identified as a modifier of XL-MTM. It was demonstrated that DNM2 expression is elevated in the *Mtm1* knock-out (KO) mouse model and in the fibroblasts of XL-MTM patients, raising the participation of DNM2 as a pathogenic element in XL-MTM. Afterward, it was generated an *Mtm1* KO mouse only expressing 50% of dynamin 2 who showed an improvement in survival and restoration of muscle functions due to reduced *Dnm2* levels (COWLING et al., 2014). This study provided a proof of concept of the therapeutic potential of the modulation of DNM2 levels for CNMs and strategies to clinically modulate DNM2 in vivo are currently in development (TASFAOUT et al., 2017, 2018).

Similarly, the therapeutic benefit of DNM2 downregulation proved to be beneficial for AR-CNM related to BIN1. $BIN1^{-/-}$ mice are unviable, but after genetic reduction of *Dnm2,* they became viable and survived for up to 18 months, showing normal muscle histology and ultrastructure. In this same study, the authors discovered BIN1 as a negative regulator of

DNM2 during muscle development and maturation, revealing a common pathway for these two proteins (COWLING et al., 2017).

DNM2 modulation is also beneficial for AD-CNM. Using allele-specific silencing RNA against the p.R465W mutation, Trochet et al. successfully reduced the levels of both mRNA and protein mutant in the HTZ mouse. This reduction was enough to restore the myopathic features in the animal (TROCHET et al., 2018).

Together, these studies suggest a shared disease mechanism by the CNMs that may be a therapeutic target. Moreover, they provide arguments in favor of the hypothesis that enhanced DNM2 activity is behind the disease development in autosomal-CNMs and XL-MTM.

I.2.3. Animal model

Almost one decade ago, a valuable tool for the study of AD-CNM was developed: a knock-in mouse model harboring the most frequent mutation found in human patients. This mouse bears the p.R465W mutation, carried by about 30% of all AD-CNM patients, and is named *KI-Dnm2*$^{R465W/+}$ or simply HTZ. The mutation is kept in the heterozygous state; homozygous animals die perinatally (DURIEUX et al., 2010b).

HTZ mice progressively develop a phenotype similar to human CNM, as evidenced by impairment of force generation, muscle atrophy and morphological abnormalities visible with oxidative histochemical staining. By three weeks of age, the muscles start to show an impairment of contractile properties. Progressive muscle atrophy is evident after two months of age: the tibialis anterior has a 20% reduction in muscle mass and fiber size is decreased by 14% (DURIEUX et al., 2010b). Muscle atrophy was shown to be triggered by the activation of autophagic genes, decreased autophagosome maturation and activation of proteasome pathways (DURIEUX et al., 2012). Hypotrophy is also correlated to a reduced number of nuclei in myofibers (FONGY et al., 2019).

Surprisingly, HTZ mice do not have an increased number of centralized nuclei, suggesting that nuclear centralization is not a major component of the pathophysiology in CNM. Even the homozygous mice, which have a severe phenotype, show no more than 10% of central nuclei, whereas human patients can present up to 90% of nuclei internalization,

suggesting that nuclear centralization is not a critical feature for disease physiopathology (DURIEUX et al., 2010b).

While mice knock-out for *Dnm2* is embryonically lethal, heterozygous null mice expressing 50% of wild-type *Dnm2* are viable with normal muscle phenotype (FERGUSON et al., 2009). However total ablation of *Dnm2* specifically on muscles caused a series of muscle abnormalities (TINELLI; PEREIRA; SUTER, 2013). Thus, these animal models demonstrate that dynamin 2 is fundamental for normal development and muscle function.

Dynamin models were also developed in other species: *Drosophila* in which there is an accumulation of pre-synaptic vesicles bind to the plasma membrane (VAN DER BLIEK; MEYEROWRTZ, 1991); *C. elegans* that shows abnormal development and locomotion (CLARK et al., 1997) and *Danio rerio,* which presents muscle weakness and abnormal neuromuscular junction (GIBBS et al., 2014).

II. Chapter 2 - Objectives

In this project, we investigated the muscle-specific impact of DNM2 mutations in autosomal dominant centronuclear myopathy (AD-CNM). The first main goal was to study the satellite cells and whether muscle regeneration is impaired in the mouse model for AD-CNM. The second objective was to better characterize the functional consequences of two mutations in cellular models, regarding myoblast fusion, cell migration, and endocytosis.

Specific objectives

1. Study of regenerative potential in the mouse model KI-*Dnm2*^{R465W}

i. Quantification of satellite cells in the gastrocnemius muscle of KI-*Dnm2*^{R465W}

ii. Study of muscle regeneration after induced lesion in the gastrocnemius muscle by histopathology

iii. Gene expression profiling of genes involved in satellite cell biology and muscle regeneration

2. Study of myogenic potential *in vitro* of myoblasts bearing two DNM2 mutations

i. Study of myogenic differentiation in vitro of mouse myoblasts with the p.R465W mutation and human myoblasts with the p.E650K mutation

ii. Quantification of myoblast migration by live imaging microscopy

iii. Define the impact of p.E650K and p.R465W mutations in the endocytic pathway

III. Chapter 3 - Methodology

III.1. Patients and next-generation sequencing

Patients were selected from the neuromuscular disorders service, at the Human Genome and Stem cells Research Center or from other partner hospitals. The diagnostic is performed by clinical examination and muscle biopsy.

31 subjects were selected based on their clinics and/or muscle biopsy suggestive of centronuclear myopathy. Peripheral blood was collected for automated DNA extraction. DNA was subjected to next-generation exome sequencing of all the genes related to neuromuscular disorders, to the identification of genetic mutation. From the 31 subjects analyzed, we could find *DNM2* mutations in 15 of them: 6 bearing p.R465W mutation and 4 with the p.R369W mutation. The mutations p.E650K, p.R522H, p.E368K, p.E368Q, and p.A618D were found in five different individuals.

III.2. Animals

The experimental procedures were approved by the Ethics Commission for the Use of Animals from Biosciences Institute (CEUA/IBUSP; Protocol 245/2016). *C57BL/6J* wild-type mice were kept under control conditions of light and temperature, with water and food *ad libitum*, at the animal house of the Human Genome and Stem Cell Research Center.

For standardization of the electric-induced lesion by electroporation protocol, a total of 48 three-month-old C57BL mice, randomly divided into eight groups of six individuals each. After electroporation, mice were sacrificed by CO_2 asphyxiation at different time points. Gastrocnemius muscles were immediately dissected. Gastrocnemius from right leg was frozen in liquid nitrogen, protected by OCT Tissue Tek medium. Gastrocnemius from left leg was directly frozen in liquid nitrogen, then pulverized and divided into two aliquots for RNA and protein extraction.

The KI-*Dnm2*$^{R465W/+}$ mouse lineage was established on C57BL/6 background as described previously (DURIEUX et al., 2010b). Mice were housed in the animal facility of the University Pierre et Marie Curie, Paris, under standard conditions of light and temperature, food and water *ad libitum*. Mice electroporated or injected with cardiotoxin and sacrificed under isoflurane anesthesia. A similar procedure of dissection and muscle storage used for

C57BL mice were employed for these mice, except that muscles for histology were mounted on gum tragacanth and frozen in isopentane cooled in liquid nitrogen bath.

Only males were included in all experiments.

III.3. Muscle lesion

Electric-induced lesion by electroporation

Animals were anesthetized with 50 µL of ketamine, xylazine, and acepromazine (3 mg/kg, 80 mg/kg and 10 mg/kg of body mass respectively) cocktail, via intraperitoneal injection. Hair from calves was removed and a conductive gel was applied on the skin. Electrodes pads (Tweezertrode, 7mm of diameter, 45-0165, Harvard Apparatus) were positioned perpendicularly to the calves and 8 pulses of 100V, duration of 20 milliseconds, with intervals of 0.5 seconds were applied to each leg, using a BTX®-ECM®830 electroporator (Harvard Apparatus). Animals were sacrificed according to the guidelines of the *Conselho Nacional de Controle de Experimentação Animal* (CONCEA) after three, five, ten, fifteen, twenty-one, thirty and sixty days post-injury and had their gastrocnemius dissected.

Cardiotoxin injury

Mice were anesthetized with isoflurane and 150 µL of a 10 µM solution of cardiotoxin (Cardiotoxin, *Naja pallida*, 217503, Merck) were injected in the middle portion of gastrocnemius muscle as described (GARRY; ANTONY; GARRY, 2016). Animals were euthanized after three, five, ten and fifteen days afterward injections and had their gastrocnemius dissected.

III.4. Cell culture of immortalized myoblasts

Human cells

Immortalized myoblast cell lines are advantageous because they have long-term survival, can be easily grown and differentiate, providing enough amounts of cells for many experiments.

Myoblasts obtained from healthy subjects and one patient with the p.E650K DNM2 mutation were kindly immortalized by the Immortalization Facility of the Myology Institute,

Paris. Briefly, once the primary culture cells were established, they were selected by CD56 expression (a known myoblast marker) to remove contaminant fibroblasts and transduced with pBABE viral vectors containing *hTERT* (human telomerase reverse transcriptase) and *CDK4* (cyclin-dependent kinase-4) genes, as well as antibiotics resistance genes. After selection with antibiotics, transduced cells were subjected to clonal selection, expansion, and characterization regarding proliferative and myogenic properties (MAMCHAOUI et al., 2011).

Once the clones were established, cells were cultivated in proliferation medium consisting of 1 volume of M199 (Invitrogen, 41150020), 4 volumes of DMEM (Invitrogen, 61965), 20% fetal bovine serum, 50 U/mL penicillin, 50 mg/mL streptomycin, 25 µg/mL fetuin (Life Technologies, 10344026), 0.5 ng/mL fibroblast growth factor-basic (bFGF; Life Technologies; PHG0026), 5 ng/mL human epidermal growth factor (hEGF; Life Technologies; PHG0311), 0.2 µg/mL dexamethasone (D4902-100mg; Sigma), 5 µg/mL insulin (91077C-1g; Sigma); or in the commercial version Skeletal Muscle Cell Growth Medium (C-23160,PromoCell) supplemented with 20% fetal bovine serum (FBS; Gibco) and antibiotics (50 U/mL penicillin, 50 mg/mL streptomycin).

For myogenic differentiation, when cell reached above 90% of confluence, growth media was switched for differentiation media containing DMEM (Invitrogen, 61965), 50 µg/mL gentamicin (15750, Invitrogen) and 10 µg/mL insulin (Sigma, 91077). Myotubes were allowed to differentiate for three and six days, then detached from flasks with trypsin, centrifuged at 300g, for 10 min at 4 °C; washed in PBS, centrifuged again and pellets were stored at -70 °C.

For high-density muscular differentiation, at time zero, cells were plated at 5000 cells/cm² and proliferation media (PM) were added to the flask. At this density, cells do not touch each other. After six hours, PM was replaced by differentiation media (DM) and the flasks were kept in the incubator for more 42 hours. Then, the cells were trypsinized and plated at 75000 cells/cm² density, in which they filled the entire plate surface and maintained in PM for six hours that was enough time to let them attach to coverslips. After six hours, PM was changed again to DM and cells were incubated for more 66 hours, when they were fixed in 4% paraformaldehyde.

Mouse cells

Myoblasts from wild-type and KI-*Dnm2*$^{R465W/+}$ mice were immortalized and kindly provided by Dr. Jocelyn Laporte's group (*Institut de Génétique et de Biologie Moléculaire et Cellulaire*, France). Immortalization was achieved by transfection with lentivirus containing the *Cdk4* gene. Immortalized myoblasts were cultured in Matrigel-coated dishes and in DMEM (Invitrogen, 61965) supplemented with 20% FBS, 1% chicken embryo extract and 50 µg/mL gentamicin (Invitrogen, 15750). Murine immortalized myoblasts KMS4 were grown in Ham's F-10 (Invitrogen) media supplemented with 20% fetal bovine serum (Invitrogen), 2.5 ng/mL of fibroblast growth factor (FGF, Invitrogen) and 50 µg/mL gentamicin.

When cells reached approximately 80% of confluence, proliferation media was switched for differentiation media composed of DMEM (Invitrogen, 61965), 2% horse serum (Gibco), 10ug/mL insulin (Sigma, 91077) and 50ug/mL gentamicin.

III.5. Fusion index

Myotubes were fixed with 4% paraformaldehyde for 10 minutes and permeabilized in 1X TBS (10 nM Tris-HCl pH 7.5, 150 mM NaCl) with 0.1% Triton™X-100 (Sigma-Aldrich) (permeabilization solution), for 30 minutes and blocked in 1X TBS with 1% fetal bovine serum (Gibco) and 0.1% Triton™X-100 (Sigma-Aldrich) for 30 minutes. Incubation with primary antibody anti-*pan*-myosin (dilution factor 1:50; Developmental Studies Hybridoma Bank, MF-20) was performed overnight at 4 °C followed by rinsing with permeabilization solution and incubation with anti-mouse AlexaFluor® 488 (Invitrogen, 11001) secondary antibody for one hour at room temperature. Slides were mounted with Vectashield® (Vector) medium, containing DAPI to counterstain nuclei. Images were acquired in the Axiophot microscope (Zeiss) with 16x magnification objective; five random fields were imaged per slide.

The total number of nuclei and nuclei inside myotubes were counted manually. Myotubes were classified according to the number of nuclei inside each myotube (categories are presented in graphs). Total fusion index, *i.e.* not considering the myotube category, was calculated as (number of nuclei inside myotube/total number of nuclei) X 100.

III.6. RNA extraction and qRT-PCR

RNA extractions from muscles and cell pellets were done with TRIzol reagent (Invitrogen), following manufacturer's instructions and resuspended with RNase free water (Invitrogen). Only RNA samples from KI-*Dnm2*$^{R465W/+}$ mice and their WT controls electroporated were obtained with RNeasy Microarray Tissue kit (Qiagen). All samples were treated with DNase. RNA yield was measured in NanoDrop spectrophotometer and 18S and 28S RNA bands integrity was checked by 1% agarose gel electrophoresis.

cDNA was synthesized with SuperScript VILO Master Mix (Invitrogen) using 1 µg of total RNA. Pairs of primers were designed for the mouse genes *Pax7, Myod, Myf5, Myog, Tgfb, Col1a2, Spry1, Myf6* and the human genes *PAX7, MYOD, MYOG, MYF5*. As endogenous control, *Tbp* was used for muscle samples from mice. *Csnk2a* and *RPLPO* were endogenous controls for mouse and human cells, respectively. The efficiency of each pair of primer was calculated by a standard curve. Primer sequences and efficiencies are listed in Table 1.

Table 1 Sequence of primers

Gene	Forward	Reverse	Amplicon length (bp)	Efficiency (%)
Col1a2	GATGGTCACCCTGGAAAACC	CACGAGCACCCTGTGGTCC	68	99.297
Csnk2a	CCATATTTCTACCCGGTGGTGA	GATTCCCCAGGCTTCATCGT	100	103.962
Myf5	CTGTCTGGTCCCGAAGAAC	GACGTGATCCGATCCACAATG	130	100.34
Myf6	GCAGAGGGCTCTCCTTTGTA	AACGTGTTCCTCTCCACTGC	106	94.126
Myod	TACAGTGGCGACTCAGATGC	TAGTAGGCGGTGTCGTAGCC	116	101.642
Myog	CTGCACTCCCTTACGTCCAT	CCCAGCCTGACAGACAATCT	103	104.651
Pax7	GAGTTCGATTAGCCGAGTGC	GTGTTTGGCTTTCTTCTCGC	100	103.238
Spry1	GGTCATAGGTCAGATCGGGTC	CTTGCCACACTGTTCGCAG	120	104.879
Tbp	TGCACAGGAGCCAAGAGTGAA	CACATCACAGCTCCCCACCA	132	101.745
Tgfb	CCCCACTGATACGCCTGAGT	AGCCCTGTATTCCGTCTCCTT	86	97.76
MYOD	TGCCACAACGGACGACTTC	CGGGTCCAGGTCTTCGAA	76	98.213
MYF5	CTCAGCAGGATGGACGTGAT	TATGCAGGAGCCGTCGTA	72	92.777
MYOG	CAGTGCCATCCAGTACATCG	AAGTTGTGGGCATCTGTAGG	225	91.198
RPLPO	GGATTACACCTTCCCACTTGCT	GCCACAAAGGCAGATGGATCA	66	97.22

Quantitative real-time PCR assays of KI-DNM2 electroporation and human myoblasts experiments were performed in 7500 Fast (Applied Biosystems) equipment, the others were done in QuantStudio5 (Applied Biosystems) equipment. Reactions for the 7500 Fast system were prepared as follows: 10 µL Sybr Green Fast (Roche), 300 nM of each primer (forward and reverse), 4 µL of 1/10 diluted cDNA and RNase free water q.s.p. 20 µL. Reactions for

QuantStudio5 system were prepared as follows: 10 µL PowerUP Sybr Green (Applied Biosystems), 300 nM of each primer (forward and reverse), 2 µL of 1:10 diluted cDNA and RNase free water *q.s.p.* 20 µL.

Relative expression was calculated by the comparative C_t method, as described (SCHMITTGEN; LIVAK, 2008).

III.7. Histological staining

Frozen tissues were sectioned in 6 µm thick sections on microtome cryostat (Microm HM 505E), transferred to poly-lysine coated slides and stored at -70 °C. Slides were equilibrated to room temperature before use.

i. Hematoxylin-eosin (HE) staining

Slides were stained for 10 minutes with hematoxylin solution and rinsed in running tap water for 10 minutes. Next, they were incubated for three minutes in eosin solution and rinsed in running tap water. Then, the muscle sections were fixed in acetic acid and dehydrated in ethanol and xylol. Slides were mounted with mounting medium and observed in a conventional upright microscope (Axio Imager.Z1, Carl Zeiss, Oberkochen, Germany), and images acquired with Axion Vision Software (Carl Zeiss). At least 5 different fields were randomly photographed per slide.

Histopathology was evaluated regarding fiber caliber variation and morphology, necrosis, centronuclear fibers, inflammatory cells infiltration, and fibrosis deposition.

ii. Acid phosphatase

Acid phosphatase enzyme is present in the lysosomes of phagocytic cells, like macrophages. Its activity is enhanced during inflammatory processes. Slides were incubated for one hour, at 37 °C in incubation solution (0.8 mL pararosaniline solution; 0.8 mL sodium nitrite 10 mg of naphthyl-AS-BI-phosphate dilute in 1 mL dimethylformamide; 5 ml veronal buffer and 13 mL deionized water). Next, slides were washed in water, counterstained with methyl green for three minutes, dehydrated in ethanol and xylol and mounted with mounting medium. Slides were observed in a conventional upright microscope (Axio Imager.Z1, Carl Zeiss, Oberkochen, Germany), and images acquired with Axion Vision Software (Carl Zeiss).

Enzyme's activity was evidenced by reddish staining. At least 5 different fields were randomly photographed per slide.

iii. Sirius red staining

Sirius red staining allows the visualization of collagen present in tissues. Slides were immersed in Bouin fixation solution for 20 minutes and rinsed in running tap water. Following, muscle sections were stained in Sirius red solution (0.2 g Sirius red in 100 mL aqueous picric acid solution) for up to one hour. After, slides were rinsed, dehydrated in ethanol and xylol and mounted with mounting medium. Slides were observed in a conventional upright microscope (Axio Imager.Z1, Carl Zeiss, Oberkochen, Germany), and images acquired with Axion Vision Software (Carl Zeiss). The positive red staining was quantified in five random fields of each slide using ImageJ software.

iv. Immunofluorescence

Developmental myosin staining

Slides were hydrated with PBS and incubated overnight at 4 °C with primary mouse anti-developmental myosin heavy chain (dMyHC) (dilution factor 1:30; Novo Castra, NCL-MHCd) and rabbit/rat anti-laminin (dilution factor 1:300; Dako, Z0097; or 1:50; Abcam, Ab80580) antibodies diluted in PBS. Then, slides were washed with PBS and incubated one hour, room temperature, with secondary antibodies: anti-mouse Cy3, anti-rabbit AF488 or anti-rat FITC. After, slides were rinsed with PBS and mounted with Vectashield® (Vector) medium, containing DAPI to counterstain nuclei.

Slides were observed in confocal microscope LSM-800 (Carl Zeiss) with EC Plan-NEOFLUAR 20X/0,5 objective. From 5 to 8 random fields were photographed per slide. Counting of positive fibers (dMyHC+) was done manually and reported as percentages in relation to the total number of fibers (also counted manually).

PAX7 staining

Slides were equilibrated to room temperature and fixed in 4% paraformaldehyde (PFA) solution for 15 minutes, washed with PBS and incubated for 5 minutes in 0.1 M glycine solution. Then, muscle sections were subjected to antigen retrieval with hot 0.01 M citric acid, followed by permeabilization in 0.2% Triton™X-100 (Sigma-Aldrich). Blocking was done with 5% fetal bovine serum and 2% bovine serum albumin in PBS with 1:100 mouse IgG Fab

fragment (Jackson Immuno Research, 015-000-007). Slides were incubated overnight at 4 °C with primary antibodies diluted in blocking solution: mouse anti-PAX7 (dilution factor 1:20; Developmental Studies Hybridoma Bank, concentrate) and rabbit anti-laminin (dilution factor 1:300; Dako, Z0097). In the day after, slides were rinsed with PBS and incubated with secondary antibodies: anti-mouse AlexaFluor® 568 and anti-rabbit AlexaFluor® 488 for one hour at room temperature. Slides were mounted with Vectashield® (Vector) medium, containing DAPI to counterstain nuclei.

Image acquisition was performed in Nikon Eclipse Ti2 confocal microscope (Nikon). Three whole muscle sections of each slide were scanned. The total number of muscle fibers was quantified in a semi-automated way, using Qupath software (BANKHEAD et al., 2017) and PAX7+ nuclei were counted manually.

III.8. Transferrin/EGF uptake assay

Immortalized myoblasts (human and mouse) were grown on coverslips placed on 12-well dish. Cells were cultured with serum-deprived media for 45 minutes and then placed on ice. Next, cells were incubated 15 minutes with 40 µg/mL of transferrin labeled with AlexaFluor-488 (Life Technologies, T13342) or 1 µg/mL of EGF labeled with AlexaFluor-488 (Life Technologies, E13345) at 37 °C. Endocytosis was stopped by adding cold media and cells were rinsed with cold PBS and fixed with 4% PFA. Coverslips were mounted in slides with Vectashield® (Vector) medium, containing DAPI to counterstain nuclei. Cells were imaged with FV-1200 confocal microscope (Olympus) and 40x oil objective; whole cells were imaged using stacks of 0.5 µm interval.

Fluorescence was measured on the sum projection of the confocal stacks. Individual cells were outlined manually and integrated density was obtained with ImageJ software. The fluorescence of three areas around each cell was measured to obtain background noise. Finally, transferrin/EGF uptake was calculated according to the formula: total cell fluorescence= fluorescence of the cell X mean fluorescence of background/cell area. At least 50 cells were measured per condition.

III.9. Live cell imaging

For quantification of cell movements, cells were recorded as follows: myoblasts were plated in 6 or 12-multiwell dishes and grown until they reach about 30% of confluence. For live imaging, the dishes were placed in an incubator to maintain cultures at 37 °C and 5% CO2 (Okolab) coupled to a Nikon Ti microscope with an XY-motorized stage (Nikon). Images were captured with a CoolSNAP HQ2 camera (Roper Scientific) every 13 minutes, during 72 hours. Then, images were assembled in Metamorph software (Molecular Devices) and cell tracking was done either with Metamorph or ImageJ. The trajectories of individual cells were traced frame by frame manually (60 frames, equivalent to 13 hours of recording).

III.10. Statistical analysis

All statistical tests were performed in GraphPad Prism software, version 5.00 for Windows (La Jolla California USA, www.graphpad.com). Values are expressed as means ± standard deviation (SD). The number of samples (n) is indicated in the respective figures' legends. Data were tested for normality for the decision of the use of a parametric or non-parametric. Comparisons between two groups were performed with the Mann-Whitney test (non-parametric). Comparisons of multiple groups were done with the Kruskal-Wallis test (non-parametric), followed by Dun's multiple comparisons. P- values <0.05 were considered significant.

IV. Chapter 4 - Skeletal muscle injury by electroporation

In this chapter, we describe the methodology of muscle injury by electroporation developed by us and employed in the study of muscle regeneration of the KI-Dnm2R465W mouse model (Chapter 5).

This manuscript was submitted and accepted for publication at Springer Nature, Methods in Molecular Biology. The publication is due to September 2019.

Skeletal muscle injury by electroporation – a model to study degeneration/regeneration pathways in muscle

Camila F Almeida, Mariz Vainzof

Laboratory of Muscle Proteins and Comparative Histopathology, Human Genome and Stem Cell Research Center, Biosciences Institute, University of São Paulo, São Paulo, Brazil

Corresponding author:

Dr. Mariz Vainzof

Human Genome and Stem Cell Research Center, IBUSP

Rua do Matão, 106 – Cidade Universitária

São Paulo, SP - CEP 05508-900. Brazil

PHONE: +55 11 3091-7736

FAX: +55 11 3091-0852

e-mail: mvainzof@usp.br

Running Head: Electroporation induced muscle injury

Resumo

O músculo esquelético possui uma notável capacidade regenerativa após sofrer lesões, devido, principalmente, ao reservatório de células precursoras denominadas células-satélite (CSs), as quais são responsáveis pelo crescimento após o nascimento e pela resposta a lesões, sejam causadas pelo exercício ou doenças. Após a lesão, a resposta regenerativa inclui a saída das CSs do estado quiescente, a sua ativação, proliferação e fusão para reparar ou formar novas miofibras. Este processo é acompanhado por inflamação, com a infiltração de células imunitárias, primariamente macrófagos. Cada fase da regeneração é altamente regulada e orquestrada por muitas moléculas e vias de sinalização. A elucidação dos mecanismos envolvidos na degeneração e regeneração muscular é de extrema importância, especialmente para o desenvolvimento de estratégias terapêuticas para doenças musculares.

Aqui, propomos um modelo de lesão muscular induzido por eletroporação, o qual se mostrou um método eficiente para provocar danos ao tecido muscular para o acompanhamento dos passos envolvidos na degeneração e regeneração. Três dias após a eletroporação, o músculo mostra sinais proeminentes de degeneração, como áreas necróticas e presença de macrófagos, seguida da regeneração, observada pelo surgimento de miofibras com núcleos centrais. Após cinco dias, a regeneração está bastante ativa, e são observadas pequenas fibras positivas para a miosina de cadeia pesada do desenvolvimento. Depois de quinze dias, observamos a regeneração geral do músculo, com fibras de diâmetro aumentado após 60 dias. Esta metodologia é uma alternativa simples e fácil de induzir a lesão muscular, podendo ser empregada no estudo de alterações na expressão gênica e do processo de recrutamento e células satélite, tanto em modelos normais como em modelos distróficos/miopáticos para o estudo de doenças neuromusculares

Palavras-chave: músculo esquelético, lesão, regeneração, eletroporação

Abstract

Skeletal muscle has a remarkable capacity to regenerate after injuries mainly due to a reservoir of precursor cells named satellite cells (SCs), which are responsible for after-birth growth and response to lesions, either by exercise or disease. Upon injury, the regenerative response includes SCs exit of quiescence, activation, proliferation, and fusion to repair or form new myofibers. This process is accompanied by inflammation, with infiltration of immune cells, primarily macrophages. Every phase of regeneration is highly regulated and orchestrated by many molecules and signaling pathways. The elucidation of players and mechanisms involved in muscle degeneration and regeneration is of extreme importance, especially for therapeutic strategies for muscle diseases.

Here we are proposing a model of muscle injury induced by electroporation, which is an efficient method to induce muscle damage in order to follow the steps involved in degeneration and regeneration. Three days after electroporation, the muscle shows prominent signals of degeneration, like areas of necrosis and infiltration of macrophages, followed by regeneration, observed by the presence of centrally nucleated myofibers. After five days, the regeneration is very active, with small dMyHC positive fibers. Fifteen days later, we observe a general regeneration of the muscle, with fibers with increased diameter after 60 days. This methodology is an easy and simple alternative to induce muscle lesion. It can be employed to study alterations in gene expression and the process of satellite cell recruitment, both in healthy and dystrophic/myopathic animal models for muscular dystrophy.

Key Words: Skeletal muscle, lesion, regeneration, electroporation

1. Introduction

After an injury, the healthy muscle is able to repair and grow new fibers. However, in the presence of mutations in a range of genes encoding for many muscular proteins, the process of regeneration is not completely efficient, and its constant activation leads to an exhaustion of this ability. Understand all the steps involved in muscle degeneration and regeneration is of major importance for a better comprehension of the neuromuscular diseases. For this, protocols to induce muscle injury are very useful to track all the steps and players of muscle regeneration. The most popular models of lesion include the use of myotoxins, chemicals, and physical methods. Although all the methods are highly efficient to provoke muscle degeneration, they can have different effects on how the tissue recovers. Thus, the choice for one method should take into account these variables, depending on the questions to be answered.

Tissue electroporation is a method for the delivery of DNA and other molecules to tissues broadly applied because it makes the plasma membrane more porous [1]. The technique consists of the application of voltage pulses that induce transient or permanent wounds in the plasma membrane.

Typically, the transmembrane potential difference of a cell is 50-70 mV, and its maintenance is necessary to preserve the membrane's integrity. The larger the membrane is, the higher is the magnitude of the transmembrane potential generated by an external electric field. Thus, electrical fields as small as 60V/cm can damage the membrane of skeletal muscle cells [2]. When the electrical field is applied, the dielectric strength of the membrane is exceeded, which causes an increase in the conductance due to pore formation [3]. During electroporation, there is also an increase in local temperature and conformational changes in proteins [2].

Three days after electroporation, the muscle shows prominent signals of degeneration, as areas of necrosis and infiltration of macrophages, followed by regeneration, observed by the

presence of centrally nucleated myofibers [4]. After 15 days, it is possible to observe a general regeneration of the muscle, but some chronic lesions could still be identified [5].

Based on these observations, we propose the use of electroporation protocol as a fast and efficient method to induce muscle damage in order to follow the steps involved in regeneration. It emerges as a simple alternative to other injury methodologies, with the benefit of adjustment of the lesion by modifying the employed parameters. This opens the possibility to study the alterations in gene expression and the process of satellite cells recruitment both in healthy and dystrophic/myopathic animal models for muscular dystrophy.

2. Materials

2.1. Electroporation induced injury

1. 1 mL disposable syringes.
2. Anesthetics: acepromazine, ketamine, and xylazine.
3. Disposable razor blades.
4. Conductive gel.
5. Pulse generator ECM830, Electro Square Porator, Harvard Apparatus.
6. Electrodes pads Tweezertrode Kit, 7 mm of diameter, stainless steel, 45-0165, Harvard Apparatus.
7. Disposable gloves.

2.2.Skeletal muscle dissection and freezing

1. Disposable gloves.
2. Surgical instruments: forceps, dissecting scissors, iris scissors, iris forceps.
3. Liquid nitrogen.
4. Tissue-Tek O.C.T. compound.
5. Talc (cryoprotectant).
6. Corks.

7. Cryogenic vial.

2.3.Skeletal muscle sectioning and pulverization

1. Microtome-Cryostat.
2. (1 mg/mL) L-poly-lysine solution
3. Microscope slides and coverslips.
4. Methylene blue solution.
5. Mortar and pestle.
6. Dry ice.
7. Liquid nitrogen.

2.4.Histological analysis

1. Hematoxylin solution.
2. Eosin solution.
3. 70%, 90%, 100% Ethanol
4. 50 - 50% Ethanol-xylol
5. Acetic acid.
6. Mounting medium.
7. Bouin's solution: 50 mL of formaldehyde, 20 mL of acetic acid and 430 mL of picric acid. Store at room temperature.
8. 0.2% Sirius red solution: 0.2g of Sirius red and 100 mL of picric acid.
9. Nail polish.

2.5.Immunofluorescence

1. Hydrophobic PAP pen.
2. Paraformaldehyde 4% solution.
3. PBS 1X.

4. Primary antibodies against laminin (1/50 dilution, Abcam - Ab80580) and developmental myosin heavy chain (dMyHC) (1/30 dilution, Vector Laboratories - VPM664).
5. Anti-rat FITC and anti-mouse Cy3 secondary antibodies.
6. DAPI diluted in the antifade mounting medium.
7. Nail polish.

2.6.Gene expression analysis

1. TRIzol reagent.
2. Spectrophotometer.
3. DNase.
4. SuperScript® VILO™ MasterMix.
5. Primers pairs for target genes (**Table 1**).
6. PowerUp SYBR Green Master Mix.
7. Real-time PCR system.

3. Methods

3.1. Animal handling and electroporation

It is recommended to work in accordance with the guidelines for animal research from your institution, respecting animal well-being (See Note 1).

1. Anesthetize animals by intraperitoneal injection of a cocktail of acepromazine, ketamine, and xylazine (3 mg/kg, 80 mg/kg and 10 mg/kg of body mass respectively) and position the animal in dorsoventral position.
2. Remove the hair from both calves and apply a drop of conductive gel to the mouse's skin (**Fig. 1**).

3. Set up the equipment: eight electrical pulses, intensity of 100V, duration of 20 milliseconds each pulse and 0.5-second interval between pulses (See Note 2).
4. Position the electrodes pads perpendicularly to muscle fibers orientation (**Fig. 1**).
5. Hold the mouse leg by its ankle and hold it tightly to avoid electrodes slipping.
6. Press the start button and wait the eight pulses be finished.
7. Place the animals back to the cage and observe them recover from anesthesia.

3.2. Animal euthanasia and muscle dissection

Animals can be euthanized after different time points from electroporation. Here we present data three, five, ten, fifteen, twenty-one, thirty and sixty days after lesion.

1. Anesthetize the mouse and sacrifice by cervical dislocation.
2. Rinse the limbs with ethanol 70%. Pinch the skin with a forceps and make an incision with a scissor and pull up the whole skin from the leg to expose muscles.
3. With a pointed forceps, pinch the calcaneal tendon, insert a scissor under it and by opening the scissors detach the whole calf muscles. Cut the tendon, hold it with forceps and cut muscles at the opposite insertion, releasing them.

a. Muscle freezing, pulverization, and cryosectioning

One muscle is prepared for sectioning and the other for biochemical studies.

1. In a small container with talc, place a slice of cork and put a generous drop of O.C.T. compound. Place the muscle perpendicularly to the cork, immersing it in O.C.T. compound. Cover everything with talc to prevent O.C.T. compound seep out.
2. Grab the cork with a forceps, make sure to keep it in a horizontal position and quickly immerge it in liquid nitrogen. Leave the sample for at least 1 minute in liquid nitrogen. The specimens can be stored in liquid nitrogen or at -80 °C freezer until sectioning. For this, pack the specimens in small plastic bags, properly identified (See Note 3).

3. Put the second muscle directly in a cryogenic vial. Sink it in liquid nitrogen and leave the vial on liquid nitrogen for at least 2 minutes. Store it on liquid nitrogen or at -80 °C freezer until pulverization.
4. Coat microscope slides with poly-lysine. Apply 10 µl of the poly-lysine solution to a slide and use another slide to spread the solution on the surface of both slides, until it dries. Make a mark with a pencil on the side that received the coating.
5. Cool the cryostat chamber to -20 °C and put the specimen disc, the blade and the specimen inside it for temperature equilibration.
6. Put a drop of water on the specimen disc to "glue" the cork with the muscle and wait until it freezes. Then, mount the specimen disc to the specimen head and align it to the blade holder.
7. Adjust the section thickness to 6 µm and cut the tissue. Transfer the muscle sections to the coated side of slides. To check if the muscle is properly positioned, stain the sections with methylene blue for a few seconds, rinse on water and observe it on a light microscope. The muscle must be in a transversal orientation, with fibers appearing round. If necessary, adjust the positioning of the specimen disc until the correct orientation is found. Then, proceed with cutting. Four to six slices suffice for each slide.
8. Cover the segment of slides with muscle sections using a piece of plastic film and store slides in a -80 °C freezer (See Note 4).
9. To pulverize muscles, use an ice bucket filled with dry ice and place the pestle and mortar in the middle of the ice to cool them down. Carefully pour liquid nitrogen in the mortar. Wait a few seconds and put the piece of muscle in the mortar and start to smash it with the pestle, until it is completely ground. Add more liquid nitrogen as it evaporates.

10. With a spatula transfer the powder to 1.5 mL microcentrifuge tubes. If wanted, the sample can be divided into aliquots. Store samples at -80 °C freezer.

b. Histological colorations

i. H&E

1. Remove slides from -80 °C and let them equilibrate to room temperature for 30 minutes.
2. Place the slides in a staining trough and pour hematoxylin solution enough to submerge the muscle sections. Stain for 8 minutes and collect the hematoxylin solution (See Note 5).
3. Put the trough under tap water and let water flow slowly for 10 minutes or until all the colorant is washed out.
4. Pour eosin solution inside the trough and stain for 2 minutes.
5. Put the trough under tap water and let water flow slowly for 10 minutes or until all the colorant is washed out.
6. Quickly dip slides in acetic acid to fix coloration.
7. Proceed to dehydration. Immerse in ethanol 70% for 3 minutes, then in ethanol 90% for 3 minutes and finally in ethanol 100%. Forthwith dip slides into an ethanol-xylol solution for 3 minutes and then in xylol for another 3 minutes (See Note 6).
8. To mount the slides, apply a drop of mounting medium over the slide and cover with a coverslip (See Note 7).
9. Seal the slides by applying nail polish around coverslips and let them dry overnight.
10. Visualize slides with a bright-field microscope. After three days, we observe an intense degeneration with infiltration of inflammatory cells. Next, at five days, there is still the infiltration of mononuclear cells, but many new fibers can be observed. At 10 days post-lesion, the tissue is cleared from cellular infiltrates and we observe centrally located nuclei. The centronucleated fibers are present even 60 days after lesion (**Fig. 2**).

c. **Sirius Red**

1. Remove slides from -80 °C and let them equilibrate to room temperature for 30 minutes.
2. Place the slides in a staining trough and pour Bouin's solution to fix muscle sections during 20 minutes (See Note 8).
3. Wash slides with tap water as many times as necessary, until water is no longer yellow.
4. Filter Sirius red solution before every use. Incubate slides in 0.2% Sirius red solution during 1 hour. Wash out all the solution with running tap water (See Notes 8 and 9).
5. Dehydrate in ethanol 90% for 2 minutes, then in ethanol 100% for 2 minutes. Immerse slides in the ethanol-xylol mixture for 2 minutes and then in xylol for another 2 minutes.
6. Mount the slides with mounting medium and coverslips. Seal the slides with nail polish.
7. Acquire images with a bright-field microscope coupled to a camera, with a 10X objective. We recommend capturing at least three fields from a section of each mouse.
8. Quantify Sirius red staining on ImageJ software. Load the file on ImageJ and convert the RGB image to grayscale. Work with the green channel image, which has the best contrast to threshold the image. Highlight the collagen (in black) by moving the threshold bar, keeping an eye on the original image to correspond black to the red staining. Once satisfied, measure the area and calculate the percentage of black to the total area of the section. No appreciable fibrosis is observed after 60 days post-injury (**Fig.3**).

d. Immunofluorescence staining

1. Remove slides from -80 °C and let them equilibrate to room temperature for 30 minutes.
2. With a hydrophobic pen, circle the sections creating a barrier.

3. Add PFA 4% on the sections. Use the volume necessary to cover all the sections. Let it fix for 15 minutes, under a fume hood.
4. Rinse PFA with PBS, three times.
5. Dilute antibodies in PBS: laminin antibody at 1/50 dilution and dMyHC at 1/30 dilution. Usually, a volume of 50 µl suffices to cover all the sections. To help spread the solution evenly cut a small square of plastic and carefully put it over the sections.
6. Incubate overnight in a wet chamber at 4 °C.
7. Wash three times with PBS for 5 minutes each.
8. Incubate with secondary antibodies diluted 1/100 in PBS for 1 hour at room temperature, in a dark humid chamber. Use a 150 µl volume per slide.
9. Wash three times with PBS for 5 minutes each. Dry all the PBS, absorbing it with a tissue paper.
10. Apply 10 µl of mounting medium and gently put a coverslip. Turn the slide over a tissue paper to remove the excess of mounting medium and eventual bubbles.
11. Let the slides dry for 30 minutes and seal with nail polish.
12. Keep slides at 4 °C, in the dark. Acquire images with a fluorescence microscope, with a 20X objective. Take representative images of the whole sections (**Fig. 4**).
13. Count the percentage of positive dMyHC fibers in relation to all fibers in the section. dMyHC+ fibers peak five days after lesion (**Fig. 4**).
14. To measure fiber's diameter, open only green channel images on ImageJ software and convert them to 8-bit. Set scales if necessary (to µm). Adjust the threshold to highlight white contours. Analyze particles using the following parameters: size 200-50000, circularity 0.00 - 1.00, show outlines, display results. Measure Feret's diameter. If necessary, exclude measurements from fibers present partially in the frame. We found

that after 60 days, the regenerated fibers increased their diameters as compared to non-injured tissue (**Fig. 5**).

e. RNA extraction

1. Get muscle powder from the freezer and keep them in dry ice.
2. Add 500 µl of TRIzol reagent. From this point, samples can be manipulated at room temperature. Homogenize samples with TRIzol using a small plastic pestle, pressuring it against the bottom of the tube. Add more 500 µl of TRIzol and gently mix with the pestle, taking care to not let TRIzol leak from the tube.
3. Let homogenates at room temperature for 5 minutes.
4. Add 200 µL of chloroform and vigorously shake by hand for 15 seconds. The color must change from a transparent pink to a milky rose.
5. Incubate for 2 minutes at room temperature.
6. Centrifuge samples at 12,000g for 15 minutes at 4 °C. Three phases will form: in the bottom a pink one, in the middle a white one and at the top an aqueous phase.
7. Remove the aqueous phase to a new 1.5 mL tube, avoiding aspirating the middle phase.
8. Add 500 µl of isopropanol and pipette up and down several times to mix well.
9. Incubate for 10 minutes at room temperature.
10. Centrifuge at 12,000g for 10 minutes at 4 °C. Depending on the initial amount of muscle, often a visible pellet forms at the bottom.
11. Carefully remove the supernatant and wash pellet with 1 mL of 75% ethanol. Vortex briefly.
12. Centrifuge at 7,500g for 5 minutes at 4 °C. Discard supernatant.
13. Air dry the pellet for 5-10 minutes (See Note 10).
14. Resuspend RNA in RNase-free water by pipetting up and down several times.
15. Incubate for 10 minutes at 60 °C.

16. Measure RNA yield with a spectrophotometer.
17. Store RNA at -80 °C.

f. cDNA synthesis and quantitative real-time PCR

1. To cDNA synthesis, use 1 µg of RNA per 20 µl reaction.
2. Add 4 µl of SuperScript® VILO™ MasterMix and RNase-free water to 20 µl.
3. Mix well and incubate at 65 °C for 10 minutes, then at 42 °C for 60 minutes and finally at 85 °C for 5 minutes.
4. Store cDNA at -20 °C.
5. To qPCR, dilute cDNA 1/10 in RNase-free water. In 96-well plates, apply 10 µl of PowerUp SYBR Green Master Mix, 2 µl of diluted cDNA and 300 nM of forward and reverse primers, and RNase-free water to 20 µl of reaction. Make triplicates for each sample and pair of primers (See Notes 11 and 12).
6. Perform PCR in a real-time PCR thermocycler using cycling conditions following the manufacturer's recommendations.
7. Calculate fold-change values according to the $2^{-\Delta\Delta CT}$ method [6]. All genes are expected to increase their expression, as a reflection of satellite cells activity and tissue remodeling. (**Fig. 6**). As tissue recovers, their expression is reduced, however, the elevated *Pax7* and *Myf5* expression even after 60 days is noteworthy (**Fig. 6a and b**).

4. Notes

1. A minimum of 5 animals age and sex-matched is suggested for significant statistical analysis.
2. The safety of electroporation is determined by the magnitude of the electric field that must be below irreversible thresholds; this can be controlled by choosing adequate pulse

amplitude and electrode configuration [7]. Adjustments of these parameters are encouraged if different degrees of the lesion are desired.

3. Once frozen, it is important to maintain the temperature of muscles, to avoid thawing and formation of artifacts.
4. Make as many slides as necessary for all histological colorations and immunofluorescence analysis. If more slides are necessary for the future, the specimen can be stored back to -80°C and cut again. Make sure that the specimen does not thaw when moved from freezer to microtome and vice-versa. Always transport specimens on dry ice.
5. Hematoxylin solution can be reused many times. The staining time can be increased or reduced if staining is too strong or weak, respectively.
6. Xylol must be manipulated under the fume hood.
7. To remove the eventually formed bubbles and excess of mounting medium, turn the slide down and gently squeeze it against a piece of tissue paper.
8. Bouin's and Sirius red solutions can be reused several times.
9. Do not let the red coloration stain inside muscle fibers. To avoid this, check slides after 20 minutes of incubation and then every 10 minutes. Stop incubation before one hour if you observe that the fibers are getting red.
10. If necessary, aspirate the ethanol with a micropipette.
11. Use SYBR green reagent compatible with your equipment.
12. PowerUp Sybr green master mix requires from 1 to 10 ng of cDNA. In this case, we are applying 10 ng.

Acknowledgements

This work was possible thanks to financial support from Fundação de Amparo à Pesquisa do Estado de São Paulo (FAPESP), CNPq and CAPES.

5. References

1. Aihara H, Miyazaki JI (1998) Gene transfer into muscle by electroporation in vivo. Nat Biotechnol 16:867–870.

2. Lee RC (2005) Cell injury by electric forces. Ann N Y Acad Sci 1066:85–91.

3. Belete H, Godin L, Stroetz R, Hubmayr R (2010) Experimental models to study cell wounding and repair. Cell Physiol Biochem 25:71–80.

4. Roche J a, Ford-Speelman DL, Ru LW et al (2011) Physiological and histological changes in skeletal muscle following in vivo gene transfer by electroporation. Am J Physiol Cell Physiol 301:C1239-50.

5. Baligand C, Jouvion G, Schakman O et al (2012) Multiparametric functional nuclear magnetic resonance imaging shows alterations associated with plasmid electrotransfer in mouse skeletal muscle. J Gene Med 14: 598-608

6. Schmittgen TD, Livak KJ (2008) Analyzing real-time PCR data by the comparative CTmethod. Nat Protoc 3: 1101-1108

7. Čorović S, Mir LM, Miklavčič D (2012) In vivo muscle electroporation threshold determination: Realistic numerical models and in vivo experiments. J Membr Biol 245:509–520.

Table 1 - Sequence of primers

Gene	Forward	Reverse	Amplicon (bp)
Col1a2	GATGGTCACCCTGGAAAACC	CACGAGCACCCTGTGGTCC	68
Myf5	CTGTCTGGTCCCGAAGAAC	GACGTGATCCGATCCACAATG	130
Myod	TACAGTGGCGACTCAGATGC	TAGTAGGCGGTGTCGTAGCC	116
Myog	CTGCACTCCCTTACGTCCAT	CCCAGCCTGACAGACAATCT	103
Pax7	GAGTTCGATTAGCCGAGTGC	GTGTTTGGCTTTCTTCTCGC	100
Tbp	TGCACAGGAGCCAAGAGTGAA	CACATCACAGCTCCCCACCA	132
Tgfb	CCCCACTGATACGCCTGAGT	AGCCCTGTATTCCGTCTCCTT	86

Fig. 1 Muscle electroporation and dissection. (A) Removal of hairs from the calf. (B) Electrode positioning. (C) After specified times, the animals are sacrificed, the skin is removed and the calcaneal tendon is pinched. (D, E) Insert a scissor under the calcaneal tendon and open it, detaching the muscle from the leg and finally cut the muscle at the opposite insertion. (F) Isolated calf muscle.

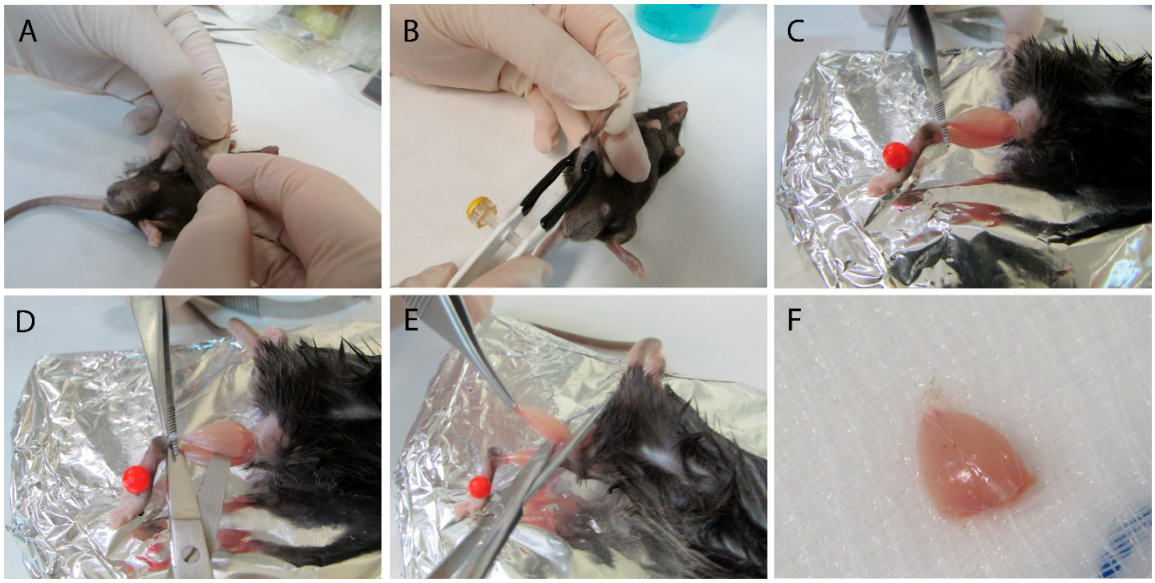

Fig. 2 Hematoxylin and eosin staining. Muscle histology at different time points after injury. At three days, we observe the infiltration of inflammatory cells and fiber degeneration. After five days, there is still cell infiltrates and new fibers start to be formed. After 10 days, centronucleated fibers appear and they are still observable 60 days post-injury.

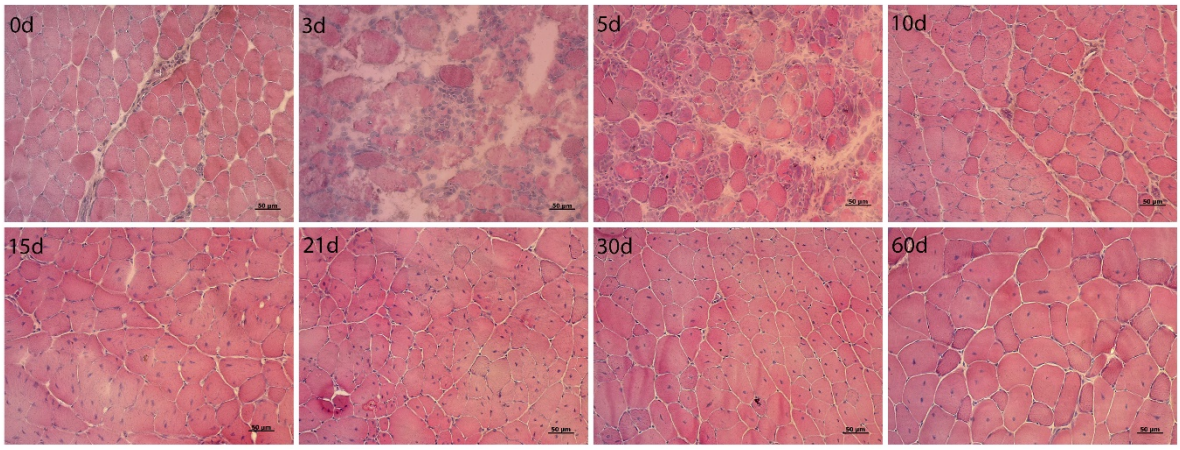

Fig.3 Sirius red staining. Quantification of the percentage of collagen deposition. Data presented as mean ± SD, n-=6 per group. Mann-Whitney test, ns=non-significant.

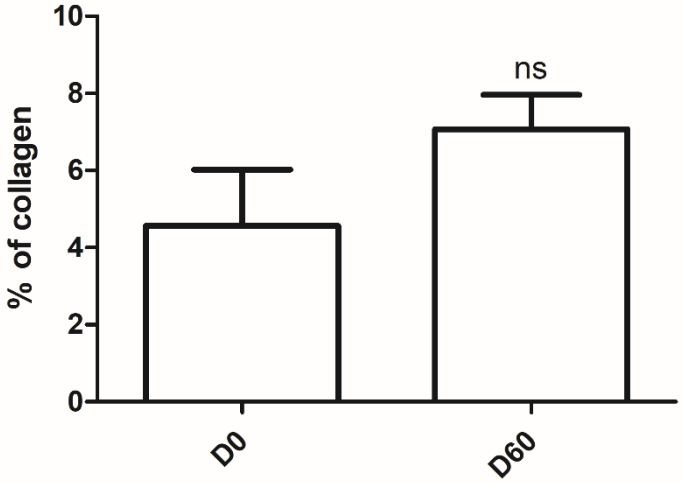

Fig. 4 Regenerating fibers are identified by dMyHC positive staining (in red).

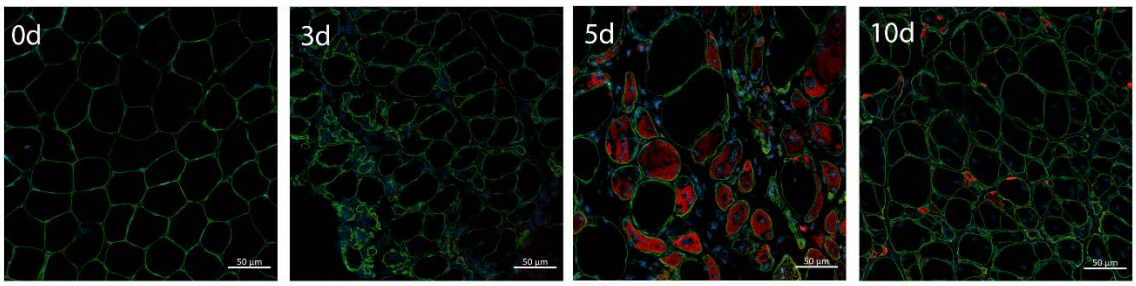

Fig. 5 Feret's diameter. Fiber's diameter is increased after lesion induced by electroporation. Data presented as mean ± SD. Mann-Whitney test, ***p<0.001.

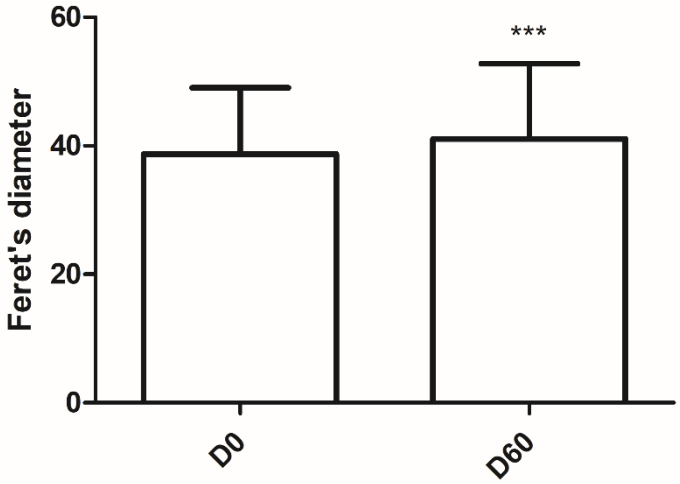

Fig. 6 Gene expression. Genes related to the myogenic program are activated upon injury, with higher expression three and five days after electroporation, reducing as muscle regenerates. Data presented as mean ± SD, n= 6 per group. Mann-Whitney test, *p<0.05, **p<0.01.

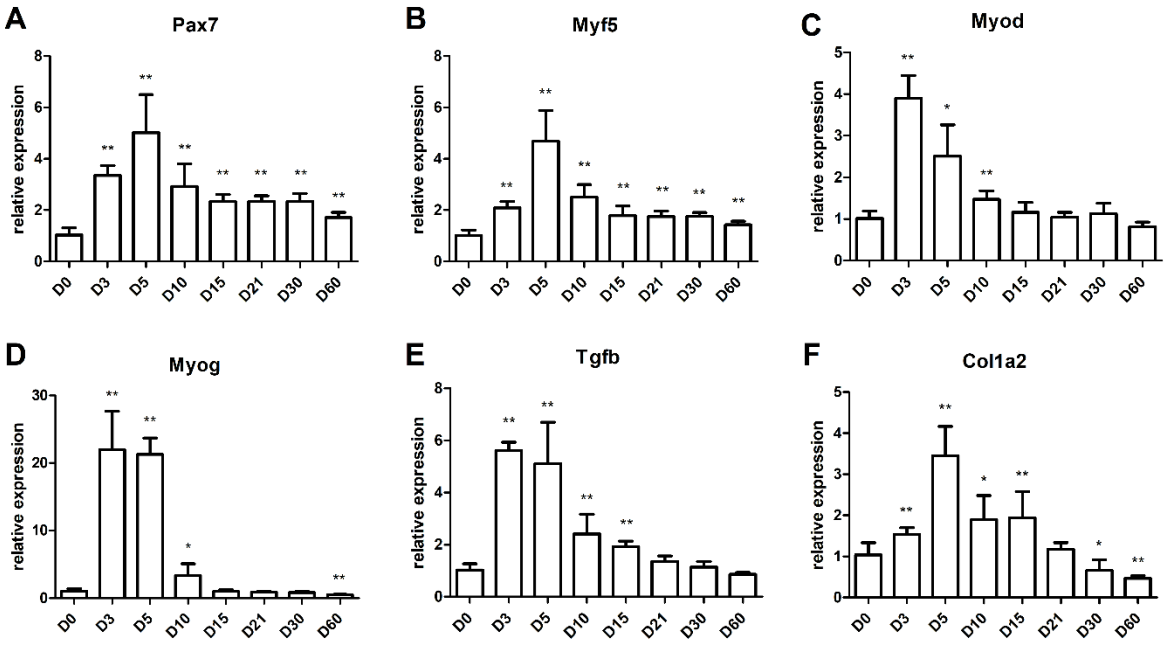

V. Chapter 5 - Muscle regeneration in centronuclear myopathy

Satellite cells deficiency and defective regeneration in DNM2 related centronuclear myopathy

Camila F. Almeida[1], Marc Bitoun[2], Mariz Vainzof[1]

[1] Laboratory of Muscle Proteins and Comparative Histopathology, Human Genome and Stem Cell Research Center, Biosciences Institute, University of São Paulo, São Paulo, Brazil

[2]Sorbonne Université, INSERM, Institute of Myology, Centre of Research in Myology, UMRS 974, F-75013, Paris, France

Corresponding author:

Dr. Mariz Vainzof

Human Genome and Stem Cell Research Center, IBUSP

Rua do Matão, 106 – Cidade Universitária

São Paulo, SP - CEP 05508-900. Brazil

PHONE: +55 11 3091-7736

FAX: +55 11 3091-0852

e-mail: mvainzof@usp.br

Resumo

As miopatias centronucleares são doenças musculares raras que têm como sinal clínico comum a fraqueza muscular e núcleos centrais na histopatologia do músculo. Mutações em vários genes têm sido associadas com formas de herança autossômica e ligada ao X. Mutações no gene da dinamina 2 são a causa genética da forma autossômica dominante (AD-CNM), caracterizada por um amplo espectro clínico, variando desde formas graves neonatais a formas moderadas em adultos.

A dinamina 2 é uma proteína expressa ubiquamente e está envolvida em muitas funções relacionadas ao tráfego e remodelamento de membranas e à dinâmica do citoesqueleto. Até o presente, algumas hipóteses e mecanismos foram propostos para explicar esta doença, porém, o impacto músculo-específico das mutações ainda necessita ser melhor explorado.

As células-satélite são a principal fonte para o crescimento muscular após o nascimento e a regeneração no músculo adulto. Neste trabalho, nós investigamos estas células no camundongo *knock-in* modelo para a AD-CNM que carrega a mutação mais comum, o KI-*Dnm2*$^{R465W/+}$. Nós encontramos uma contagem reduzida de células-satélite no músculo gastrocnêmio e uma regeneração muscular menos eficiente após a lesão induzida por duas metodologias diferentes. Nossos dados proveem evidências de que o número e a função destas células estão alterados e isto pode contribuir para o desenvolvimento da doença.

Abstract

Centronuclear myopathies are rare muscle diseases that share muscle weakness as the main clinical feature and central nuclei at muscle histopathology. Mutations in several genes have been associated with X-linked and autosomal forms. Mutations in dynamin 2 gene were found to be the genetic cause of the autosomal dominant form (AD-CNM), characterized by a wide clinical spectrum, ranging from severe neonatal to milder adult forms.

Dynamin 2 is a ubiquitously expressed protein, involved in many functions related to trafficking and remodeling of membranes and cytoskeleton dynamics. To date, several hypotheses and mechanisms have been proposed to explain the disease, but the muscle-specific impact of the mutations still needs to be further investigated.

Satellite cells are the main source for muscle growth after birth and during regeneration in adult tissue. Here, we investigated these cells in the knock-in mouse model for AD-CNM bearing the most common mutation, the KI-*Dnm2*$^{R465W/+}$. We found a lower counting of satellite cells in the gastrocnemius muscle and defective muscle regeneration after induced injury by two different methodologies. Our data provide evidence that the number and function of these cells are altered and this may contribute to the disease development.

Introduction

Centronuclear myopathies (CNM) form a group of rare congenital myopathies, clinically and genetically heterogeneous, characterized mainly by muscle weakness. Clinical signals vary from severe hypotonia in newborns to moderate and mild muscle weakness in patients with early-adulthood onset. The main histological feature is a high incidence of centrally positioned nuclei (ROMERO; BITOUN, 2011).

Mutations in several genes have been identified as the cause of autosomal dominant, autosomal recessive and X-linked forms of inheritance, but mutations in *MTM1, BIN1,* and *DNM2* genes represent most of the reported cases (BITOUN et al., 2005; LAPORTE et al., 1996; NICOT et al., 2007).

The autosomal dominant centronuclear myopathy (AD-CNM) is due to mutations in the dynamin 2 gene (*DNM2*) (BITOUN et al., 2005), which lead to a wide clinical spectrum. Neonatal cases are characterized by severe hypotonia, generalized weakness, facial weakness with open mouth, ptosis, and ophthalmoplegia (BITOUN et al., 2007). Late-childhood or adult-onset patients present delayed motor milestones, diffuse muscle weakness mainly affecting limbs and face, accompanied by ptosis and ophthalmoplegia (FISCHER et al., 2006; HANISCH et al., 2011). In the majority of cases, the disease progresses slowly, with normal cardiac and respiratory functions (FISCHER et al., 2006). Histologically, there is predominance and atrophy of type I fibers, centralized nuclei and radiating sarcoplasmic strands (SEWRY; WALLGREN-PETTERSSON, 2017).

More than 20 different mutations in *DNM2* have been found as causative of AD-CNM (BÖHM et al., 2012), and some specific mutations are associated to Charcot-Marie-Tooth neuropathy (SIDIROPOULOS et al., 2012) and hereditary spastic paraplegia (SAMBUUGHIN et al., 2015). Dynamin 2 belongs to the family of large GTPases (OBAR et al., 1990) that participates in various membrane-remodeling processes throughout the cell and trafficking events, including clathrin-independent and dependent endocytosis, intracellular membrane trafficking, microtubules and actin networks dynamics (DURIEUX et al., 2010a; FERGUSON; DE CAMILLI, 2012). In membrane trafficking events, DNM2 oligomers form a helical structure around the neck of the nascent vesicle and GTP hydrolysis leads to vesicle release in the cytoplasm (WARNOCK; BABA; SCHMID, 1997).

DNM2 is ubiquitously expressed, however, to date there is no satisfying explanation for the muscle-specific impact of mutations. Dynamin 2 mRNA and protein expression are both normal in patients (BITOUN et al., 2005, 2009), while protein localization may be altered, with cytosolic accumulation in DNM2 mutant models (DURIEUX et al., 2010b; KENNISTON; LEMMON, 2010). On one hand, this points to a dominant-negative effect of the heterozygous mutations, resulting in loss of function. On the other hand, as several DNM2 mutations increase oligomer stability and GTPase activity (KENNISTON; LEMMON, 2010; WANG et al., 2010), this would imply in a gain of function mechanism.

The most frequent mutation p.R465W in the DNM2 gene, found in 30% of patients, was used to develop the knock-in mouse model KI-*Dnm2*$^{R465W/+}$. This model develops a phenotype similar to human patients, characterized by a progressive myopathy with impairment of contractile properties, muscle atrophy, and structural disorganization. Moreover, histological analysis shows no sign of regeneration, inflammation or fibrosis deposition (DURIEUX et al., 2010b).

A suggestion that regeneration could be impaired in the group of CNM diseases raised from studies in a mouse model of X-linked MTM1 form of CNM that showed alteration in satellite cell quantity and behavior (LAWLOR et al., 2012). Satellite cells (SCs) are known to orchestrate muscle regeneration in adult muscle. Although in particular cases they can retain their regenerative capacity (BOLDRIN; ZAMMIT; MORGAN, 2015), SCs have been emerging as direct players in the mechanisms of many neuromuscular disorders (DUMONT et al., 2015; KUDRYASHOVA; KRAMEROVA; SPENCER, 2012; ROSS et al., 2012). DNM2 shares some functions with MTM1 protein and it has been shown that MTM1 is a negative regulator of DNM2, being both proteins engaged in a common pathway, controlling muscle mass and maximal force (COWLING et al., 2014).

Based on this and on a recent study in which a lower number of satellite cells was found in tibialis anterior muscle from KI-*Dnm2*$^{R465W/+}$ mouse (FONGY et al., 2019), we hypothesized that these cells could also present functional alterations; hence we used KI-*Dnm2*$^{R465W/+}$ mice to study possible dysfunction of the satellite cell population. This study complements the pathomechanisms of AD-CNM, as we show a reduced number of PAX7+ satellite cells and defective regeneration in the KI-*Dnm2*$^{R465W/+}$ mouse model.

Methods

Animals

The KI-*Dnm2*^{R465W} mouse line was established as previously described (DURIEUX et al., 2010b). Animals were housed under controlled light and temperature conditions, with water and food *ad libitum*. Seven or eight heterozygous (HTZ) animals were randomly divided into the groups of electric-induced injury experiments; three animals per group were used for cardiotoxin injection experiment. The wild-type (WT) littermates were used as controls. All animals were males and with three months of age. All procedures were performed under isoflurane anesthesia, according to French guidelines. Animal studies conform to the French laws and regulations concerning the use of animals for research and were approved by an external Ethical committee (approval no. 00351.02 delivered by the French Ministry of Higher Education and Scientific Research).

Muscle injury

To induce muscle degeneration, we used two different techniques. The first one is an electric-induced injury protocol established in our laboratory, which causes damage by electric shock delivered using an electroporation device[1]. Briefly, the hairs from the calves were removed and the electrodes pads were positioned perpendicularly to muscle fibers orientation. The muscles were injured by applying eight electrical pulses at an intensity of 100 Volts, during 20 milliseconds each pulse, separated by a 0.5-second interval (ECM830, Electro Square Porator, Harvard Apparatus). The second injury procedure was done by the classical cardiotoxin injection (GARRY; ANTONY; GARRY, 2016). We injected 150 μL of 10 μM cardiotoxin solution (Cardiotoxin, *Naja pallida*, 217503, Merck) in both gastrocnemius muscles. Animals were euthanized by cervical dislocation three, five, ten and fifteen days post-lesion.

[1] The methodology is described in details in Chapter 4 of this thesis

Histopathology

Gastrocnemius muscles were harvested and immediately frozen in liquid nitrogen-cooled isopentane. The muscles were cut in 6 µm cryosections and stained with hematoxylin-eosin (HE) to evaluate histological alterations and Sirius red to quantify collagen deposit.

Images were captured on a conventional upright microscope (Axio Imager.Z1, Carl Zeiss) and with Axion Vision Software (Carl Zeiss). Quantification of Sirius red staining was done on five different random fields of muscle section, using ImageJ software.

Immunohistochemistry

Muscle cryosections were labeled with primary antibodies including rabbit anti-laminin (1:300; Dako, Z0097), mouse anti-developmental myosin heavy chain (dMyHC) (1:30, Novo Castra, NCL-MHCd) and mouse anti-PAX7 (1:20; Developmental Studies Hybridoma Bank, concentrate), overnight at 4°C. Secondary antibodies were anti-rabbit AlexaFluor® 488 (Invitrogen, A-11008), anti-mouse Cy3 (Sigma Aldrich, C2181) or AlexaFluor® 568 (Invitrogen, A-11004). Secondary antibodies were incubated 1 hour and sections were counterstained with DAPI diluted in mounting medium Vectashield® (Vector Laboratories). The sections were visualized on a Carl Zeiss (LSM800) confocal microscope and images captured with ZenBlue software.

For PAX7 staining, muscle sections were submitted to antigen retrieval with hot citric acid and blocking with mouse IgG Fab fragment (1:100, Jackson Immuno Research). Whole muscle section imaging was performed in Nikon Eclipse Ti2 microscope. Counting of dMyHC+ fibers and PAX7+ nuclei was done manually. The total number of fibers was calculated in a semi-automated fashion, in QuPath software (BANKHEAD et al., 2017). Fiber's diameter was measured on laminin stained sections, using ImageJ software, according to Treat-NMD guidelines (SOP DMD_M.1.2.001).

RNA extraction, cDNA synthesis, and qPCR

Total RNA was extracted using RNeasy Microarray Tissue Mini Kit (Qiagen) following the manufacturer's instructions. Quantity and quality of RNA were assessed with Nanodrop 8000 Spectrophotometer (Thermo Scientific) and agarose gel electrophoresis. To obtain

cDNA, 1 µg of RNA was reverse transcribed using SuperScript VILO Master mix (Invitrogen) according to the manufacturer's instructions.

For qPCR, specific primers were designed for each gene of interest and *Tbp* was used as the endogenous control (Table 1). Amplification was done with SybrGreen Master Mix (Roche). The run was performed in 7500 Applied Biosystems thermocycler. Results were analyzed with 7500 Software v2.0.6. Relative expression of the target genes was calculated as mean values of $2^{-\Delta\Delta CT}$.

Table 2 Sequence of primers. bp: base-pair.

Gene	Forward	Reverse	Amplicon length (bp)
Col1a2	GATGGTCACCCTGGAAAACC	CACGAGCACCCTGTGGTCC	68
Myf5	CTGTCTGGTCCCGAAGAAC	GACGTGATCCGATCCACAATG	130
Myf6	GCAGAGGGCTCTCCTTTGTA	AACGTGTTCCTCTCCACTGC	106
Myod	TACAGTGGCGACTCAGATGC	TAGTAGGCGGTGTCGTAGCC	116
Myog	CTGCACTCCCTTACGTCCAT	CCCAGCCTGACAGACAATCT	103
Pax7	GAGTTCGATTAGCCGAGTGC	GTGTTTGGCTTTCTTCTCGC	100
Spry1	GGTCATAGGTCAGATCGGGTC	CTTGCCACACTGTTCGCAG	120
Tbp	TGCACAGGAGCCAAGAGTGAA	CACATCACAGCTCCCCACCA	132
Tgfb	CCCCACTGATACGCCTGAGT	AGCCCTGTATTCCGTCTCCTT	86

Statistical analysis

Graphs and statistical analysis were done in GraphPad Prism software, version 5.00. Differences between two groups were assessed using tests indicated in figure's captions and data are presented as the mean ± standard deviation (SD) (*$p < 0.05$, **$p < 0.01$, ***$p<0.001$).

Results

PAX7-positive cells number is reduced in KI-Dnm2^{R465W} mice

To investigate the satellite cells in HTZ mice, we first analyzed the expression of *Pax7* mRNA in the gastrocnemius muscle of three-month-old animals, by quantitative real-time PCR. We found a decrease of 70% in *Pax7* expression (p=0.0079) as compared to the wild-type control (Figure 1).

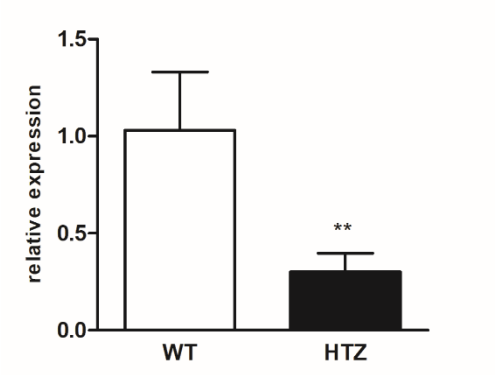

Figure 13 Pax7 mRNA expression in HTZ mice as compared to WT values. Relative expression was calculated by $2^{-\Delta\Delta Ct}$ method using WT values as the normalizer sample. Mann-Whitney test, n=5 individuals per genotype, **p<0.01

Next, we immunostained muscle sections for PAX7 and counted the number of PAX7-positive (PAX7+) nuclei in relation to the total number of fibers. The counting revealed a reduced number of cells positive for PAX7 (Figure 2), demonstrating that reduced *Pax7* expression resulted from the reduction of the satellite cell population in HTZ mice.

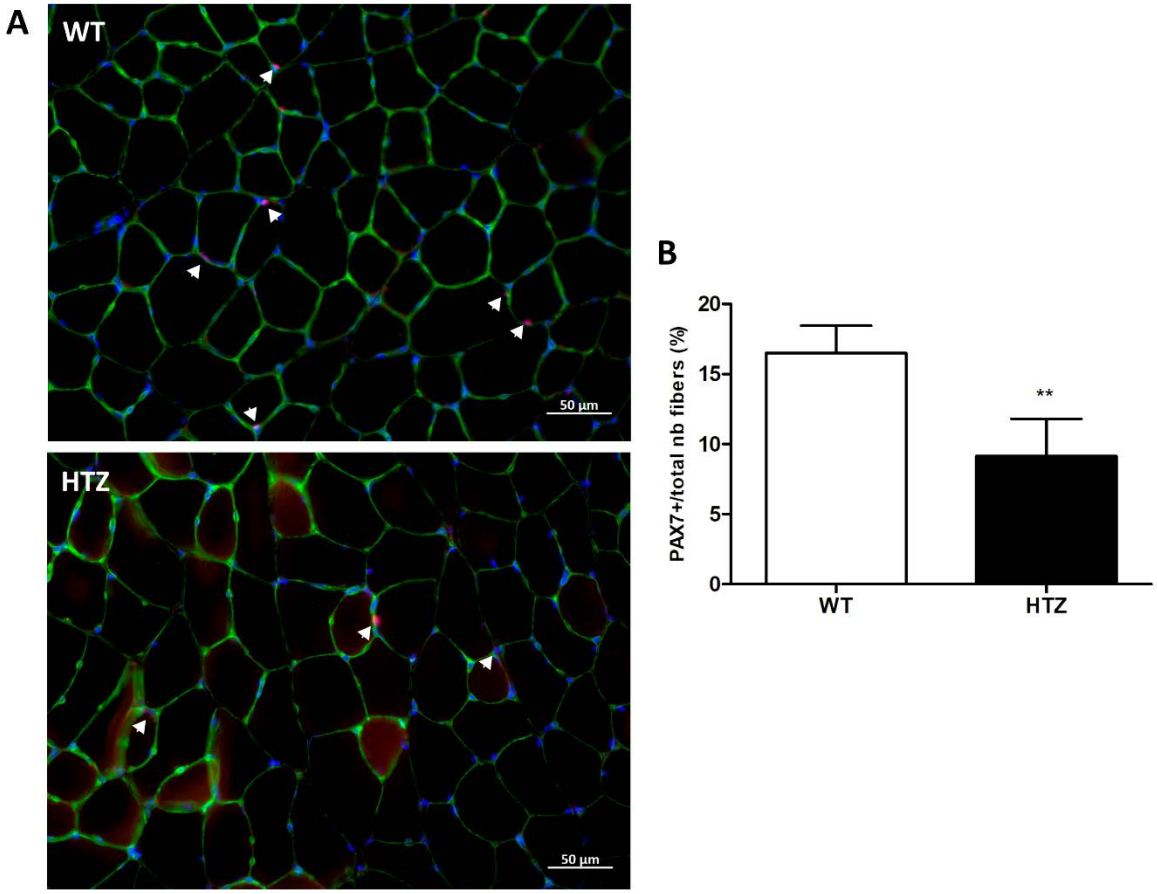

Figure 14 Number of satellite cells in gastrocnemius muscle of HTZ mice in comparison to WT. (A) Representative images of PAX7 staining in WT and HTZ muscle sections. Laminin (green) antibody was used to delimit fiber membrane; PAX7 stain in bright pink/purple indicated by white arrows (B) The number of satellite cells is presented in relation to total fiber number in transverse cross-sections. Mann-Whitney test, n= 6 – 7 transversal sections from 3 animals of each genotype, **p<0.01

Muscle mass of HTZ mice did not recover after acute lesion

To test the impact of the reduced number of satellite cells in the gastrocnemius of HTZ mice, we provoked muscle injury by electric shock (EP) and cardiotoxin (CTX) injection and followed muscle regeneration after three, five, ten and fifteen days. We then measured the absolute mass of gastrocnemius at each time point, and relative mass by total body weight. Uninjured muscles from WT and HTZ showed no significant differences in the gastrocnemius mass (Supplementary Figure 19) or gastrocnemius/body weight ratio (Figure 3A). After EP lesion, gastrocnemius mass of WT animals decreased slightly, with a significant reduction after 5 and 10 days, but it returned to normal levels after 15 days. For HTZ the reduction was substantial and muscle mass did not recover after 15 days (Figure 3A).

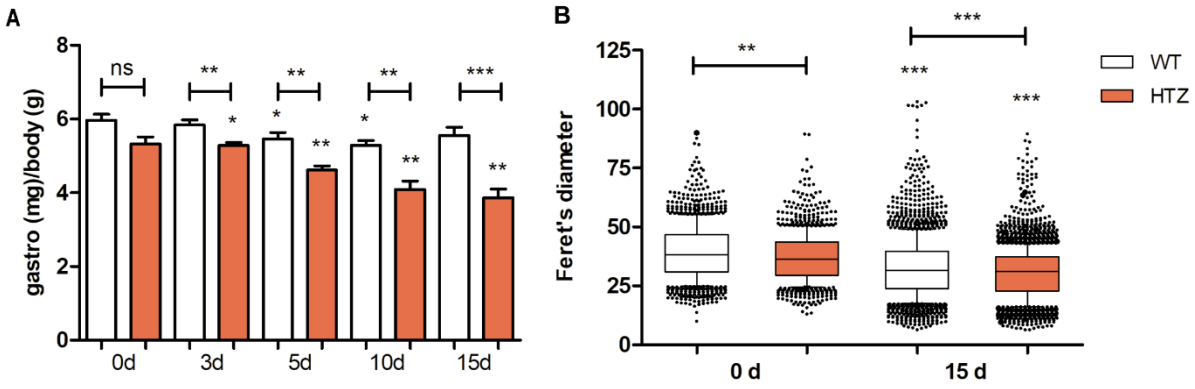

Figure 15 Loss of muscle mass and reduced fiber diameter after EP lesion. (A) gastrocnemius mass relative to total body weight. Mann-Whitney test, n=5 individuals per genotype at time point zero, n=8 individuals per genotype at the other time points; ns=non-significant; *p<0.05, **p<0.01, ***p<0.001 (B) Feret's diameter of myofibers before and after EP injury. Kruskal-Wallis test followed by Dunn's multiple comparison test; n=1278 fibers in WT 0d, n=1152 fibers in HTZ 0d, n=2081 fibers in WT 15d and n=3291 fibers in HTZ 15d; **p<0.01, ***p<0.001.

By measuring the minimal Feret's diameter of fibers, we found that HTZ mice have smaller fibers than WT before EP injury. Fifteen days after injury, WT and HTZ fibers had their diameter reduced compared to the same genotype before lesion, and the mean size is still smaller in HTZ mice (28.9 µm) than the mean of WT (33.2 µm) (Figure 3B). Data from CTX-injured muscles are in Supplementary Figure 18. The fiber density (number of fibers per area) before the injury in HTZ mice is higher than in WT, a reflection of the smaller fiber's size. After lesion, the fiber density in WT increased, while in HTZ it remained equal to uninjured muscle, although lower than WT after 15 days (Figure 4).

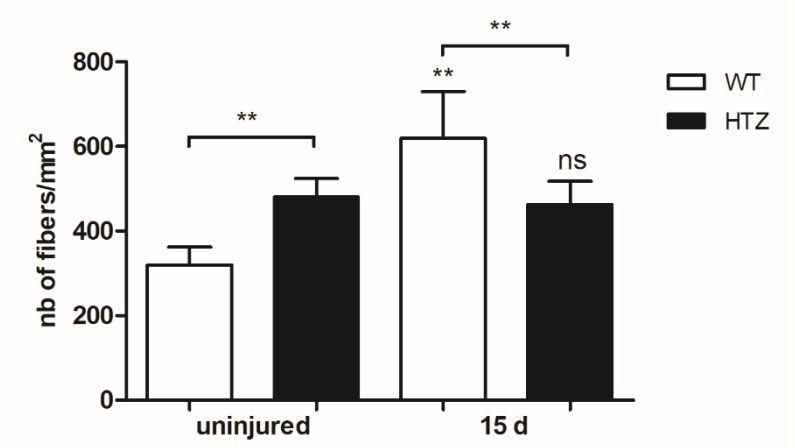

Figure 16 Number of fibers per area. The fiber density in uninjured HTZ muscle is higher than in WT, reflecting their smaller size. After CTX lesion, fiber density in WT muscle increased, while in HTZ it remained the same to uninjured muscle. Mann-Whitney-test, n= 6 – 8 transversal sections from 3 animals of each genotype/time point; ns= non-significant, **p<0.01.

Histopathology following muscle injury

Regardless of the injury method, skeletal muscle regeneration occurred in similar ways, featured by a peak of necrosis, followed by restoration by new fibers formation and tissue remodeling (Figure 5 and Figure 6). Muscles of HTZ animals, three days post-electroporation (EP) injury or cardiotoxin injection (CTX), in HE staining showed fibers in the metabolic stage of necrosis, identified by a pale color, and infiltration of inflammatory cells, invading muscle fibers. WT muscles presented the same features and, in addition, we noted the presence of the first small regenerating fibers. In general, CTX caused a more pronounced degeneration (Figure 6).

After five days, we observed a still ongoing necrotic process, with the presence of many inflammatory cells in muscles from HTZ animals. At this point, we noted the first regenerating fibers. For control muscles, the necrotic process is still present, but to a lesser extent and the proportion of regenerating fibers is notably higher.

Ten days post-injury, HTZ muscles had some remaining necrotic areas and many small regenerating fibers, especially in CTX injury, whilst WT muscles appeared to be in a more advanced stage of regeneration. At 15 days, WT muscles regenerated completely, with central nuclei. HTZ muscles were also regenerated, but the new fibers seemed smaller and central nuclei appeared larger.

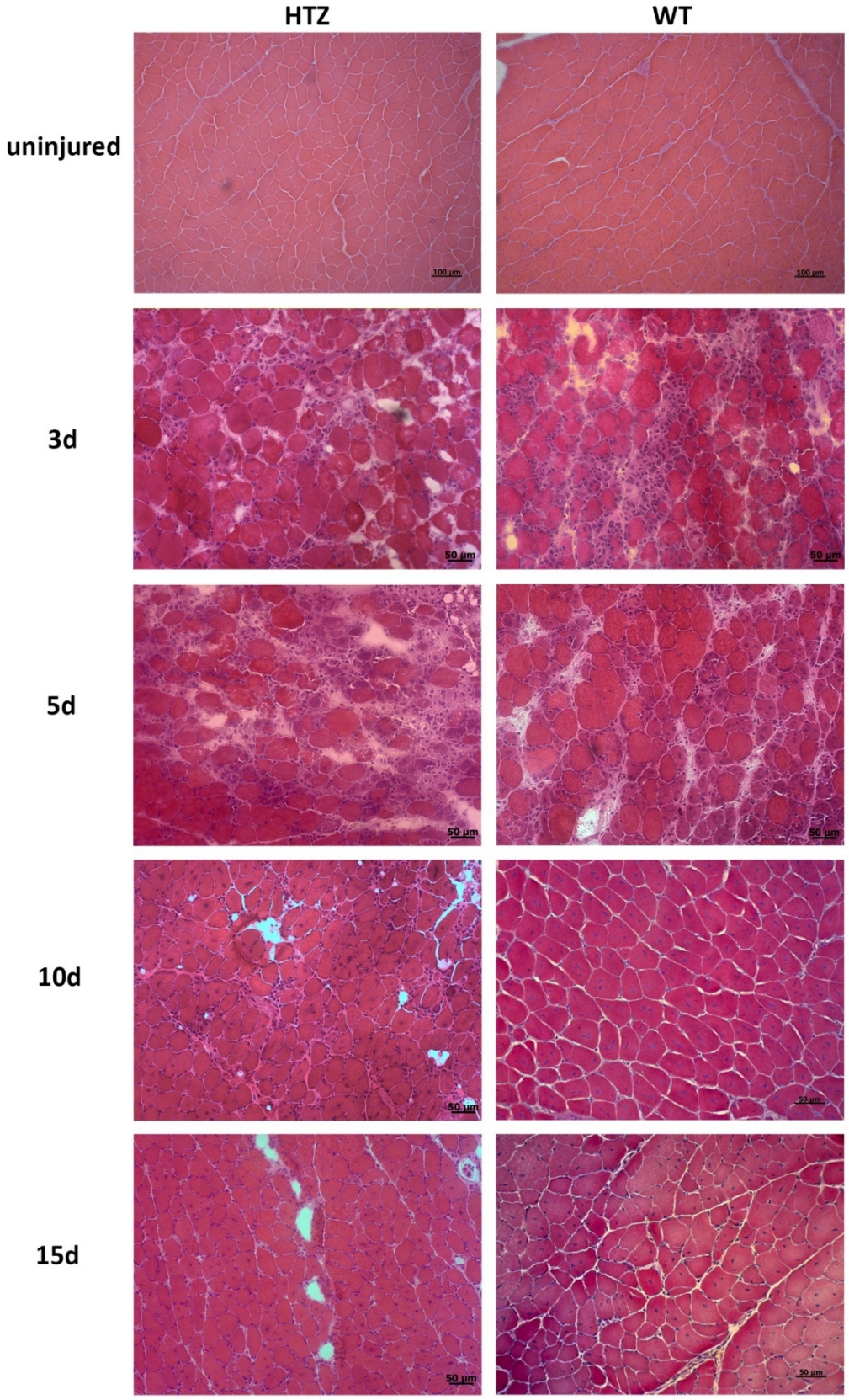

Figure 17 Representative images of HE staining of muscles before and after electroporation-induced injury. Muscle necrosis is identified by pale fibers and infiltration of inflammatory cells. Regenerating fibers are visualized by five days post-lesion. At 15 days, muscle fibers are regenerated and have central nuclei. Scale bars= 100 µm at day 0 (uninjured) and 50 µm for the other time points.

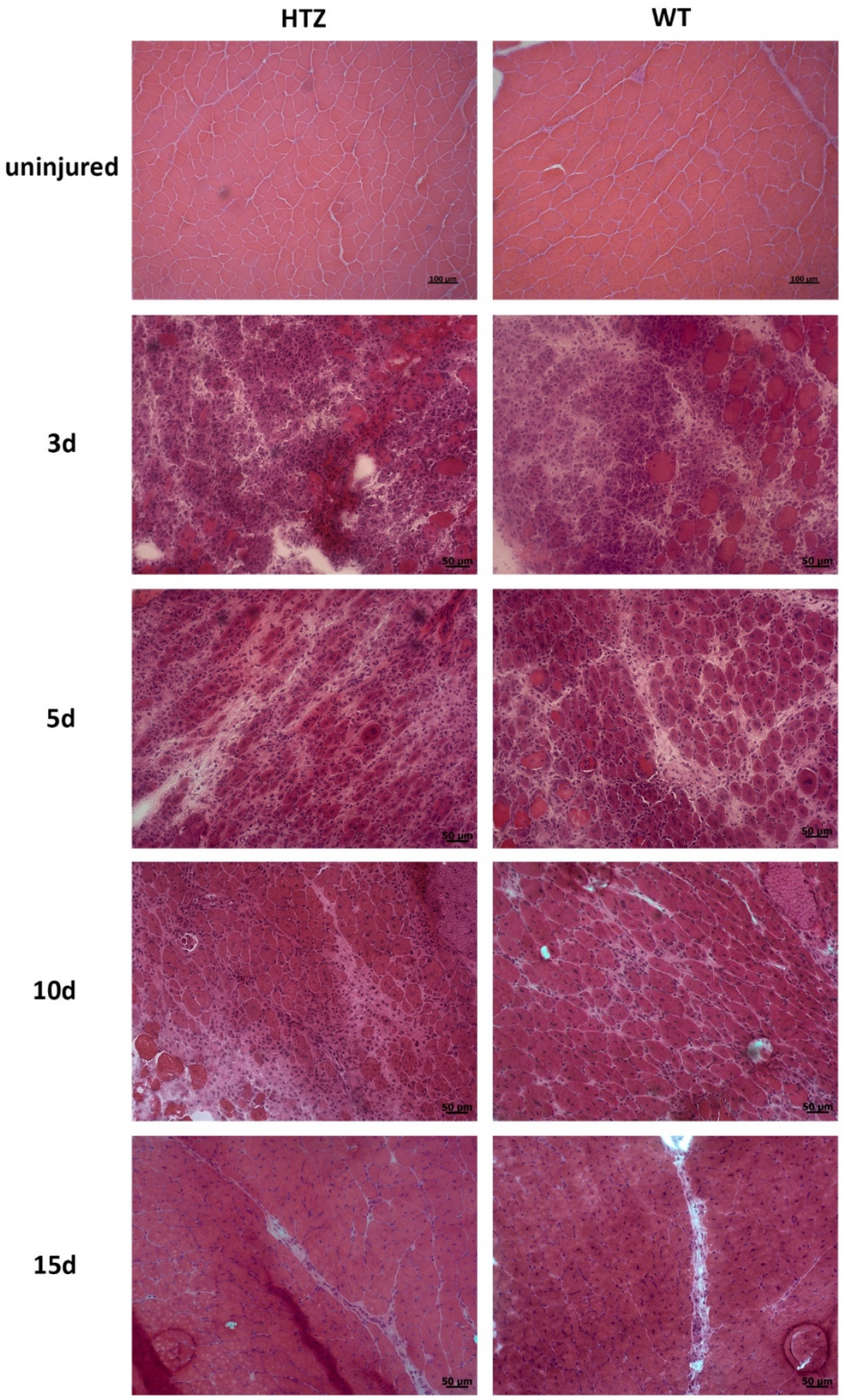

Figure 18 Representative images of HE staining of muscles before and after cardiotoxin injection. Cardiotoxin provoked a pronounced necrosis at three days, remaining few myofibers with preserved architecture. By five days, more regenerating fibers are identified in WT than in HTZ. After 10 days, some infiltrate of inflammatory cells is still observable in HTZ muscle. At 15 days, muscles are regenerated with central nuclei. Scale bars= 100 µm at day 0 (uninjured) and 50 µm for the other time points.

Fibrosis is defined as excessive production of components of the extracellular matrix, as a result of an inefficient regeneration. We assessed deposition of fibrotic tissue after injury with Sirius Red that stains collagens. We observed an increased collagen content in both WT and HTZ muscles fifteen days after EP lesion (Figure 7A), but the gastrocnemius from HTZ mice had a significantly higher increase in the percentage of fibrosis (Figure 7B). We also measured the expression of *Tgfb1*, a profibrotic gene and a collagen gene, *Col1a2* (Figure 7C and D). Both genes were activated by the degeneration process, with HTZ mice showing higher expression of *Tgfb1* at days three and ten (Figure 7C). The relative expression of *Tgfb1* and *Col1a2* in CTX-injured muscles were similar and are shown in Supplementary Figure 26 and Figure 25.

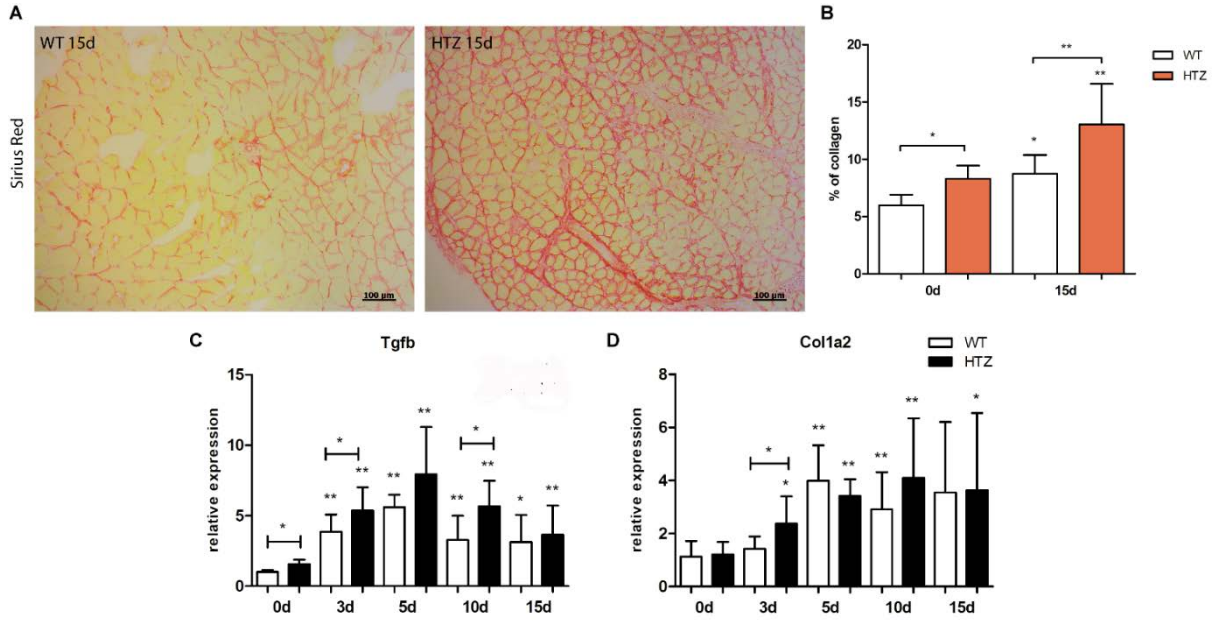

Figure 19 Fibrosis quantification. (A) Representative images of Sirius red staining in WT and HTZ muscles, showing a stronger staining on HTZ. Scale bar= 100 µm. (B) Quantification of Sirius red staining on muscles fifteen days after electroporation. Mann-Whitney test, *p<0.05, **p<0.01, n=5 individuals for day zero, n=8 individuals for day 15. Five different images were taken from random fields per animal. (C) Relative expression of Tgfb1 and (D) Col1a2 mRNA. Mann-Whitney test, *p<0.05, **p<0.01, n=5 individuals per genotype for day zero, n=8 individuals per genotype at the other time points. Relative expression values were calculated by $2^{-\Delta\Delta Ct}$ method using WT values as the normalizer sample.

Formation of new myofibers

We evaluated new fibers formation by the expression of developmental myosin heavy chain (Figure 8). Three days after EP, we observed the first dMyHC-positive fibers in WT, but none in HTZ. Five days post-EP there is the highest proportion of positive fibers in both HTZ and WT mice (Figure 8). At 10 days, no positive fiber was observed in WT muscle, although in HTZ around 5% of fibers were positive (Figure 8 and Figure 9).

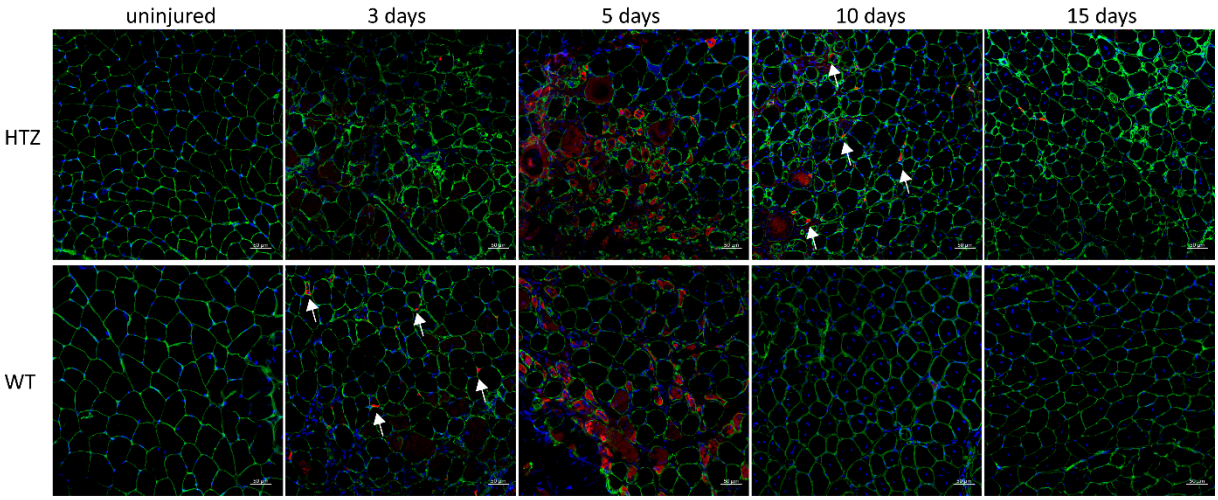

Figure 20 Formation of new myofibers after EP. New myofibers express developmental myosin heavy chain (in red). Membranes were delimited with laminin antibody (in green), nuclei were stained with DAPI (in blue) (representative images). The first dMyHC-positive fibers appeared at three days in WT (white arrows). At 10 days, some dMyHC-positive fibers were still present in HTZ (white arrows) Scale bar= 50 µm.

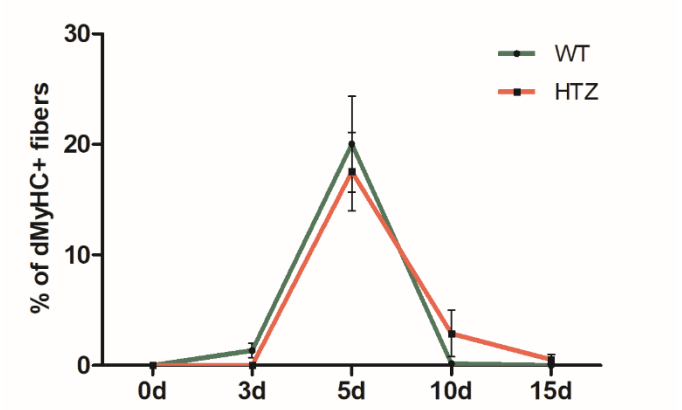

Figure 21 Quantification of dMyHC-positive fibers in relation to total number of fibers after EP lesion. No positive fibers were found before lesion. After three days, the first dMyHC-positive fibers appeared in WT. For both genotypes, the peak of positive fibers was at five days, declining at 10 days and returning to zero after 15 days. HTZ presented around 5% of positive fibers at day 10. N=5 individuals per genotype at time point zero, n=8 individuals per genotype after lesion. Five to seven random fields were counted per animal.

Muscles injected with cardiotoxin degenerated more intensely and elicited a strongest regenerative response. CTX treatment induced more pronounced differences between HTZ

and WT mice (Figure 10). At three days post-CTX, we found about 25% of dMyHC+ fibers in WT muscles, whilst HTZ presented less than 1%. At five days, both genotypes reached their highest percentage of dMyHC+ fibers (about 70% for WT), but again, for HTZ muscles, this percentage was considerably lower, around 30%. After 10 days, all WT fibers lost dMyHC expression, while 5% of HTZ fibers showed positive staining (Figure 11).

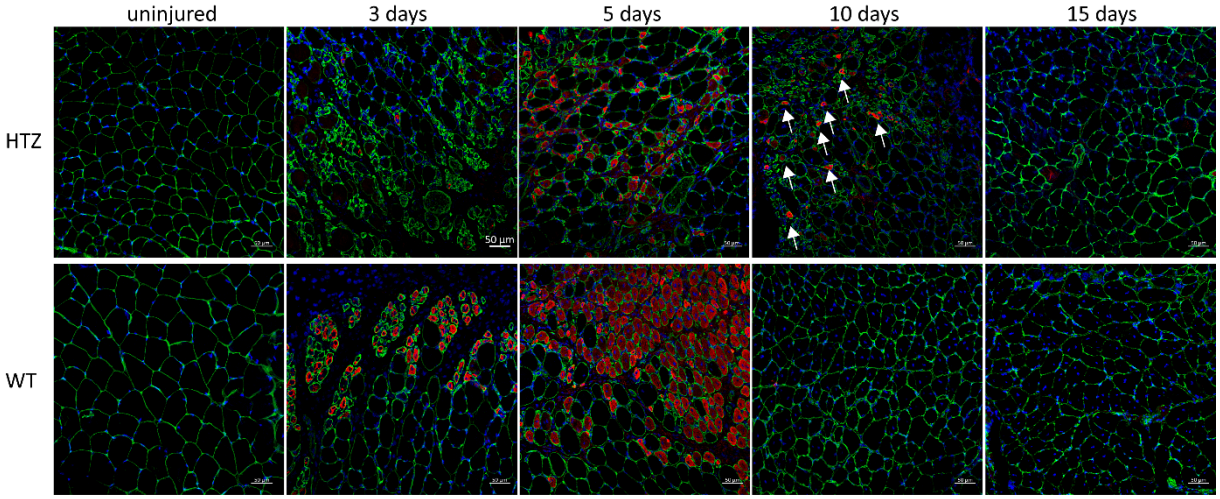

Figure 22 Formation of new myofibers after CTX injection. New myofibers express developmental myosin heavy chain (in red). Membranes were delimited with laminin antibody (in green), nuclei were stained with DAPI (in blue) (representative images). After three days, many fibers were dMyHC-positive in WT, while in HTZ no positive fibers were detected. At five days, we found the highest number of dMyHC-positive fibers. At 10 days, some dMyHC-positive fibers were still present in HTZ (white arrows), while none was present in WT. Scale bar= 50 µm.

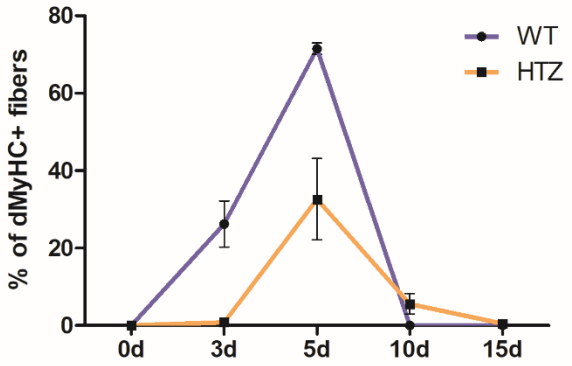

Figure 23 Quantification of dMyHC-positive fibers in relation to total number of fibers after CTX lesion. No positive fibers were found before lesion. After three days, an important quantity of dMyHC-positive fibers was already present in WT. For both genotypes, the peak of positive fibers was at five days, but at a lower proportion in HTZ. Following, there is a decline at 10 days and returning to zero after 15 days. HTZ presented around 5% of positive fibers at day 10. N=5 individuals per genotype at time point zero, n=3 individuals per genotype after lesion. Five to seven random fields were counted per animal.

Gene expression of myogenic regulatory factors

In view of the satellite cell deficiency in HTZ mice, we analyzed the activation of genes related to the regeneration pathway by measuring their expression before and after lesion. We studied the myogenic regulatory factors (MRFs) and genes important to satellite cell regulation.

In addition to *Pax7* expression in uninjured muscles, we also quantified its expression after lesion, to obtain an indirect measurement of satellite cell population dynamics during regeneration. *Pax7* expression raised significantly after lesion by both methods in WT muscles (Figure 12 and Supplementary Figure 23), peaking at 5 days and reducing at 10 days. After 15 days, although muscles seemed fully regenerated and no dMyHC+ fibers were detected, *Pax7* expression was still significantly increased as compared to uninjured muscles.

In HTZ mice, *Pax7* also activated after injury (Figure 12), at significant levels after 5, 10 and 15 days, when compared uninjured HTZ muscles, but at lower levels when compared to WT uninjured (Figure 12). Thus, *Pax7* expression was substantially reduced in HTZ during all the course of regeneration, as compared to WT at the same time point.

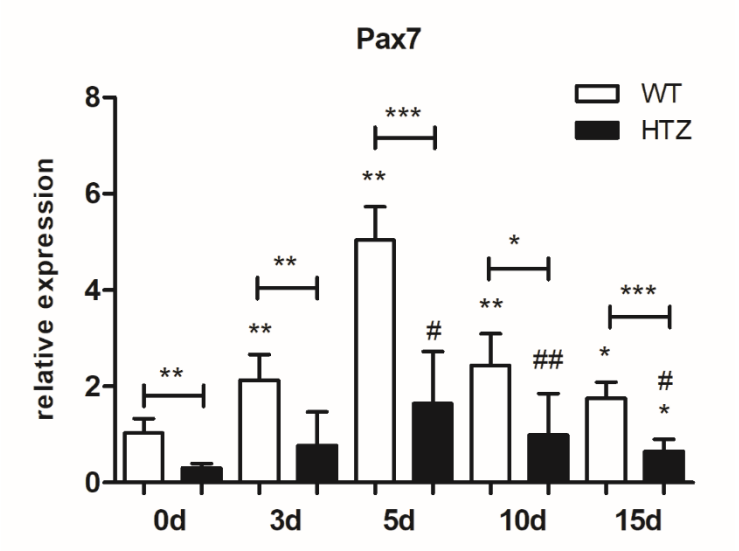

Figure 24 Relative expression of Pax7 mRNA measured by qRT-PCR after electroporation injury and calculated by $2^{-\Delta\Delta Ct}$ method. Relative expression values normalized to WT uninjured, showing that the activation of Pax7 occurs at lower levels in HTZ. Mann-Whitney test, n=5 individuals per genotype at time point zero, n=8 individuals per genotype after lesion. Asterisks (*) denote differences in relation to WT uninjured, number sign (#) in relation to HTZ uninjured. * and # p<0.05, ** and ## p<0.01, *** p<0.001.

As *Pax7*, the relative expression of *Myf5* is lower in HTZ mice in the uninjured muscle (Figure 14). Unlike WT, *Myf5* is not significantly activated after lesion in HTZ and its expression is significantly lower compared to injured WT muscles after 3, 5, 10 and 15 days post-injury by EP (Figure 14) and CTX (Supplementary Figure 24).

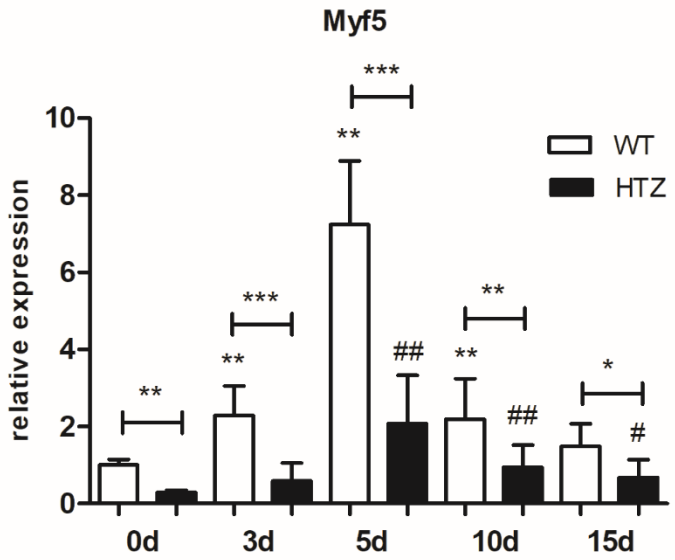

Figure 25 Myf5 expression during regeneration. Relative expression of Myf5 mRNA measured by qRT-PCR after electroporation injury and calculated by $2^{-\Delta\Delta Ct}$ method. Relative expression values normalized to WT uninjured, showing that in HTZ Myf5 expression is lower before and during regeneration. Mann-Whitney test, n=5 individuals per genotype at time point zero, n=8 individuals per genotype after lesion. Asterisks (*) denote differences in relation to WT uninjured, number sign (#) in relation to HTZ uninjured. * and # p<0.05, ** and ## p<0.01, *** p<0.001.

Myod was similarly expressed in WT and HTZ mice in uninjured tissue (Figure 15). Nevertheless, its expression is only slightly increased in HTZ after EP lesion regarding the expression measured in WT, which increased after EP and CTX lesions (Figure 15; Supplementary Figure 25). In general, relative expression values were higher in the CTX experiment (Supplementary Figure 25).

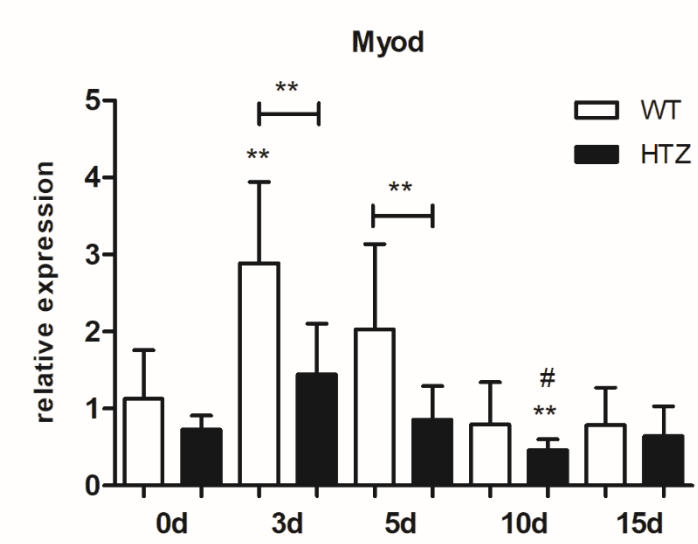

Figure 26 Relative expression of Myod mRNA measured by qRT-PCR after electroporation injury and calculated by $2^{-\Delta\Delta Ct}$ method. Relative expression values normalized to WT uninjured, showing that in HTZ Myod expression is lower than in WT at days three and five. Mann-Whitney test, n=5 individuals per genotype at time point zero, n=8 individuals per genotype after lesion. Asterisks (*) denote differences in relation to WT uninjured, number sign (#) in relation to HTZ uninjured. * and # p<0.05, ** p<0.01.

We also assessed the expression of *Myog*, which is important for myofiber maturation. As expected, *Myog* expression is increased after injury, peaking at five days, in both mutant and normal mice. Interestingly, *Myog* has an increased expression in non-injured HTZ mice, however, after injury, the activation of myogenin expression is less pronounced than in normal muscles (Figure 16A; Supplementary Figure 25). Here, we also detected a stronger response of CTX-injured than EP-injured muscles and sustained expression of *Myog* until the fifteenth day (Supplementary Figure 25).

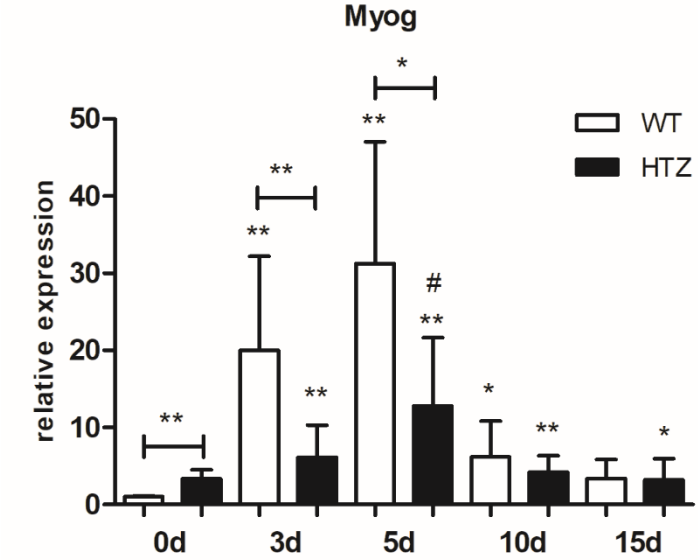

Figure 27 Relative expression of Myog mRNA measured by qRT-PCR after electroporation injury and calculated by $2^{-\Delta\Delta Ct}$ method. Relative expression values normalized to WT uninjured, showing that in HTZ Myog expression is higher in uninjured muscle, the activated after lesion, but lower than in WT at days three and five. Mann-Whitney test, n=5 individuals per genotype at time point zero, n=8 individuals per genotype after lesion. Asterisks (*) denote differences in relation to WT uninjured, number sign (#) in relation to HTZ uninjured. * and # p<0.05, ** p<0.01.

Next, we measured the expression of *Myf6* that is important for muscle maturation during development. We detected a similarly reduced expression of *Myf6* after injury in HTZ and WT (Figure 17). The values obtained from CTX-injured muscles followed the same tendency (Supplementary Figure 26).

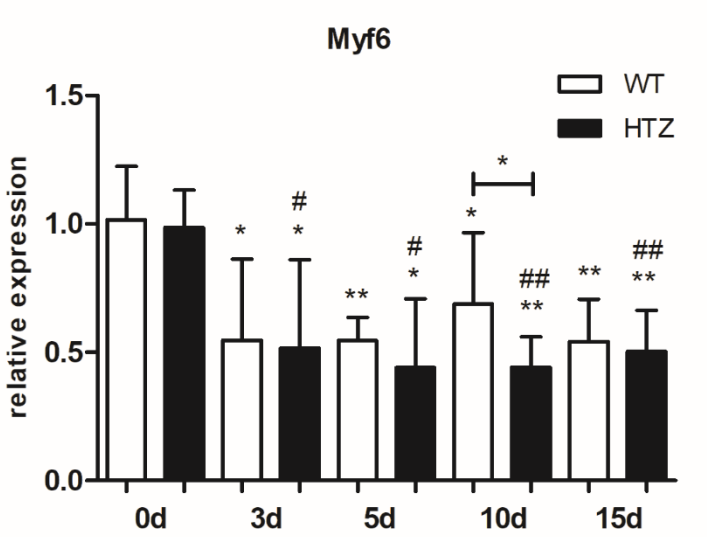

Figure 28 Relative expression of Myf6 mRNA measured by qRT-PCR after electroporation injury and calculated by $2^{-\Delta\Delta Ct}$ method. Relative expression values normalized to WT uninjured, showing that after lesion there is a downregulation of Myf6 in both genotypes. Mann-Whitney test, n=5 individuals per genotype at time point zero, n=8 individuals per genotype after lesion. Asterisks (*) denote differences in relation to WT uninjured, number sign (#) in relation to HTZ uninjured. * and # $p<0.05$, ** and ## $p<0.01$.

Finally, we verified the expression of a gene important for the return of satellite cells to quiescence after regeneration, *Spry1*. HTZ mice presented a higher expression of *Spry1* before EP lesion (Figure 18). As expected, *Spry1* expression was reduced three days after lesion in WT muscle and a subsequent increase occurred as the regeneration proceeded to reach higher values than in uninjured muscles after 10 and 15 days. The same occurred with the HTZ mouse. A similar time course was measured after CTX treatment leading to more pronounced differences between WT and HTZ muscles (Supplementary Figure 28).

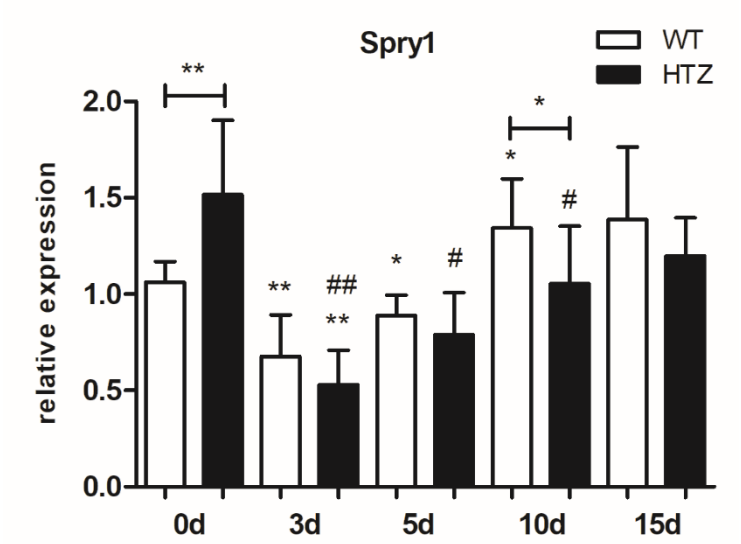

Figure 29 Relative expression of Spry1 mRNA measured by qRT-PCR after electroporation injury and calculated by $2^{-\Delta\Delta Ct}$ method. Relative expression values normalized to WT uninjured, showing that in HTZ Spry1 expression is higher in uninjured muscle. After lesion, it is reduced and progressively increase as the muscle regenerates. Mann-Whitney test, n=5 individuals per genotype at time point zero, n=8 individuals per genotype after lesion. Asterisks (*) denote differences in relation to WT uninjured, number sign (#) in relation to HTZ uninjured. * and # $p<0.05$, ** and ## $p<0.01$.

Discussion

Skeletal muscle has a remarkable regenerative capacity that relies mainly on the muscle-specific stem cells called satellite cells. In this work, we sought to investigate whether these cells have their properties affected by a mutation in dynamin 2. First, we found a significantly lower number of SC in the gastrocnemius muscle of KI-*Dnm2*^{R465W} mouse, verified by *Pax7* mRNA expression and *in situ* quantification of Pax7+ cells in muscle. In addition, we identified a defective regeneration, evidenced by a lower level of regenerating fibers, altered expression of genes related to the myogenic program, loss of mass of regenerated muscle in mutant mice and consequent higher collagen deposition.

Pax7-positive cells number is reduced in KI-Dnm2^{R465W} mice

To date, dynamin 2 has been found engaged in a series of different functions, mainly related to membrane trafficking and cytoskeleton dynamics. This functional diversity reflects in the complexity of the physiopathology seen in autosomal-dominant centronuclear myopathy. The knock-in mouse model KI-*Dnm2*^{R465W} (HTZ) has helped to reveal many mechanisms behind AD-CNM. This mouse presents an impairment of contractile properties and develops atrophy. Studies published in the last nine years have found consistent evidence to explain, at least in parts, this phenotype. HTZ mice present an impaired actin-dependent

trafficking (GONZÁLEZ-JAMETT et al., 2017), alterations in calcium homeostasis (FRAYSSE; GUICHENEY; BITOUN, 2016), perturbation of excitation-contraction coupling (KUTCHUKIAN et al., 2017) and desmin network disorganization (FRANCK et al., 2019), which can explain the contractile properties alterations. Atrophy may develop as a result of the impairment of autophagy and the recent finding of a lower number and altered distribution of nuclei (FONGY et al., 2019).

Satellite cells are the principal source of cells for muscle post-natal growth and regeneration. Impairment in satellite cell population has been documented in various neuromuscular disorders as an important component of disease development (BLAU; WEBSTER; PAVLATH, 1983; CASTETS et al., 2011; KUDRYASHOVA; KRAMEROVA; SPENCER, 2012; ROSS et al., 2012). In the group of centronuclear myopathies, a reduced number and delayed proliferation of satellite cells were identified in the X-linked form (LAWLOR et al., 2012). Here, we found that HTZ mice have a 70% reduction in *Pax7* expression and also a reduced number of PAX7+ nuclei as evidenced by *in situ* counting. PAX7 is the major regulator of satellite cell activity, being essential for muscle development and regeneration (SEALE et al., 2000). During muscle development and regeneration, both cells that will form the satellite cell pool or commit with the muscular program express *Pax7* (OLGUIN; OLWIN, 2004). The growth of muscle after birth has been long believed to occur through the expansion of the cross-sectional area, with the accretion of myonuclei just in the first weeks, ceasing by the weaning (WHITE et al., 2010). In contrast, there are data that point to the contribution of satellite cells for muscle growth and maintenance during different life stages (CHAKKALAKAL et al., 2014; SCHULTZ, 1996), even in aging (KEEFE et al., 2015). Recently, the contribution of Pax7+ cells to muscle growth was proved to be essential during the puberty phase in mice (BACHMAN et al., 2018). Thus, the reduced satellite cell population in HTZ mice can compromise muscle growth and maintenance, as well as muscle regeneration.

Muscle mass of HTZ mice did not recover after acute lesion

Different protocols of muscle injury are available that can be grouped according to the agent employed: physical, chemical or toxins. Despite all these methods being able to provoke an acute muscle degeneration followed by regeneration, they are not completely identical and it is documented important differences among them (HARDY et al., 2016) which can mask or

unveil important data, as shown in an investigation of the regeneration in *Myf5*-null mice, in which a specific role of *Myf5* was only revealed by the freeze-injury method (GAYRAUD-MOREL et al., 2007).

Since HTZ mice do not experience cycles of degeneration and regeneration as part of its pathology, we sought to examine the behavior of satellite cells during regenerative myogenesis after acute injury provoked by electroporation and cardiotoxin injection.

By measuring the mass of gastrocnemius post-lesion, we found that while WT mice are able to recover muscle mass loss after lesion, in HTZ mice the mass of gastrocnemius did not return to its normal after 15 days. This is also evidenced by fiber's diameter, as HTZ fibers presented a smaller size. These data show that in HTZ mice the regeneration is less efficient or delayed compared to WT mice, as a consequence of the reduced satellite cell population.

Histopathology following muscle injury

In the morphological analysis after injury, we noted that HTZ muscle underwent an intense degeneration, evidenced by abnormal tissue architecture, pale fibers and infiltration of mononuclear cells at day three. At day five, new fibers started to be formed and by day 15 the muscle seemed completely regenerated. However, by comparing each time point of HTZ muscle with WT muscle, we could detect some differences that suggest a slower regeneration response in HTZ animals. After 5 days, HTZ muscles have more mononuclear cells infiltrates, while in WT muscles we observed a predominance of new fibers over inflammation. At day 10, WT muscles are visually completed regenerated, but in HTZ muscles there are still areas with mononuclear cells. These observations apply for both injury methods, but the differences are more striking in cardiotoxin-injected muscles.

To confirm whether the HTZ muscles were less efficient to regenerate, we assessed the fibrosis deposition as an indicative of regenerative success. TGF-β1 is known as a profibrogenic factor (DELANEY et al., 2017), controlling the synthesis, remodeling, and degradation of extracellular matrix and it attracts fibroblasts to the site of injury, which promotes the synthesis of extracellular matrix proteins (IHN, 2002). TGF-β1 has also a role in the attraction of inflammatory cells to injured tissues (WAHL et al., 1992). The expression of *Tgfb1* and *Col1a2* genes were equally activated in normal and mutant tissue. Nevertheless,

we found a higher increase in collagen deposits in HTZ muscles, confirming that, although the regeneration was properly activated, it occurred less efficiently and part of the tissue had to be replaced by fibrotic tissue.

Formation of new myofibers

New muscle fibers expressed developmental myosin heavy chain. In EP-injured muscles, we detected the emerging of the first dMyHC+ fibers at day three only in WT muscle, but the persistence of positive fibers in HTZ muscle at day ten, when WT showed none positive fiber. In CTX-injured the same was observed, but with more pronounced differences. HTZ muscles showed a remarkable smaller percentage of dMyHC+ fibers than WT. Moreover, the number of the first positive fibers appearing three days after the lesion in WT animals is higher, while in HTZ, they aroused only at five days and a small percentage persisted at day ten, indicating a delayed regeneration.

After 15 days, WT muscle showed an increased fiber density, suggesting hyperplasia, while in the HTZ, the fiber density remained equal to uninjured muscle, evidencing also a less efficient regeneration.

Gene expression of myogenic regulatory factors

Several mutant mice for MRFs have been developed to decipher the role of each of these genes for muscle development and enabled the discovery of their role for muscle formation. However, as the studies are more focused on development, how these genes work for muscle homeostasis and regeneration in adult tissue is still not completely understood. Thus, studies of mutant mice during adult regeneration is worthwhile, not only to give insights into healthy muscle biology but also in the context of muscle diseases, in which satellite cells have been demonstrated as important players.

PAX7 is the major marker of satellite cells (SEALE et al., 2000) and efficient muscle regeneration relies on PAX7+ cells (SAMBASIVAN et al., 2011; VON MALTZAHN et al., 2013). The genetic ablation of *Pax7* in adult satellite cells leads to a loss of these cells and failure to regenerate (GÜNTHER et al., 2013). This loss of SCs is a consequence of a defective proliferation and inhibition of myogenesis, processes under the control of *Pax7* (OUSTANINA; HAUSE; BRAUN, 2004) by the coordination of the expression of genes related to cell

proliferation and repression of genes of terminal muscle differentiation (SOLEIMANI et al., 2012).

Pax7 expression is detected in proliferating cell and even in cells that will differentiate, marked by *Myod* expression; it is downregulated only for terminal differentiation occur (ZAMMIT, 2006). Accordingly, in our experiments, we saw upregulation of *Pax7* after injury (Figure 11). In HTZ, when we normalized expression levels to HTZ uninjured muscles, we detect an increment in *Pax7* expression, showing that the remaining SCs are still functional; however, we compared to WT uninjured muscles, actually they showed a less pronounced expression, suggesting that there is no mechanism to compensate the initial small number of cells that could be overcome by a higher proliferative rate.

Spry1 is an important regulator of myoblast quiescence, especially for the return to quiescence after activation and proliferation for damage repair (SHEA et al., 2010). Therefore, the increased expression of *Spry1* could impose a constraint to maintain quiescence, delaying SC activation in the presence of the mutation.

Reduced expression of *Myf5* in uninjured HTZ mice is also consistent with a reduced number of satellite cells, as *Myf5* is also present in most part of quiescent satellite cells (BEAUCHAMP et al., 2000) and its expression is directly regulated by *Pax7* (MCKINNELL et al., 2008). This reduced expression of *Myf5* can also be interpreted as a reduction in the number of cells primed to the myogenic program, since *Myf5* is the earliest marker of skeletal muscle program (SASSOON et al., 1989) and one of the first genes readily transcribed upon activation (CRIST; MONTARRAS; BUCKINGHAM, 2012). Moreover, *Myf5* expression in SCs is crucial to muscle regeneration (GAYRAUD-MOREL et al., 2007; USTANINA et al., 2007), as it regulates myogenic commitment (KUANG et al., 2007). Likewise *Pax7*, *Myf5* is also induced upon injury, but once again, at lower levels in HTZ mice, indicating that fewer cells are being produced for muscle repair. In a normal situation, despite not being translated, SCs maintain high levels of *Myf5* transcription. This is advantageous because once activated, the cells can promptly translate large amounts of MYF5 protein (CRIST; MONTARRAS; BUCKINGHAM, 2012). Consequently, in this scenario, HTZ SCs are also in a disadvantage, as we detected only 30% of the *Myf5* expression seen in WT mice.

Myod is important for the determination of muscle fate. Quiescent cells do not express *Myod* but activated proliferating myoblasts express it (BENTZINGER; WANG; RUDNICKI, 2012). We observed the peak of *Myod* expression three days after lesion, indicating that the majority of the cells primed to repair the lesion were already produced at this time point. Correspondingly, this precedes the peak of dMyHC+ fibers that was observed at five days. However, in HTZ mice the activation of *Myod* was also at lower levels than in WT mice, reinforcing that their SCs are giving rising to fewer myoblasts.

Myog and *Myf6* (or *Mrf4*) participate more directly in the myotube differentiation, leading to the expression of proteins specific of mature muscle during development (BUCKINGHAM, 1994; HASTY et al., 1993; VENUTI et al., 1995). In opposition, recent work found that myogenin is not indispensable for muscle terminal maturation, at least in zebrafish, but essential for fusion (GANASSI et al., 2018). With the injury, *Myog* was dramatically upregulated three days after, but in HTZ at much lower levels, emphasizing the delayed regeneration and less new myofibers at five days.

Myogenin levels in adult muscle are low, but in muscle with a mixed composition of slow and fast fibers, like gastrocnemius, the expression tends to concentrate on slow fibers (HUGHES et al., 1993). In AD-CNM there is a predominance of slow type I fibers, this could justify the higher expression of myogenin found in uninjured HTZ muscles, but there is no change in the fiber typing in Tibialis anterior muscles from HTZ mice (KUTCHUKIAN et al., 2017). Thus, the higher expression of myogenin is in agreement with muscle immaturity.

Myf6 is the most abundant MRF in adult muscle, evenly distributed among the different fiber and muscle types (HUGHES et al., 1993; VOYTIK et al., 1993), consistent to its role in later fiber maturation. No MYF6 RNA or protein is detected in activated or proliferating satellite cells (PAVLATH et al., 2003). Accordingly, after injury, we detected a significant decrease in *Myf6* mRNA, which slowly started to increase as regeneration progress (PAVLATH et al., 2003), but no significant differences were detected in HTZ muscles. In addition, at 15 days, the expression did not recover to normal levels in WT and HTZ muscles, maybe because this may happen after a long time. Our results suggest that later fiber maturation subsequent to regeneration is not altered in HTZ muscle but it would be necessary to evaluate the muscles after a long time to confirm this hypothesis.

It was shown that in C2C12 cells and primary myoblasts, the GTPase activity of dynamin 2 is required in later stages of myoblasts membrane fusion (LEIKINA et al., 2013), by association of dynamin 2 to TKS5 protein at the invadosome and strengthening of dynamin-actin bundles, driving membranes fusion (CHUANG et al., 2019). Other study demonstrated that the clathrin-mediated endocytosis is also necessary to C2C12 cells form myotubes (SHIN et al., 2014). This specific function of dynamin 2 could have a direct relationship with the muscular phenotype in centronuclear myopathy. In opposition, no alterations in the fusion index were found in cultured primary myoblasts of HTZ mice (FONGY et al., 2019).

How dynamin 2 acts on satellite cells is not clear and further investigations are necessary to define the mechanism by which the mutant dynamin 2 leads to satellite cell loss. The absence of dMyHC+ in uninjured muscles makes unlikely that SCs are being more recruited in HTZ muscles. It would be relevant to check satellite cells in AR-CNM, to verify if SC defects are common to all CNM.

Taken together, our results suggest that albeit all the molecular pathways are activated for muscle regeneration, the overall outcome is compromised in HTZ animals. Although a defective satellite cell population is a non-specific feature of centronuclear myopathy, our findings contribute with one more layer to the comprehension of the disease, especially to the understanding of the muscle-specific impact of *DNM2* mutations in CNM.

References

BACHMAN, J. F. et al. Prepubertal skeletal muscle growth requires Pax7-expressing satellite cell-derived myonuclear contribution. **Development**, v. 145, n. 20, p. dev167197, 2018.

BANKHEAD, P. et al. QuPath: Open source software for digital pathology image analysis. **Scientific Reports**, v. 7, n. 1, 2017.

BEAUCHAMP, J. R. et al. Expression of CD34 and Myf5 defines the majority of quiescent adult skeletal muscle satellite cells. **Journal of Cell Biology**, v. 151, n. 6, p. 1221–1233, 2000.

BENTZINGER, C. F.; WANG, Y. X.; RUDNICKI, M. A. Building muscle: molecular regulation of myogenesis. **Cold Spring Harb Perspect Biol**, v. 4, n. 2, p. a008342, 2012.

BITOUN, M. et al. Mutations in dynamin 2 cause dominant centronuclear myopathy. **Nature Genetics**, v. 37, n. 11, p. 1207–1209, 2005.

BITOUN, M. et al. Dynamin 2 mutations cause sporadic centronuclear myopathy with neonatal onset. **Annals of Neurology**, v. 62, n. 6, p. 666–670, 2007.

BITOUN, M. et al. Dynamin 2 mutations associated with human diseases impair clathrin-mediated receptor endocytosis. **Human Mutation**, v. 30, n. 10, p. 1419–1427, 2009.

BLAU, H. M.; WEBSTER, C.; PAVLATH, G. K. Defective myoblasts identified in Duchenne muscular dystrophy. **Proceedings of the National Academy of Sciences of the United States of America**, v. 80, n. 15, p. 4856–60, ago. 1983.

BÖHM, J. et al. Mutation spectrum in the large gtpase dynamin 2, and genotype-phenotype correlation in autosomal dominant centronuclear myopathy. **Human Mutation**, v. 33, n. 6, p. 949–959, 2012.

BOLDRIN, L.; ZAMMIT, P. S.; MORGAN, J. E. Satellite cells from dystrophic muscle retain regenerative capacity. **Stem Cell Research**, v. 14, n. 1, p. 20–29, 2015.

BUCKINGHAM, M. Muscle Differentiation: Which myogenic factors make muscle? **Current Biology**, v. 4, n. 1, p. 61–63, 1994.

CASTETS, P. et al. Satellite cell loss and impaired muscle regeneration in selenoprotein N deficiency. **Human Molecular Genetics**, v. 20, n. 4, p. 694–704, 2011.

CHAKKALAKAL, J. V. et al. Early forming label-retaining muscle stem cells require p27kip1 for maintenance of the primitive state. **Development**, v. 141, n. 8, p. 1649–1659, 2014.

CHUANG, M. C. et al. Tks5 and Dynamin-2 enhance actin bundle rigidity in invadosomes to promote myoblast fusion. **Journal of Cell Biology**, 2019.

COWLING, B. S. et al. Reducing dynamin 2 expression rescues X-linked centronuclear

myopathy. **Journal of Clinical Investigation**, v. 124, n. 3, p. 1350–1363, 2014.

CRIST, C. G.; MONTARRAS, D.; BUCKINGHAM, M. Muscle satellite cells are primed for myogenesis but maintain quiescence with sequestration of Myf5 mRNA targeted by microRNA-31 in mRNP granules. **Cell Stem Cell**, v. 11, n. 1, p. 118–126, 2012.

DELANEY, K. et al. The role of TGF-β1 during skeletal muscle regeneration. **Cell Biology International**, v. 41, n. 7, p. 706–715, 2017.

DUMONT, N. A. et al. Dystrophin expression in muscle stem cells regulates their polarity and asymmetric division. **Nature Medicine**, v. 21, n. 12, p. 1455–1463, 2015.

DURIEUX, A. C. et al. Dynamin 2 and human diseases. **Journal of Molecular Medicine**, v. 88, n. 4, p. 339–350, 2010a.

DURIEUX, A. C. et al. A centronuclear myopathy-dynamin 2 mutation impairs skeletal muscle structure and function in mice. **Human Molecular Genetics**, v. 19, n. 24, p. 4820–4836, 2010b.

FERGUSON, S. M.; DE CAMILLI, P. Dynamin, a membrane-remodelling GTPase. **Nature Reviews Molecular Cell Biology**, v. 13, n. 2, p. 75–88, 2012.

FISCHER, D. et al. Characterization of the muscle involvement in dynamin 2-related centronuclear myopathy. **Brain**, v. 129, n. 6, p. 1463–1469, 2006.

FONGY, A. et al. Nuclear defects in skeletal muscle from a Dynamin 2-linked centronuclear myopathy mouse model. **Scientific Reports**, v. 9, 2019.

FRANCK, A. et al. Clathrin plaques and associated actin anchor intermediate filaments in skeletal muscle. **Molecular Biology of the Cell**, v. 30, n. 5, p. 579–590, 2019.

FRAYSSE, B.; GUICHENEY, P.; BITOUN, M. Calcium homeostasis alterations in a mouse model of the Dynamin 2-related centronuclear myopathy. **Biology Open**, v. 5, n. 11, p. 1691–1696, 2016.

GANASSI, M. et al. Myogenin promotes myocyte fusion to balance fibre number and size. **Nature Communications**, v. 9, n. 1, 2018.

GARRY, G. A.; ANTONY, M. L.; GARRY, D. J. Cardiotoxin induced injury and skeletal muscle regeneration. **Methods in Molecular Biology**, v. 1460, p. 61–71, 2016.

GAYRAUD-MOREL, B. et al. A role for the myogenic determination gene Myf5 in adult regenerative myogenesis. **Developmental Biology**, v. 312, n. 1, p. 13–28, 2007.

GONZÁLEZ-JAMETT, A. M. et al. Dynamin-2 mutations linked to Centronuclear Myopathy impair actin-dependent trafficking in muscle cells. **Scientific Reports**, v. 7, n. 1, 2017.

GÜNTHER, S. et al. Myf5-positive satellite cells contribute to Pax7-dependent long-term

maintenance of adult muscle stem cells. **Cell Stem Cell**, v. 13, n. 5, p. 590–601, 2013.

HANISCH, F. et al. Phenotype variability and histopathological findings in centronuclear myopathy due to DNM2 mutations. **Journal of Neurology**, v. 258, n. 6, p. 1085–1090, 2011.

HARDY, D. et al. Comparative Study of Injury Models for Studying Muscle Regeneration in Mice. **PloS one**, v. 11, n. 1, p. e0147198, 2016.

HASTY, P. et al. Muscle deficiency and neonatal death in mice with a targeted mutation in the myogenin gene. **Nature**, v. 364, n. 6437, p. 501–506, 1993.

HUGHES, S. M. et al. Selective accumulation of MyoD and myogenin mRNAs in fast and slow adult skeletal muscle is controlled by innervation and hormones. **Development**, v. 118, n. 1137–1147, 1993.

IHN, H. The role of TGF-beta signaling in the pathogenesis of fibrosis in scleroderma. **Arch Immunol Ther Exp (Warsz)**, v. 50, n. 5, p. 325–331, 2002.

KEEFE, A. C. et al. Muscle stem cells contribute to myofibres in sedentary adult mice. **Nature Communications**, v. 6, 2015.

KENNISTON, J. A.; LEMMON, M. A. Dynamin GTPase regulation is altered by PH domain mutations found in centronuclear myopathy patients. **EMBO Journal**, v. 29, n. 18, p. 3054–3067, 2010.

KUANG, S. et al. Asymmetric Self-Renewal and Commitment of Satellite Stem Cells in Muscle. **Cell**, v. 129, n. 5, p. 999–1010, 2007.

KUDRYASHOVA, E.; KRAMEROVA, I.; SPENCER, M. J. Satellite cell senescence underlies myopathy in a mouse model of limb-girdle muscular dystrophy 2H. **Journal of Clinical Investigation**, v. 122, n. 5, p. 1764–1776, 2012.

KUTCHUKIAN, C. et al. Impaired excitation–contraction coupling in muscle fibres from the dynamin2R465W mouse model of centronuclear myopathy. **Journal of Physiology**, v. 595, n. 24, p. 7369–7382, 2017.

LAPORTE, J. et al. A gene mutated in X-linked myotubular myopathy defines a new putative tyrosine phosphatase family conserved in yeast. **Nature Genetics**, v. 13, n. 2, p. 175–182, 1996.

LAWLOR, M. W. et al. Myotubularin-deficient myoblasts display increased apoptosis, delayed proliferation, and poor cell engraftment. **American Journal of Pathology**, v. 181, n. 3, p. 961–968, 2012.

LEIKINA, E. et al. Extracellular annexins and dynamin are important for sequential steps in

myoblast fusion. **Journal of Cell Biology**, v. 200, n. 1, p. 109–123, 2013.

MCKINNELL, I. W. et al. Pax7 activates myogenic genes by recruitment of a histone methyltransferase complex. **Nature Cell Biology**, v. 10, n. 1, p. 77–84, 2008.

NICOT, A. S. et al. Mutations in amphiphysin 2 (BIN1) disrupt interaction with dynamin 2 and cause autosomal recessive centronuclear myopathy. **Nature Genetics**, v. 39, n. 9, p. 1134–1139, 2007.

OBAR, R. A. et al. Molecular cloning of the microtubule-associated mechanochemical enzyme dynamin reveals homology with a new family of GTP-binding proteins. **Nature**, v. 347, n. 6290, p. 256–261, 1990.

OLGUIN, H. C.; OLWIN, B. B. Pax-7 up-regulation inhibits myogenesis and cell cycle progression in satellite cells: A potential mechanism for self-renewal. **Developmental Biology**, v. 275, n. 2, p. 375–388, 2004.

OUSTANINA, S.; HAUSE, G.; BRAUN, T. Pax7 directs postnatal renewal and propagation of myogenic satellite cells but not their specification. **EMBO Journal**, v. 23, n. 16, p. 3430–3439, 2004.

PAVLATH, G. K. et al. Regeneration of transgenic skeletal muscles with altered timing of expression of the basic helix-loop-helix muscle regulatory factor MRF4. **American Journal of Pathology**, v. 162, n. 5, p. 1685–1691, 2003.

ROMERO, N. B.; BITOUN, M. Centronuclear myopathies. **Seminars in Pediatric Neurology**, v. 18, p. 250–256, 2011.

ROSS, J. et al. Defects in glycosylation impair satellite stem cell function and niche composition in the muscles of the dystrophic largemydmouse. **Stem Cells**, v. 30, n. 10, p. 2330–2341, 2012.

SAMBASIVAN, R. et al. Pax7-expressing satellite cells are indispensable for adult skeletal muscle regeneration. **Development**, v. 138, n. 17, p. 3647–3656, 2011.

SAMBUUGHIN, N. et al. Adult-onset autosomal dominant spastic paraplegia linked to a GTPase-effector domain mutation of dynamin 2. **BMC Neurology**, v. 15, n. 1, 2015.

SASSOON, D. et al. Expression of two myogenic regulatory factors myogenin and MyoDI during mouse embryogenesis. **Nature**, v. 341, n. 6240, p. 303–307, 1989.

SCHULTZ, E. Satellite cell proliferative compartments in growing skeletal muscles. **Developmental Biology**, v. 175, n. 1, p. 84–94, 1996.

SEALE, P. et al. Pax7 is required for the specification of myogenic satellite cells. **Cell**, v. 102, n. 6, p. 777–786, 2000.

SEWRY, C. A.; WALLGREN-PETTERSSON, C. Myopathology in congenital myopathies. **Neuropathology and Applied Neurobiology**, v. 43, n. 1, p. 5–23, 2017.

SHEA, K. L. et al. Sprouty1 regulates reversible quiescence of a self-renewing adult muscle stem cell pool during regeneration. **Cell stem cell**, v. 6, n. 2, p. 117–29, 5 fev. 2010.

SHIN, N. Y. et al. Dynamin and endocytosis are required for the fusion of osteoclasts and myoblasts. **Journal of Cell Biology**, v. 207, n. 1, p. 73–89, 2014.

SIDIROPOULOS, P. N. M. et al. Dynamin 2 mutations in Charcot-Marie-Tooth neuropathy highlight the importance of clathrin-mediated endocytosis in myelination. **Brain**, v. 135, n. 5, p. 1395–1411, 2012.

SOLEIMANI, V. D. et al. Transcriptional Dominance of Pax7 in Adult Myogenesis Is Due to High-Affinity Recognition of Homeodomain Motifs. **Developmental Cell**, v. 22, n. 6, p. 1208–1220, 2012.

USTANINA, S. et al. The Myogenic Factor Myf5 Supports Efficient Skeletal Muscle Regeneration by Enabling Transient Myoblast Amplification. **Stem Cells**, v. 25, n. 8, p. 2006–2016, 2007.

VENUTI, J. M. et al. Myogenin is required for late but not early aspects of myogenesis during mouse development. **Journal of Cell Biology**, v. 128, n. 4, p. 563–576, 1995.

VON MALTZAHN, J. et al. Pax7 is critical for the normal function of satellite cells in adult skeletal muscle. **Proceedings of the National Academy of Sciences**, v. 110, n. 41, p. 16474–16479, 2013.

VOYTIK, S. L. et al. Differential expression of muscle regulatory factor genes in normal and denervated adult rat hindlimb muscles. **Developmental Dynamics**, v. 198, n. 3, p. 214–224, 1993.

WAHL, S. M. et al. Transforming growth factor-beta in synovial fluids modulates Fc gamma RII (CD16) expression on mononuclear phagocytes. **J Immunol**, v. 148, n. 2, p. 485–490, 1992.

WANG, L. et al. Dynamin 2 mutants linked to centronuclear myopathies form abnormally stable polymers. **Journal of Biological Chemistry**, v. 285, n. 30, p. 22753–22757, 2010.

WARNOCK, D. E.; BABA, T.; SCHMID, S. L. Ubiquitously expressed dynamin-II has a higher intrinsic GTPase activity and a greater propensity for self-assembly than neuronal dynamin-I. **Mol Biol Cell**, v. 8, n. 12, p. 2553–2562, 1997.

WHITE, R. B. et al. Dynamics of muscle fibre growth during postnatal mouse development. **BMC Developmental Biology**, v. 10, n. 21, 2010.

ZAMMIT, P. S. Pax7 and myogenic progression in skeletal muscle satellite cells. **Journal of Cell Science**, v. 119, n. 9, p. 1824–1832, 2006.

Supplementary data

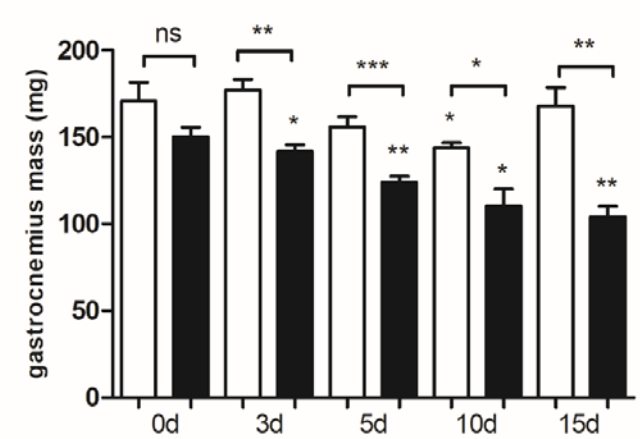

Figure 30 Reduction in gastrocnemius mass after lesion by electroporation. Mann-Whitney test, n=5 individuals per genotype at time point zero, n=8 individuals per genotype at the other time points; ns=non-significant; *p<0.05; **p<0.01, ***p<0.001

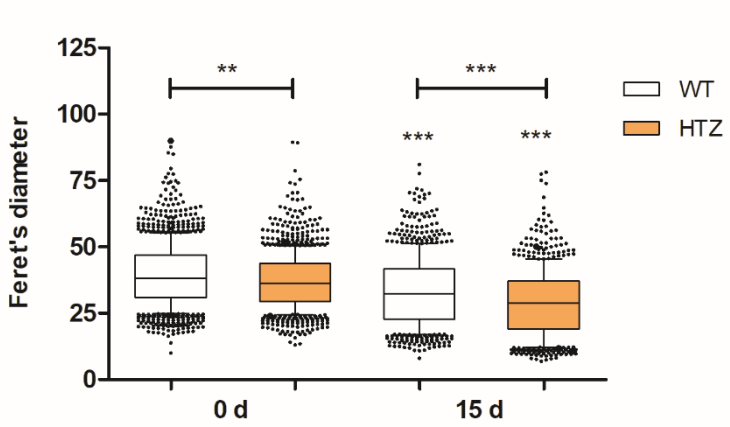

Figure 31 Feret's diameter of myofibers before and after cardiotoxin injury. Kruskal-Wallis test followed by Dunn's multiple comparison test; n=1278 fibers in WT 0d, n=1152 fibers in HTZ 0d, n=809 fibers in WT 15d and n=664 fibers in HTZ 15d; **p<0.01, ***p<0.001.

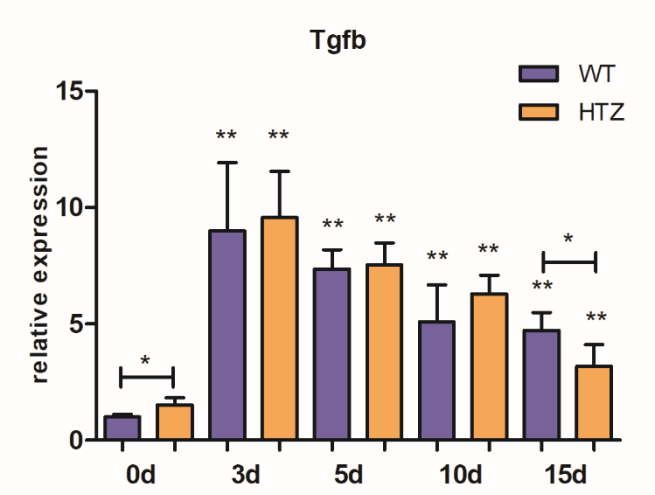

Figure 32 Relative expression of Tgfb mRNA measured by qRT-PCR after cardiotoxin injury. Mann-Whitney test, *p<0.05, **p<0.01, n=5 individuals per genotype for day zero, n=3 individuals per genotype at the other time points. Relative expression values were calculated by $2^{-\Delta\Delta Ct}$ method using WT values as the normalizer sample.

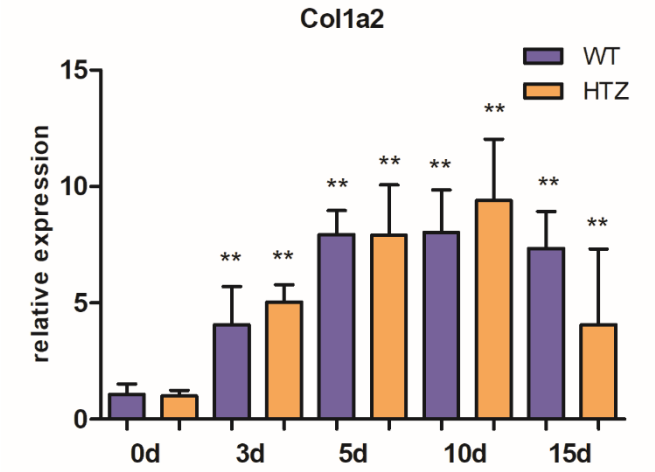

Figure 33 Relative expression of Col1a2 mRNA measured by qRT-PCR after cardiotoxin injury. Mann-Whitney test, **p<0.01, n=5 individuals per genotype for day zero, n=3 individuals per genotype at the other time points. Relative expression values were calculated by $2^{-\Delta\Delta Ct}$ method using WT values as the normalizer sample.

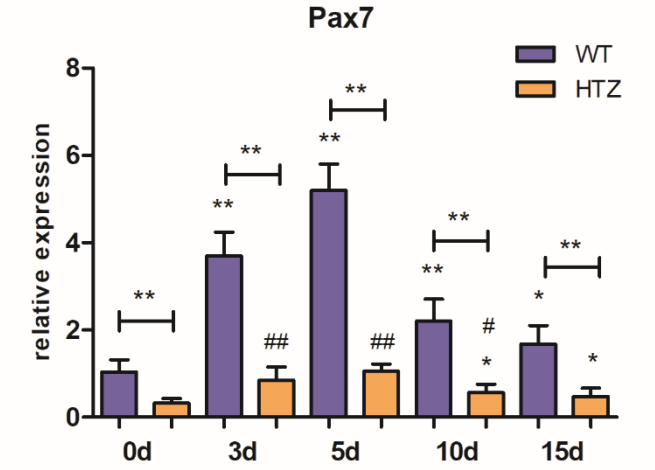

Figure 34 Relative expression of Pax7 mRNA measured by qRT-PCR after cardiotoxin injury. Mann-Whitney test. Asterisks (*) denote differences in relation to WT uninjured, number sign (#) in relation to HTZ uninjured. * and # p<0.05, ** and ## p<0.01. n=5 individuals per genotype for day zero, n=3 individuals per genotype at the other time points. Relative expression values were calculated by $2^{-\Delta\Delta Ct}$ method using WT values as the normalizer sample.

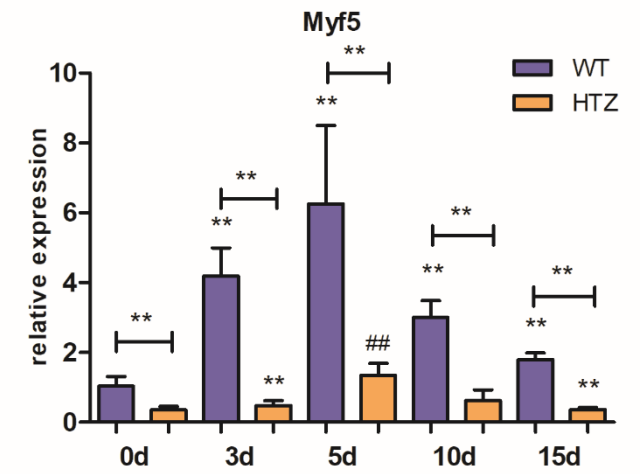

Figure 35 Relative expression of Myf5 mRNA measured by qRT-PCR after cardiotoxin injury. Mann-Whitney test Asterisks (*) denote differences in relation to WT uninjured, number sign (#) in relation to HTZ uninjured. ** and ## p<0.01. n=5 individuals per genotype for day zero, n=3 individuals per genotype at the other time points. Relative expression values were calculated by $2^{-\Delta\Delta Ct}$ method using WT values as the normalizer sample.

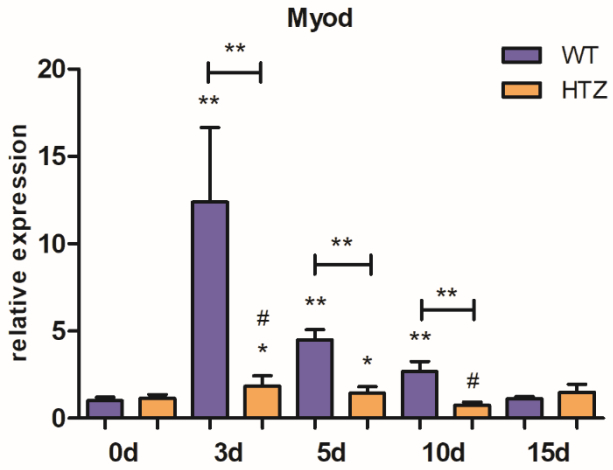

Figure 36 Relative expression of Myod mRNA measured by qRT-PCR after cardiotoxin injury. Mann-Whitney test. Asterisks (*) denote differences in relation to WT uninjured, number sign (#) in relation to HTZ uninjured. * and # p<0.05, ** p<0.01. n=5 individuals per genotype for day zero, n=3 individuals per genotype at the other time points. Relative expression values were calculated by $2^{-\Delta\Delta Ct}$ method using WT values as the normalizer sample.

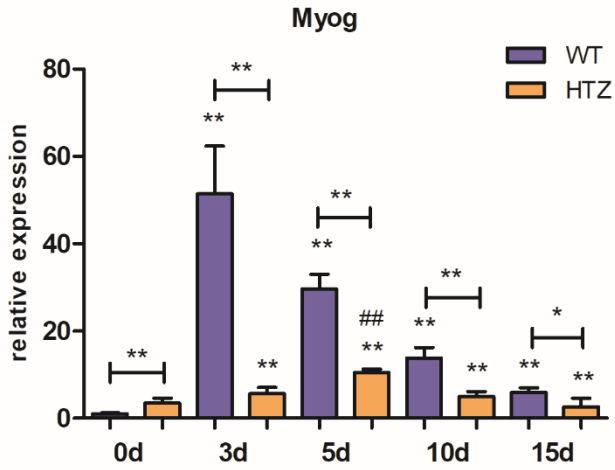

Figure 37 Relative expression of Myog mRNA measured by qRT-PCR after cardiotoxin injury. Mann-Whitney test. Asterisks (*) denote differences in relation to WT uninjured, number sign (#) in relation to HTZ uninjured. * p<0.05, ** and ## p<0. 01. n=5 individuals per genotype for day zero, n=3 individuals per genotype at the other time points. Relative expression values were calculated by $2^{-\Delta\Delta Ct}$ method using WT values as the normalizer sample.

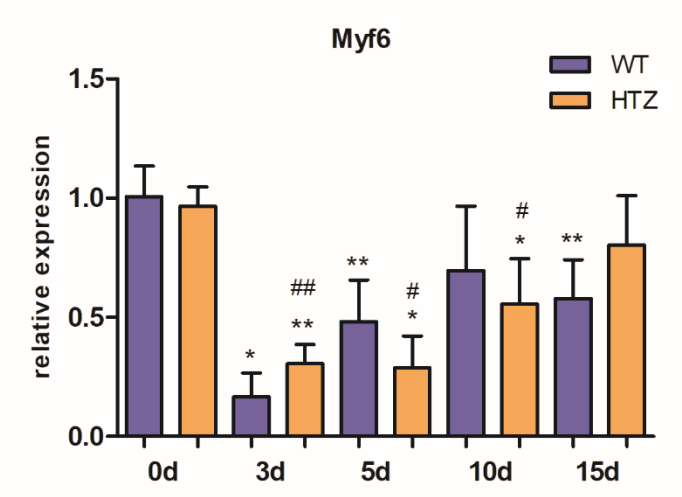

Figure 38 Relative expression of Myf6 mRNA measured by qRT-PCR after cardiotoxin injury. Mann-Whitney test. Asterisks (*) denote differences in relation to WT uninjured, number sign (#) in relation to HTZ uninjured. * and # p<0.05, ** and ## p<0.01. n=5 individuals per genotype for day zero, n=3 individuals per genotype at the other time points. Relative expression values were calculated by $2^{-\Delta\Delta Ct}$ method using WT values as the normalizer sample.

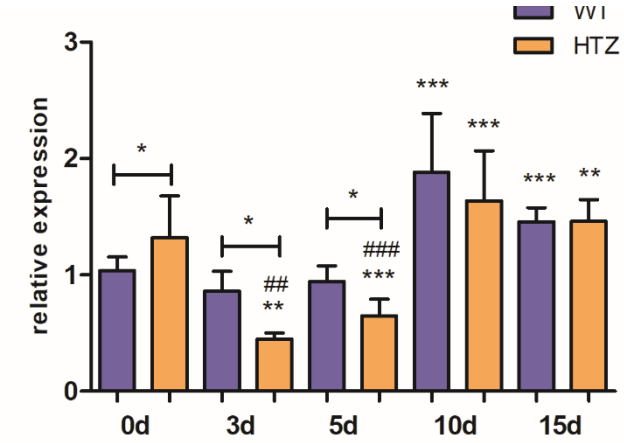

Figure 39 Relative expression of Spry1 mRNA measured by qRT-PCR after cardiotoxin injury. Mann-Whitney test. Asterisks (*) denote differences in relation to WT uninjured, number sign (#) in relation to HTZ uninjured. * and # p<0.05, ** and ## p<0.01, *** and ### p<0.001. n=5 individuals per genotype for day zero, n=3 individuals per genotype at the other time points. Relative expression values were calculated by $2^{-\Delta\Delta Ct}$ method using WT values as the normalizer sample.

VI. Chapter 6 - Functional characterization of DNM2 mutations

Myogenic properties of human and mouse immortalized myoblasts carrying *DNM2* mutations

Camila F. Almeida[1], Vincent Mouly[2], Jocelyn Laporte[3], Marc Bitoun[2], Mariz Vainzof[1]

[1] Laboratory of Muscle Proteins and Comparative Histopathology, Human Genome and Stem Cell Research Center, Biosciences Institute, University of São Paulo, São Paulo, Brazil

[2]Sorbonne Université, INSERM, Institute of Myology, Centre of Research in Myology, UMRS 974, F-75013, Paris, France

[3]Institut de Génétique et de Biologie Moléculaire et Cellulaire (IGBMC), Illkirch 67404, France

Corresponding author:

Dr. Mariz Vainzof

Human Genome and Stem Cell Research Center, IBUSP

Rua do Matão, 106 – Cidade Universitária

São Paulo, SP - CEP 05508-900. Brazil

PHONE: +55 11 3091-7736

FAX: +55 11 3091-0852

e-mail: mvainzof@usp.br

Resumo

A dinamina 2 é uma GTPase ubiquamente expressa conhecida principalmente pelo seu papel na endocitose. Entretanto, muitas outras funções foram descritas nos últimos anos, destacando a sua importância para múltiplas atividades críticas para o funcionamento adequado das células. Mutações no gene DNM2 são responsáveis pela miopatia centronuclear, uma doença que causa fraqueza muscular progressiva e atrofia. O impacto músculo-específico das mutações não é completamente compreendido. Neste estudo, nós investigamos o impacto funcional de duas mutações encontradas em pacientes humanos, p.R46W e p.E650K, utilizando mioblastos imortalizados derivados de um camundongo modelo e de um paciente humano. Pela análise da diferenciação miogênica *in vitro*, nós encontramos alterações na expressão de genes regulatórios miogênicos em mioblastos com a mutação p. R465W e a formação de miotubos de tamanho reduzido por células com a mutação p. E650K. Pela análise da migração celular, nós observamos que ambas mutações limitam a capacidade migratória. Finalmente, nós encontramos uma redução na taxa de endocitose dos mioblastos murinos com a mutação p.R465W, mas uma discreta alteração nos mioblastos humanos com a mutação p.E650K. Assim, nossos resultados mostram que as mutações p.R465W e p.E650K podem impactar no desenvolvimento muscular, pela alteração na expressão de genes reguladores da miogênese e na fusão de mioblastos, provavelmente como uma consequência do prejuízo à capacidade migratória e a possível redução na endocitose.

Abstract

Dynamin 2 is a ubiquitously expressed large GTPase mainly known by its role in endocytosis. However, many other activities have been identified in the last years, underscoring its importance to multiple activities critical to proper cell functioning. Mutations in the *DNM2* gene are responsible for centronuclear myopathy, a disease that causes progressive muscle weakness and atrophy. The muscle-specific impact of the mutations is not fully understood. In this study, we investigated the functional impact of two mutations found in human patients, p.R465W and p.E650K, using immortalized myoblasts derived from a mouse model and a human patient. By analyzing *in vitro* myogenic differentiation, we found altered expression of myogenic regulatory genes on p.R465W myoblasts and the formation of smaller myotubes by p.E650K cells. Studying cellular migration, we observed that both mutations limit the cell migratory capacity. Finally, we found a reduced endocytosis rate on mouse myoblasts bearing the p.R465W mutation, but a discrete alteration in the human p.E650K myoblasts. Therefore, our results showed that p.R465W and p.E650K mutations can impact on muscle development, by altering the gene expression of myogenic regulatory factors and myoblasts fusion, probably as a consequence of impaired migratory capacities, and possible reduction of endocytosis.

Introduction

Dynamin 2 (DNM2) belongs to a superfamily of large GTPases involved in membrane-remodeling events including fission and fusion of intracellular vesicles (RAMACHANDRAN; SCHMID, 2018). Dynamins are also important for actin cytoskeleton dynamics (GU et al., 2010). Dynamin 2 is composed of five distinct structural domains: an N-terminal GTPase domain is the effector of GTP hydrolysis (CHEN et al., 2004). The middle domain (MD) participates in DNM2 self-assembly and in conformational change induced by GTP hydrolysis (SMIRNOVA et al., 1999). The pleckstrin homology (PH) domain binds to phosphoinositides at the plasma membrane, directing dynamin to the membrane (KLEIN et al., 1998). The GTPase Enhancing Domain (GED) is proposed to participate in DNM2 self-oligomerization, is a positive regulator of GTPase activity and together with MD forms a structurally essential stalk (SEVER; MUHLBERG; SCHMID, 1999). Finally, the proline-rich domain (PRD) interacts with the SH3 domain-containing proteins which are DNM2 partners (HEYMANN; HINSHAW, 2009).

Mutations in the *DNM2* gene were identified as the genetic cause of the autosomal dominant form of centronuclear myopathy (AD-CNM) (BITOUN et al., 2005). AD-CNM is characterized by a wide spectrum of clinical manifestations, including muscle weakness, atrophy, ptosis and ophthalmoplegia (ROMERO; BITOUN, 2011). The histological hallmark is the presence of many nuclei positioned in the central region of the muscle fiber (ROMERO; BITOUN, 2011). Although dynamin 2 has a ubiquitous expression, AD-CNM-linked mutations mainly affect skeletal muscle, suggesting that dynamin 2 has a tissue-specific function or at least its functions are more sensitive for this tissue.

By now, more than 20 mutations were found in AD-CNM patients and they are mostly concentrated on the MD and PH domains. The most common mutation is p.R465W found in approximately 30% of patients and it was used to produce a knock-in mouse model that presents a myopathic phenotype, with impairment of contractile properties and muscle atrophy (DURIEUX et al., 2010). Few mutations localize to GED domain, including p.E650K (BITOUN et al., 2009).

The muscle-specific role of dynamin 2 is not totally understood. In muscle, it localizes at the plasma membrane, the I-band, and the perinuclear regions. It partially co-localizes with the microtubule network, at the neuromuscular junction and nearby sarcomeric Z-disks close

to triads (COWLING et al., 2011; DURIEUX et al., 2010) suggesting a role in T-tubule organization (TINELLI; PEREIRA; SUTER, 2013). The expression levels of both RNA and protein are unaltered in fibroblasts and muscle from patients, showing equal expression and stability of the normal and mutated proteins (BITOUN et al., 2005, 2009; ECHANIZ-LAGUNA et al., 2007; KIERDASZUK et al., 2013; KOUTSOPOULOS et al., 2013); however, localization of DNM2 may be changed in mutant models, with cytosolic accumulation in vitro (JAMES et al., 2014; KENNISTON; LEMMON, 2010; KIERDASZUK et al., 2013; KOUTSOPOULOS et al., 2011; LIU; LUKIYANCHUK; SCHMID, 2011) and in vivo (CHIN et al., 2015; DURIEUX et al., 2010; GONZÁLEZ-JAMETT et al., 2017). These data favor for a dominant-negative effect of the heterozygous mutations, resulting in loss of function. Nonetheless, some studies point out that several DNM2 mutations increase oligomer stability and GTPase activity (KENNISTON; LEMMON, 2010; WANG et al., 2010) suggestive of a gain of function. Several pathogenic mechanisms have been proposed including calcium homeostasis deregulation (FRAYSSE; GUICHENEY; BITOUN, 2016; KUTCHUKIAN et al., 2017), defects in neuromuscular junction (DOWLING et al., 2012; GIBBS et al., 2013; ROBB et al., 2011), clathrin-mediated endocytosis impairment (BITOUN et al., 2009), actin kinetics impairment (GONZÁLEZ-JAMETT et al., 2017), desmin cytoskeleton alterations (FRANCK et al., 2019; HNIA et al., 2011) and nuclear abnormalities (FONGY et al., 2019).

In the present work, we sought to further expand the pathomechanisms linked to two dynamin 2 mutations in mouse and in human cell models, exploring the impact of these mutations on myogenic differentiation, cell migration, and clathrin-mediated endocytosis. We found an impaired expression of myogenic regulatory genes on p.R465W myoblasts and the formation of smaller myotubes by p.E650K cells. Regarding cellular migration, we found that both mutations impact on cells migratory capacity. Finally, we found a reduced endocytosis rate on mouse p.R465W myoblasts, while unaltered endocytosis in human p.E650K cells.

Methodology

Cell culture

Myoblasts cultures were established from muscle biopsies performed in healthy subjects aged between 20 and 38-years-old and one male patient with the p.E650K DNM2 mutation when he was 35-years-old. Primary myoblasts were immortalized by the Immortalization Facility of the Myology Institute (Paris, France) as previously described (MAMCHAOUI et al., 2011). Immortalized myoblasts were cultured in proliferation medium consisting of 1 volume of M199 (Invitrogen, 41150020), 4 volumes of DMEM (Invitrogen, 61965), 20% fetal bovine serum (FBS, Invitrogen), 50 U/mL penicillin, 50 mg/mL streptomycin, 25 µg/mL fetuin (Life Technologies, 10344026), 0.5 ng/mL fibroblast growth factor-basic (bFGF; Life Technologies; PHG0026), 5 ng/mL human epidermal growth factor (hEGF; Life Technologies; PHG0311), 0.2 µg/mL dexamethasone (D4902-100mg; Sigma), 5 µg/mL insulin (91077C-1g; Sigma).

For myogenic differentiation, when cell reached above 90% of confluence, growth media was switched for differentiation media containing DMEM (Invitrogen, 61965), 50 µg/mL gentamicin (15750, Invitrogen) and 10 µg/mL insulin (Sigma, 91077). Myotubes were allowed to differentiate for three and six days, then detached from flasks with trypsin, centrifuged at 300 g, for 10 min at 4°C; washed in PBS, centrifuged again and pellets were used for subsequent analyses.

For high-density muscular differentiation, at time zero, cells were plated at 5000 cells/cm² in proliferation media (PM). At this density, cells do not touch each other. After six hours, PM was replaced by differentiation media (DM) for more 42 hours. Then, the cells were trypsinized and plated at 75000 cells/cm² density, in which they filled the entire plate surface and maintained in PM for six hours that was enough time to let them attach to coverslips. Thereafter, PM was changed again to DM and cells were incubated for more 66 hours and fixed in 4% paraformaldehyde.

Myoblasts from wild-type (WT2) and KI-*Dnm2*$^{R465W/+}$ (R465W) mice were immortalized by transfection with lentivirus containing the *Cdk4* gene (RABAI et al., 2019). Immortalized myoblasts were cultured in Matrigel-coated dishes in DMEM (Invitrogen, 61965) supplemented with 20% FBS, 1% chicken embryo extract and 50 µg/mL gentamicin

(Invitrogen, 15750). Murine immortalized myoblasts KMS4 (WT1), derived from wild-type C57BL/6, were grown in Ham's F-10 (Invitrogen) media supplemented with 20% FBS, 2.5 ng/mL of fibroblast growth factor (FGF, Invitrogen) and 50 μg/mL gentamicin.

When cells reached approximately 80% of confluence, PM was switched for DM composed of DMEM (Invitrogen, 61965), 2% horse serum (Invitrogen), 10 μg/mL insulin (Sigma, 91077) and 50 μg/mL gentamicin.

Fusion index

Myotubes were fixed with 4% paraformaldehyde for 10 minutes and permeabilized in 1X TBS (10 nM Tris-HCl pH 7.5, 150 mM NaCl) containing 0.1% Triton™X-100 (Sigma-Aldrich) (permeabilization solution) for 30 minutes and blocked in 1X TBS with 1% FBS and 0.1% Triton™X-100 (Sigma-Aldrich) for 30 minutes. Incubation with primary antibody anti-*pan*-myosin (dilution factor 1:50; Developmental Studies Hybridoma Bank, MF-20) was performed overnight at 4°C followed by rinsing with permeabilization solution and incubation with anti-mouse AlexaFluor® 488 (Invitrogen, 11001) secondary antibody for one hour at room temperature. Slides were mounted with Vectashield® (Vector) medium, containing DAPI to counterstain nuclei. Images were acquired in the Axiophot microscope (Zeiss) with 16x magnification objective; five random fields were imaged per slide.

The total number of nuclei and nuclei inside myotubes were counted manually. Myotubes were classified according to the number of nuclei inside each myotube (categories are presented in graphs). Total fusion index, *i.e.* not considering the myotube category, was calculated as (number of nuclei inside myotube/total number of nuclei) X 100.

RNA extraction and qRT-PCR

RNA extractions from cell pellets were done with TRIzol reagent (Invitrogen), following manufacturer's instructions and resuspended with RNase free water (Invitrogen). All samples were treated with DNase. RNA yield was measured in NanoDrop spectrophotometer and 18S and 28S RNA bands integrity was checked by 1% agarose gel electrophoresis. cDNA was synthesized with SuperScript VILO Master Mix (Invitrogen) using 1 μg of total RNA. Pairs of primers were designed for the mouse genes *Pax7, Myod, Myf5, Myog,* and the human genes *MYOD, MYOG,* and *MYF5*. *Csnk2a* and *RPLPO* were endogenous controls for mouse and human cells, respectively. Primer sequences are listed on the Supplementary Table 1.

Quantitative real-time PCR assays of human myoblasts experiments were performed in 7500 Fast (Applied Biosystems) equipment and the assays for mouse myoblasts were done in QuantStudio5 (Applied Biosystems) equipment. Reactions for 7500 Fast system were prepared as follows: 10 μL Sybr Green Fast master mix (Roche), 300 nM of each primer (forward and reverse), 4 μL of 1:10 diluted cDNA and RNase free water *q.s.p.* 20 μL. Reactions for QuantStudio5 system were prepared as follows: 10 μL PowerUP Sybr Green master mix (Applied Biosystems), 300 nM of each primer (forward and reverse), 2 μL of 1:10 diluted cDNA and RNase free water *q.s.p.* 20 μL. Relative expression was calculated by the comparative C_t method, as described (SCHMITTGEN; LIVAK, 2008).

Live cell imaging

For quantification of cell movements, cells were recorded as follows: myoblasts were plated in 12-multiwell dishes and grown until they reach about 30% of confluence. For live imaging, the dishes were placed in an incubator to maintain cultures at 37 °C and 5% CO_2 (Okolab) coupled to a Nikon Ti microscope with an XY-motorized stage (Nikon). Images were captured with a CoolSNAP HQ2 camera (Roper Scientific) every 13 minutes, during 72 hours. Then, images were assembled in Metamorph software (Molecular Devices) and cell tracking was done either with Metamorph or ImageJ. The trajectories of individual cells were traced frame by frame manually (60 frames, equivalent to 13 hours of recording). The analyzed parameters were calculated with SkyPad add-in for Microsoft Excel (CADOT; GACHE; GOMES, 2014).

Transferrin/EGF uptake assay

Immortalized myoblasts (human and mouse) were grown on coverslips placed on 12-well dish. Cells were cultured with serum-deprived media for 45 minutes and then placed on ice. Next, cells were incubated 15 minutes with 40 μg/mL of transferrin labeled with AlexaFluor-488 (Life Technologies, T13342) or 1 μg/mL of EGF labeled with AlexaFluor-488 (Life Technologies, E13345) at 37°C. Endocytosis was stopped by adding cold media and cells were rinsed with cold PBS and fixed with 4% PFA. Coverslips were mounted in slides with Vectashield® (Vector) medium, containing DAPI to counterstain nuclei. Cells were imaged with FV-1200 confocal microscope (Olympus) and 40x oil objective; whole cells were imaged using stacks of 0.5 μm interval.

Fluorescence was measured on the sum projection of the confocal stacks. Individual cells were outlined manually and integrated density was obtained with ImageJ software. The fluorescence of three areas around each cell was measured to obtain background noise. Finally, transferrin uptake was calculated according to the formula: total cell fluorescence= fluorescence of the cell X mean fluorescence of background/cell area. More than 100 cells were measured per condition.

Statistical analysis

All statistical tests were performed in GraphPad Prism software, version 5.00 for Windows (La Jolla California USA). Values are expressed as means ± standard error of the mean (SEM). Comparisons between two groups were performed with the Mann-Whitney test (non-parametric). Comparisons of multiple groups were done with the Kruskal-Wallis test (non-parametric), followed by Dunn's multiple comparisons. P values <0.05 were considered significant. Sample numbers and statistical tests are indicated in the figure's captions.

Results

Myogenic differentiation

To verify whether the p.R465W mutation had effects on myoblast differentiation, we induced the cells to fuse and form myotubes for three and six days. Fusion index was previously assessed in primary myoblasts culture (FONGY et al., 2019) and in immortalized myoblasts (RABAI et al., 2019), and no significant differences were found regarding their fusion capacity. Thus, we focused on the expression analysis of myogenic markers before and after differentiation. Morphologically, we did not detect evident differences between WT and R465W myotubes (Figure 1), in accordance with previous studies.

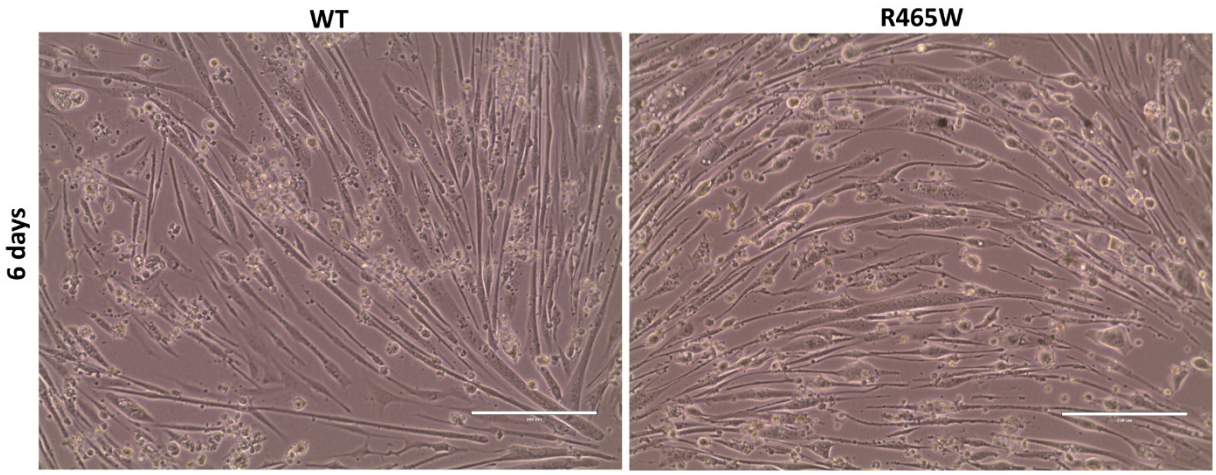

Figure 40 Myogenic differentiation of WT and R465W myoblasts in vitro after six days showing a similar pattern of myotube formation. Representative image of light microscopy. Scale bar = 200 µm.

Next, we quantified the expression of the satellite cell marker *Pax7* and the three main myogenic regulatory factors (*Myf5, Myod*, and *Myog*). R465W myoblasts showed a reduced expression of *Pax7* (Figure 2). After the induction for myogenic differentiation, *Pax7* was downregulated in WT and mutant cells, although in WT the difference was not significantly different relative to WT myoblasts. However, the difference between WT and R465W myotubes persisted (Figure 2).

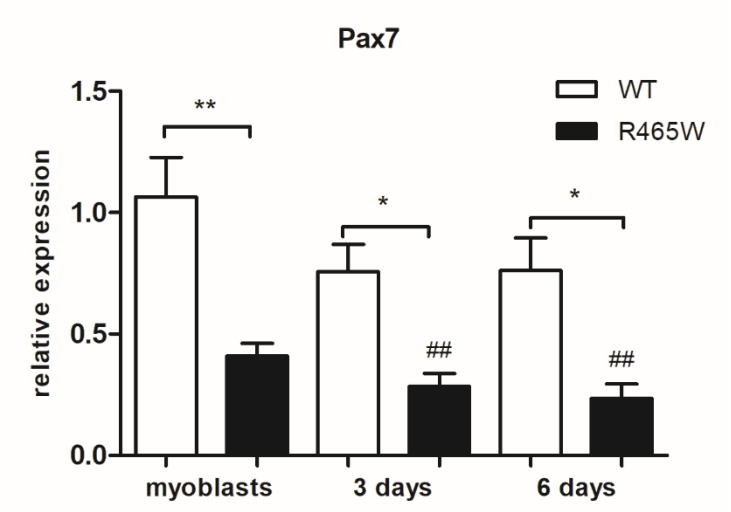

Figure 41 Relative expression of Pax7 gene in proliferating myoblasts and myotubes differentiated for three and six days. Relative expression calculated using $2^{-\Delta\Delta Ct}$ method, using WT myoblasts as the normalizer sample. Asterisks (*) denote differences between WT and R465W cells in the same condition, and number signs (#) in relation to WT myoblasts. Statistical analysis was performed using Mann-Whitney test; n=5 independent experiments; *p<0.05, ** and ## p<0.01.

The expression of *Myf5* was similar in WT and R465W in proliferating myoblasts. After the start of differentiation, *Myf5* expression remained unchanged in WT cells, while in R465W myotubes it was significantly activated (Figure 3).

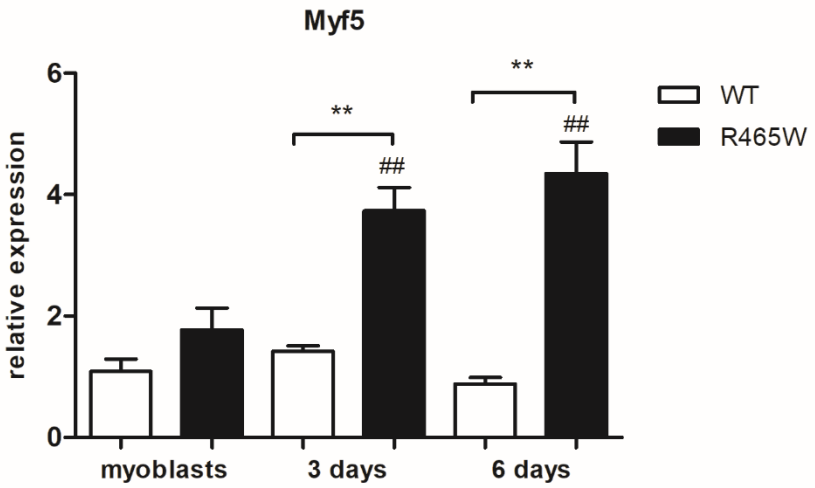

Figure 42 Relative expression of Myf5 gene in proliferating myoblasts and myotubes differentiated for three and six days. Relative expression calculated using $2^{-\Delta\Delta Ct}$ method, using WT myoblasts as the normalizer sample. Asterisks (*) denote differences between WT and R465W cells in the same condition, and number signs (#) in relation to WT myoblasts Statistical analysis was performed using Mann-Whitney test; n=5 independent experiments; ** and ## p<0.01.

Myod had strikingly reduced expression in R465W myoblast as compared to WT, which slightly increased after differentiation, but remained unchanged in WT myoblasts (Figure 4).

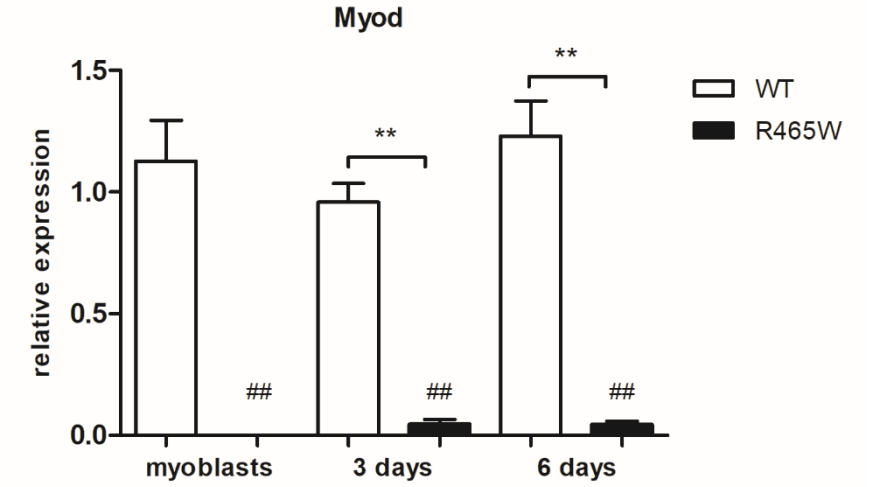

Figure 43 Relative expression of Myod gene in proliferating myoblasts and myotubes differentiated for three and six days. Relative expression calculated using $2^{-\Delta\Delta Ct}$ method, using WT myoblasts as the normalizer sample. Asterisks (*) denote differences between WT and R465W cells in the same condition, and number signs (#) in relation to WT myoblasts. Statistical analysis was performed using Mann-Whitney test; n=5 independent experiments; ** and ## p<0.01.

Finally, we quantified *Myog* expression and we found a reduced expression in R465W myoblasts. Following differentiation, there was an upregulation, but at lower rates in R465W myotubes (Figure 5).

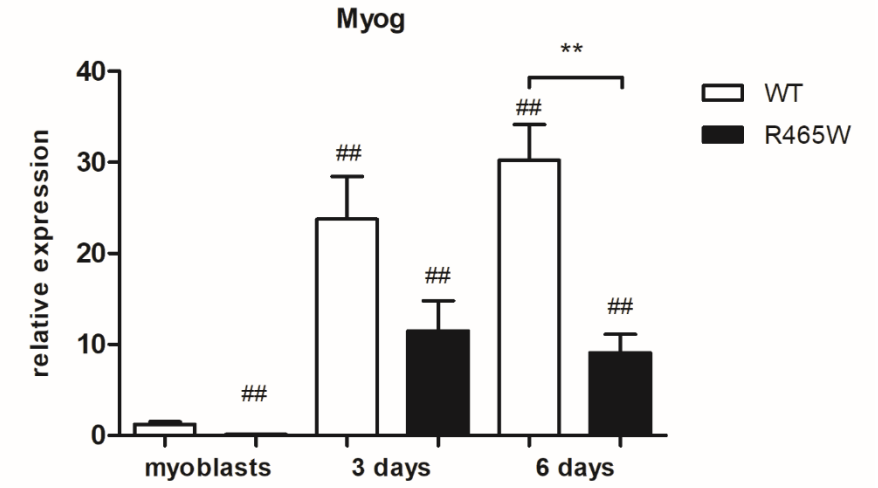

Figure 44 Relative expression of Myog gene in proliferating myoblasts and myotubes differentiated for three and six days. Relative expression was calculated using $2^{-\Delta\Delta Ct}$ method, using WT myoblasts as the normalizer sample. Asterisks (*) denote differences between WT and R465W cells in the same condition, and number signs (#) in relation to WT myoblasts. Statistical analysis was performed using Mann-Whitney test; n=5 independent experiments; ** and ## p<0.01.

Next, we evaluated the expression of the myogenic regulatory factors in human immortalized myoblasts harboring another DNM2 mutation; i.e. p.E650K, after myogenic differentiation for three and six days. Regarding the expression of *MYF5*, p.E650K myoblasts showed an increased expression in relation to control myoblasts. After the start of differentiation, *MYF5* mRNA levels dropped considerably, but they continued higher in E650K myotubes (Figure 6).

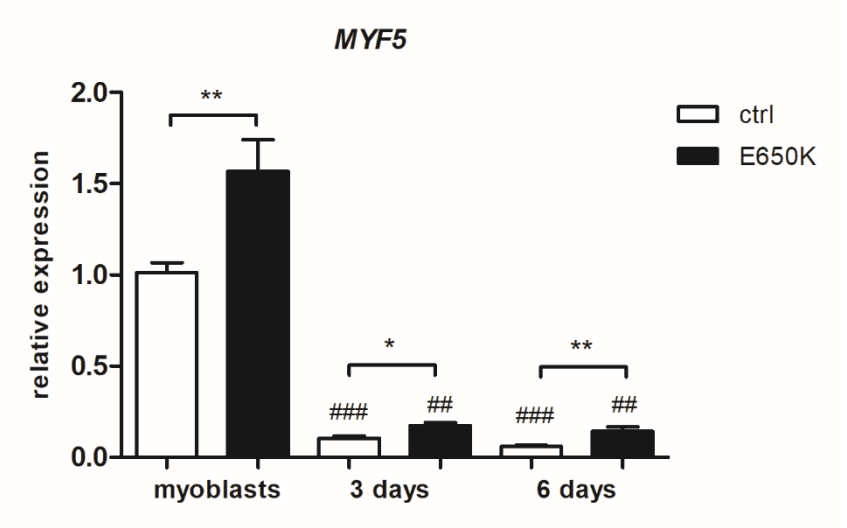

Figure 45 Relative expression of MYF5 gene in proliferating myoblasts and myotubes differentiated for three and six days. Relative expression was calculated using $2^{-\Delta\Delta Ct}$ method, using control myoblasts as the normalizer sample. Asterisks (*) denote differences in relation between control and E650K cells in the same condition and number signs (#) to control myoblasts. Statistical analysis was performed using Mann-Whitney test; n=4 independent experiments; *p<0.05, ** and ## p<0.01, *** and ### p<0.001.

MYOD gene showed no alteration in its expression after differentiation and no significant differences were found in p.E650K myoblasts in comparison to control cells (Figure 7).

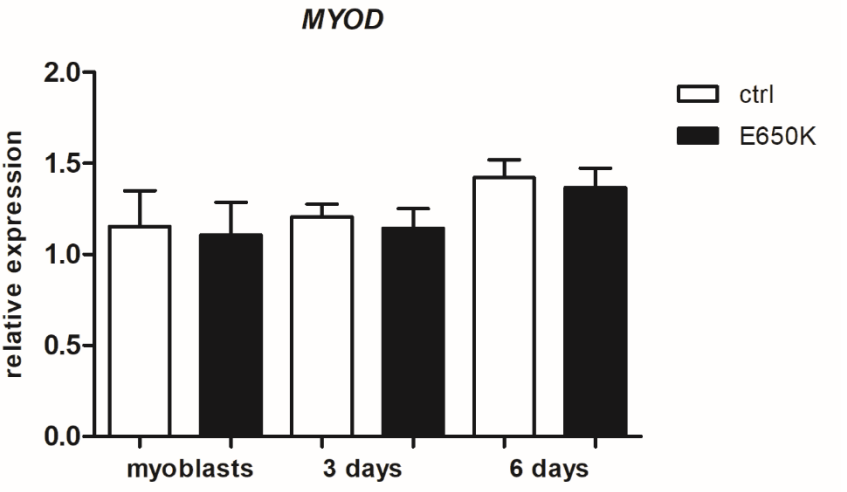

Figure 46 Relative expression of MYOD gene in proliferating myoblasts and myotubes differentiated for three and six days. Relative expression was calculated using $2^{-\Delta\Delta Ct}$ method, using control myoblasts as the normalizer sample. Statistical analysis was performed using Mann-Whitney test and no significant changes were found; n=4 independent experiments.

After differentiation, *MYOG* expression increased significantly in both control and E650K myotubes (Figure 8) but no change was noticed between WT and mutant cells.

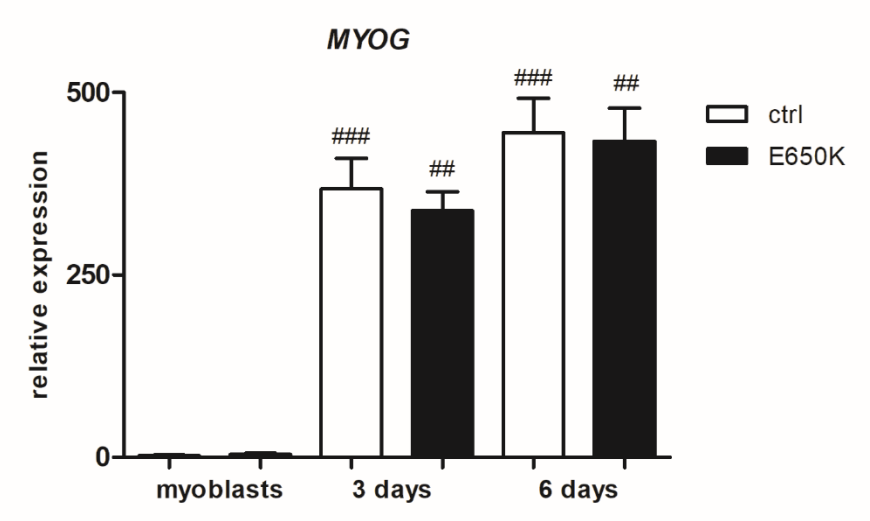

Figure 47 Relative expression of MYOG gene in proliferating myoblasts and myotubes differentiated for three and six days. Relative expression was calculated using $2^{-\Delta\Delta Ct}$ method, using control myoblasts as the normalizer sample. Number signs denote differences in relation to control myoblasts. Statistical analysis was performed using Mann-Whitney test; n=4 independent experiments; ## p<0.01, ### p<0.001.

To calculate the fusion index of control and E650K myoblast, we differentiated them at a high density, to ensure that differentiation process was started on confluent cells for both genotypes and to guarantee that they would not be able to proliferate. By doing this, we avoid higher or lower fusion indexes being influenced by differences in cell numbers or in proliferative capacity, under these conditions. First, we counted the number of myotubes formed, that is, the number of structures positive for myosin heavy chain staining present per field. The two control and the E650K lines were able the form equal numbers of myotubes (Figure 9).

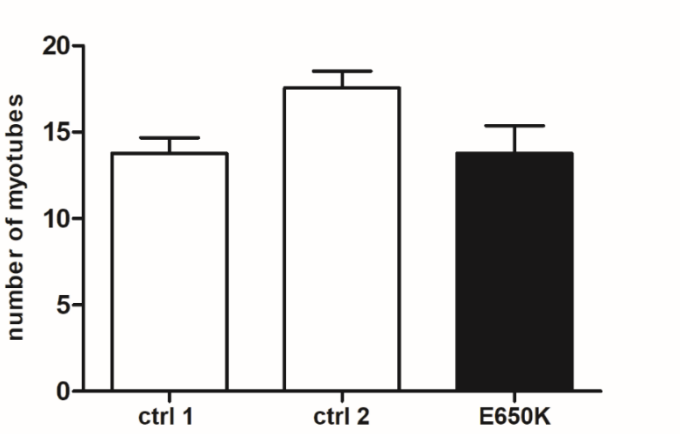

Figure 48 Average numbers of myotubes formed by control and E650K myoblasts after three days of differentiation started with cells plated at high density. No significant differences were found with one-way analysis of variance and Tukey's multiple-comparison test; data are presented as mean ± SEM; three independent experiments were performed independently.

The total fusion index was calculated by counting the total number of nuclei inside myotubes divided by the total number of nuclei present in the field. Control myotubes had a fusion index superior to 50%, while E650K showed a fusion index of about 20% after three days of differentiation (Figure 10).

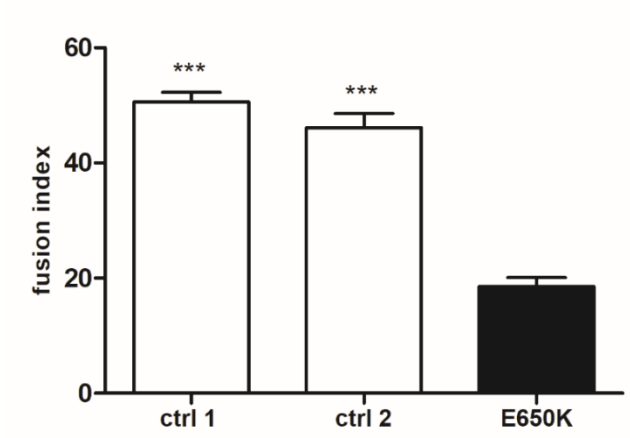

Figure 49 Total fusion index of control and E650K myoblasts after three days of differentiation started with cells plated at high density. Statistical differences calculated with Kruskal-Wallis test and post-hoc Dunn's multiple-comparison; asterisks correspond to differences between E650K and control cells; data are presented as mean ± SEM; three independent experiments were performed independently; ***p<0.001.

We also observed that the E650K myotubes were smaller and contained fewer nuclei (Figure 11). Then, we classified the myotubes according to the number of nuclei and we verified that the E650K myoblasts formed mainly smaller myotubes with two to six nuclei, and a small proportion of bigger myotubes with more than seven nuclei (less than 30% of myotubes), while the majority of myotubes contained more than seven nuclei in controls (Figure 12).

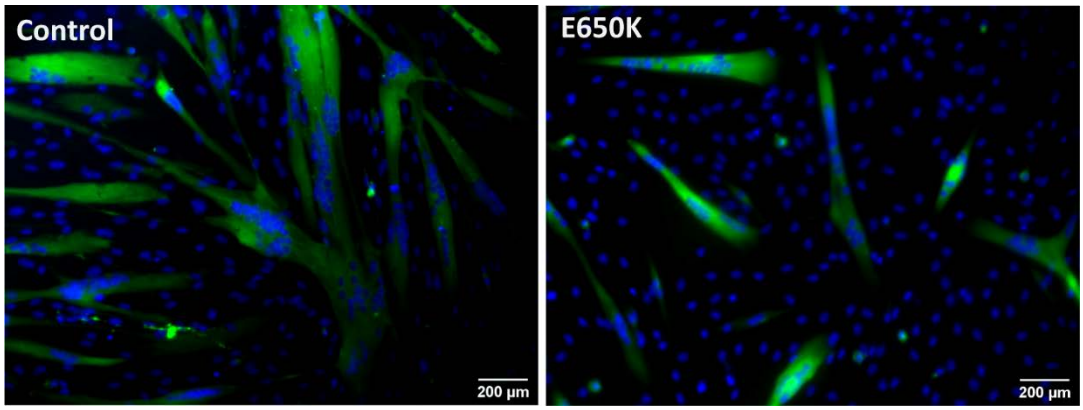

Figure 50 Representative images of control and E650K myotubes formed after three days of differentiation started with cells plated at high density. Nuclei in blue and pan-myosin heavy chain in green.

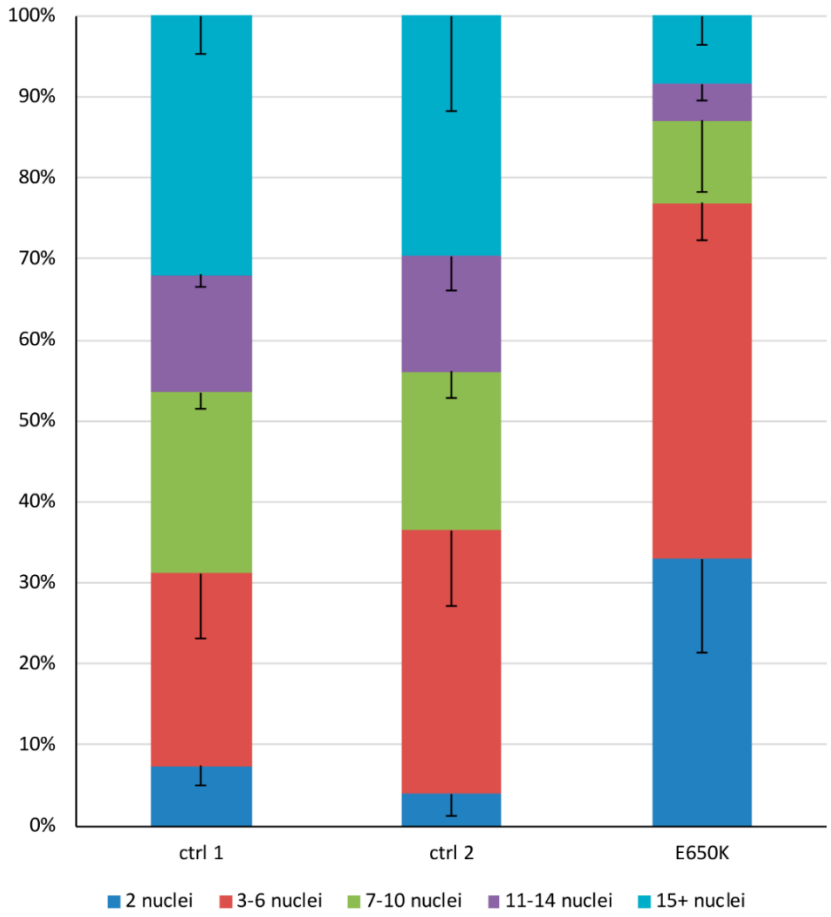

Figure 51 E650K myoblasts form mainly smaller myotubes containing two to six nuclei. Percentages of myotubes containing different numbers of nuclei. Data presented as mean ± SD. Three independent experiments were performed independently.

Cell migration assay

Dynamin 2 is involved in actin network dynamics. By its turn, actin remodeling is crucial for cell movements and migration. Based on these, we evaluated how myoblasts migrate during the proliferative stage to verify whether dynamin 2 mutations influence on cell migration properties. We recorded wild-type and mutated myoblasts for 72 hours and tracked individual cells. From their X; Y coordinates along time, we calculated the distance and the median speed, then we calculated for how long they were moving, how many times they paused and the duration of pauses.

The median speed developed by R465W and E650K mutated cells was reduced in comparison to control myoblasts. Consequently, both cells traveled shorter distances than control cells (Figure 13).

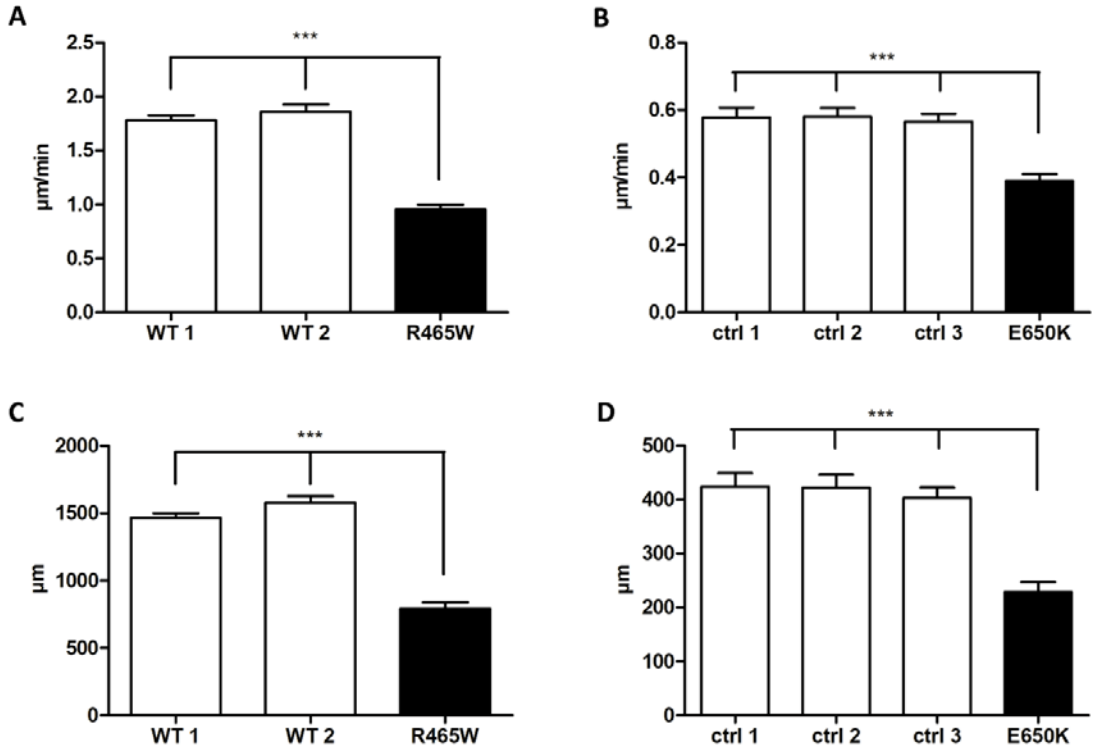

Figure 52 Cell migration assay. Median speed when moving and total distance traveled by mouse (A and C) and human (B and D) myoblasts. Statistical differences were assessed with Kruskal-Wallis test and post-hoc Dunn's multiple-comparison; asterisks correspond to differences between mutant and control cells; data are presented as mean ± SEM; two independent experiments were performed independently; n=40 to 42 cells of each line; ***p<0.001.

This reduced velocity and shorter coursed distance can be attributed to the following observations. The R465W and E650K myoblasts were in movement during a less percentage of the time analyzed in comparison to normal myoblasts (Figure 14).

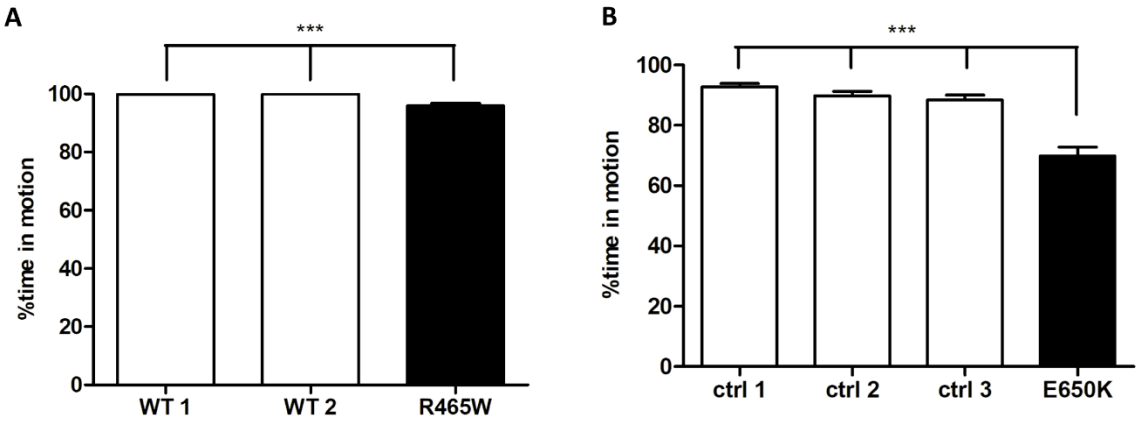

Figure 53 Cell migration assay. Percentage of time in motion of mouse (A) and human myoblasts (B). Statistical differences were assessed with Kruskal-Wallis test and post-hoc Dunn's multiple-comparison; asterisks correspond to differences between mutant and control cells; data are presented as mean ± SEM; two independent experiments were performed independently; n=40 to 42 cells of each line; ***p<0.001.

In addition, the number of pauses done by each cell and the time they stayed motionless are higher. Of note, the average pausing time for R465W cells was approximately 30 minutes, while for E650K cells this time was of 235 minutes (Figure 15).

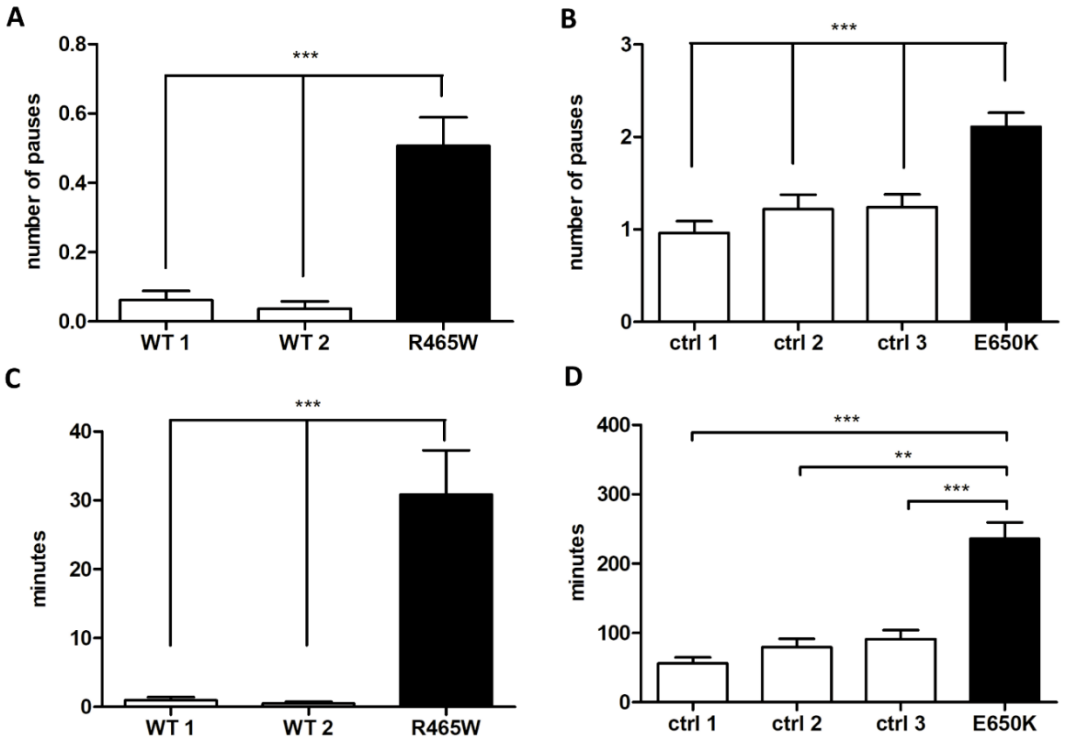

Figure 54 Cell migration assay. Number and duration of pauses made by mouse (A and C) and human (B and D) myoblasts. Statistical differences were assessed with Kruskal-Wallis test and post-hoc Dunn's multiple-comparison; asterisks correspond to differences between mutant and control cells; data are presented as mean ± SEM; two independent experiments were performed independently; n=40 to 42 cells of each line; **p<0.01, ***p<0.001.

Collectively, these experiments showed a new important phenotype caused by the mutations that can have a direct impact on muscle differentiation.

Transferrin and EGF endocytosis

We assessed the endocytosis capability of cultured immortalized myoblasts harboring the p.R465W and p.E650K DNM2 mutations. In mouse-derived p.R465W myoblasts, we found a significant increase in transferrin uptake as compared to two wild-type controls (Figure 16A). However, by visual observations, we suspected that R465W myoblasts were bigger than wild-type ones (Figure 16C). We measured their areas and found that R465W were indeed bigger what directly influences on endocytosis capability (Figure 16D). Thus, we divided fluorescence values by the cell area, to normalize transferrin uptake values. By doing this, transferrin uptake was decreased in R465W myoblasts (Figure 16B).

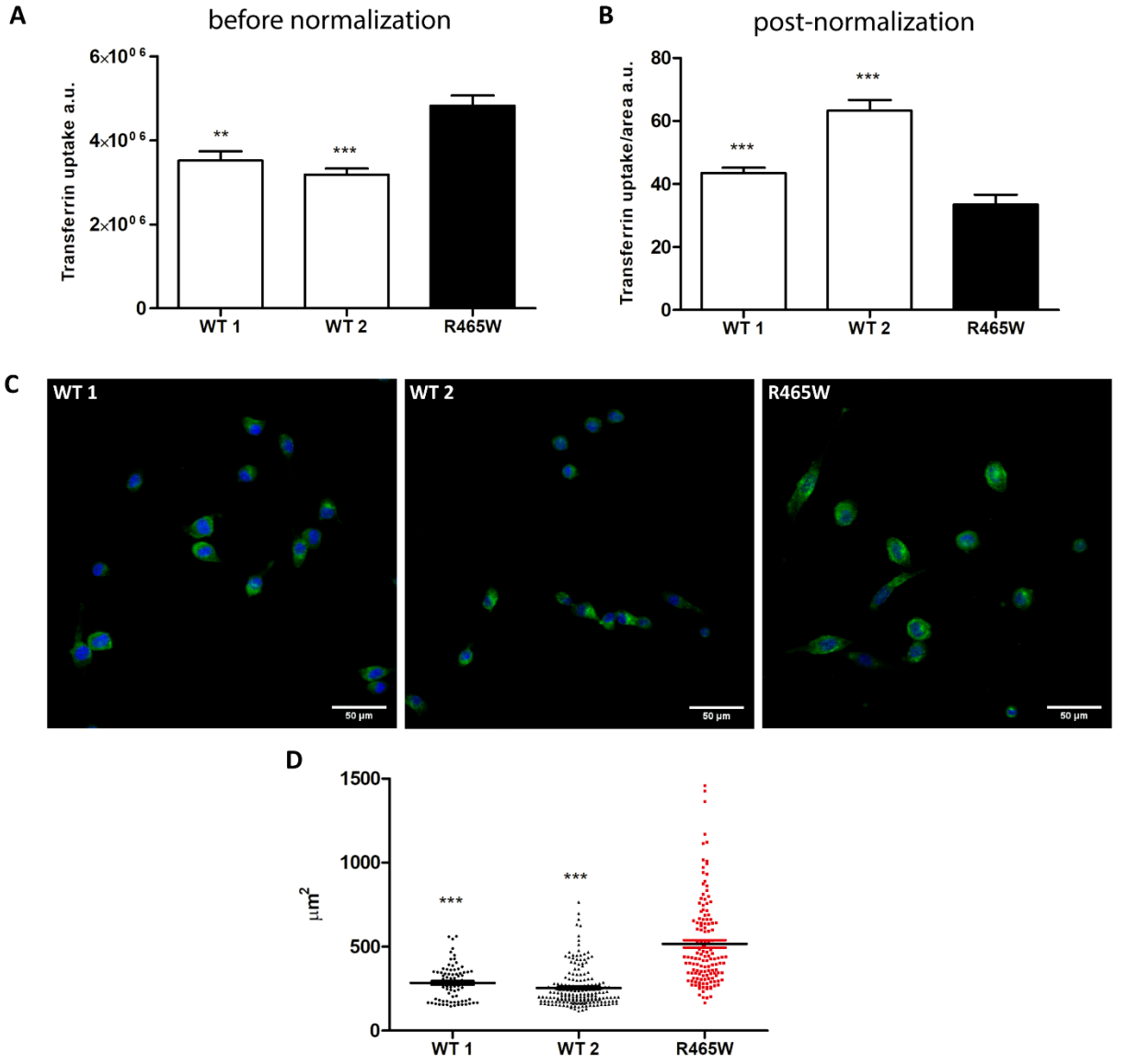

Figure 55 Endocytosis assay on p.R465W mutant myoblasts. (A) Transferrin uptake in murine p.R465W and WT immortalized myoblasts after 15 minutes of incubation before normalization. (B) Transferrin uptake normalized by cell surface area, showing decreased levels by mutant cells. (C) Confocal images of murine immortalized myoblasts. Fluorescent transferrin in green and DAPI in blue. Scale bar=50 µm. (D) Measurement of cell surface area confirmed that mutant myoblasts are bigger Data are presented as mean ± SEM; n=83 for WT1, n=187 for WT2, n=139 cells for R465W. Two experiments were performed independently. Asterisks denote differences between R465W and WT myoblasts calculated with Kruskal-Wallis test, post-hoc Dunn's multiple-comparison, ***p<0.001.

EGF receptor internalization occurs via both clathrin-dependent and independent endocytosis. In EGF uptake assay, we observed the same effect of cell size, the decrease was significant in relation to wild-type control 2 and equal to wild-type 1 (Figure 17).

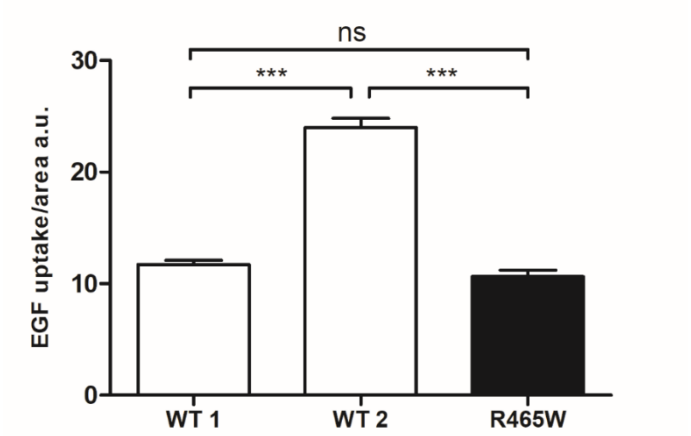

Figure 56 EGF uptake by murine p.R465W immortalized myoblasts after 15 minutes of incubation. Data are presented as mean ± SEM; n=174 for WT1, n=189 for WT2, n=162 cells for R465W. Two experiments were performed independently. Asterisks denote differences between R465W and WT myoblasts calculated with Kruskal-Wallis test, post-hoc Dunn's multiple-comparison, ***p<0.001, ns=non-significant.

We also quantified transferrin and EGF uptake in human-derived myoblasts bearing the p.E650K mutation compared to four different control cell lines. There was also variability on the cell's size, albeit not so discrepant as in murine cells. Thus, the fluorescence values were all normalized by the cell surface's area. In both assays, it is noteworthy the variability among the different control cell lines (Figure 18 and Figure 19).

In transferrin uptake assay, except for control 2, we saw a decreased transferrin uptake by E650K myoblasts, but there is variability among the controls (Figure 18).

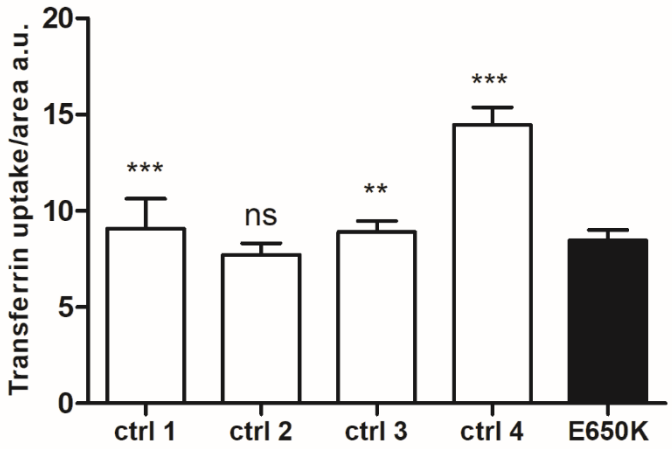

Figure 57 Transferrin uptake by human immortalized myoblasts after 15 minutes of incubation. Data are presented as mean ± SEM; n=196 for ctrl 1, n=189 for ctrl 2, n=113 cells for ctrl 3, n=245 for ctrl 4, n=365 for E650K cells. Four experiments were performed independently. Asterisks denote differences between E650K and control myoblasts calculated with Kruskal-Wallis test, post-hoc Dunn's multiple-comparison, ** p<0.01, ***p<0.001, ns=non-significant.

In EGF uptake assay, we found an increased EGF uptake by mutant myoblasts as compared to controls number 1 and 2. However, in comparison to controls number 3 and 4, E650K myoblasts showed a decreased and a normal EGF uptake, respectively (Figure 19).

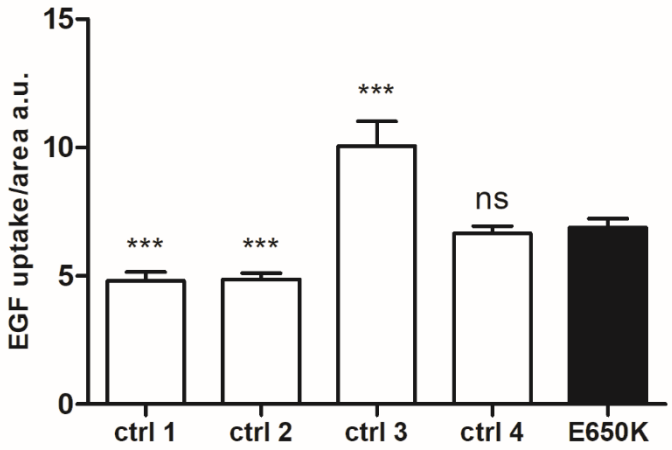

Figure 58 EGF uptake by human immortalized myoblasts after 15 minutes of incubation. Data are presented as mean ± SEM; n=306 for ctrl 1, n=333 for ctrl 2, n=276 cells for ctrl 3, n=315 for ctrl 4, n=290 for E650K cells. Four experiments were performed independently. Asterisks denote differences between E650K and control myoblasts calculated with Kruskal-Wallis test, post-hoc Dunn's multiple-comparison, ***p<0.001, ns=non-significant.

Thus, receptor endocytosis may be a variable process in human myoblasts, so, based on these results, we are not able to draw a definitive conclusion on the effect of the p.E650K mutation.

Discussion

Dynamin 2 is a large GTPase ubiquitously expressed that interacts with diverse proteins, then exerting many functions. Mutations in *DNM2* are the genetic cause of autosomal dominant centronuclear myopathy, a muscle disease characterized by the development of muscle weakness and central nuclei in muscle fibers. Several mechanisms and hypotheses have been proposed to explain the disease; however, the muscle-specific impact of the mutations is still not fully understood.

In this work, we sought to further explore the functional consequences of two DNM2 mutations located in two distinct domains, regarding the effects on myoblast differentiation, cell migration, and endocytosis rate.

Myogenic differentiation

Pax7 had reduced expression in R465W myoblasts as compared to WT cells, similarly to our results found in gastrocnemius muscle of HTZ mouse (Chapter 4 of this thesis). PAX7 is present not only in quiescent satellite cells but also during the proliferative stage promoting proliferation and influencing *Myod* expression (ZAMMIT, 2006). With the start of myoblast fusion, its expression is downregulated, as we observed in our analysis in WT and R465W cells, but at lower levels in R465W cells. Thus, the lower levels of *Pax7* seen in R465W mutant may limit the myogenic program as evidenced here by the altered expression of *Myod*. Alternatively, as *Pax7* downregulation was not statistically significant in WT cells, we cannot rule out that this is an effect of the mononuclear cells that were not induced to fuse or differentiated within the culture system.

The upregulation of *Myf5* in R465W cells after the start of differentiation was unexpected, since MYF5 usually is more active during the proliferative stage, as shown in C2C12 myoblasts (YOSHIDA et al., 1998), however, this could be a compensatory mechanism, since *Myod* depletion in mice stimulates *Myf5* upregulation (RUDNICKI et al., 1992). MYF5 is present in almost all quiescent satellite cells (BEAUCHAMP et al., 2000) and it is important to control the stemness of the satellite cell reserve pool (GAYRAUD-MOREL et al., 2013). But MYF5 also has a dual and apparently contradictory role by both defining muscle fate (VALDEZ et al., 2000) and is incompatible with differentiation (BEAUCHAMP et al., 2000). *Myod* expression remained constant in WT cells, while in R465W it was almost absent and only

slightly increased after differentiation. In C2C12 myoblasts, it was demonstrated that MYOD and MYF5 are regulated in a cell cycle-dependent manner: at G1 phase, which corresponds to the entry in differentiation, MYOD reaches its highest expression, whilst MYF5 expression is the lowest. In G0 (quiescent) stage, the opposite is observed: the highest MYF5 levels and absence of MYOD, leading to failed differentiation (KITZMANN et al., 1998). In the light of these facts about the activity of MYF5 and MYOD, although R465W myoblasts formed some myotubes and expressed myogenin at equal levels than WT cells, many cells still remained mononucleated in our cultures and these data are compatible with the upregulation of MYF5 and the very low expression of MYOD. In addition, *Myod* downregulation was observed in C2C12 myoblasts that constituted a reserve population in differentiating cultures (YOSHIDA et al., 1998), which might also be the case in our culture. In summary, as demonstrated by previous studies and here, the p.R465W mutation probably does not influence on fusion properties of mutated myoblasts, nevertheless, the altered expression on MRFs suggest that the myogenic potential may be disturbed.

In human E650K myoblasts, *MYOD* and *MYOG* had an expression equivalent to control values, indicating that the mutation does not interfere in these genes. However, E650K myoblasts showed a poor myogenicity *in vitro* evidenced by a reduced fusion index and predominance of smaller myotubes. Interestingly, MYF5 is upregulated in E650K myoblasts and persisted higher in relation to control cells even after the induction of differentiation. This may be behind the poor differentiation, as high levels of MYF5 were shown to impair the differentiation of C2C12 myoblasts (KITZMANN et al., 1998). Thus, the p.E650K mutation seems to have an inverted effect from the p.R465W mutation. The expression of regulatory factors is unchanged, except for *MYF5*, but the fusion is impacted, resulting in a reduced myogenic potential, as observed by the lower number of fused myoblasts, a lower fusion index and the presence of myoblasts with a smaller number of nuclei. These results are in accordance to previous studies in which it was demonstrated that dynamin 2 is important for myoblast fusion (CHUANG et al., 2019; LEIKINA et al., 2013; SHIN et al., 2014). For the first time, we are demonstrating that a disease-causing mutation on DNM2 might impact on myoblast fusion and differentiation. And even if the mechanisms are not exactly similar, both mutations are impairing the myogenic potential.

Cell migration assay

Cell migration involves the integration of several steps of assembly and disassembly of focal adhesions, cytoskeleton dynamics, and membrane remodeling. The migratory cycle can be summarized in the following steps: extension of the cellular protrusion, which is conducted by actin polymerization, formation of stable adhesions at the leading edge, translocation of the cell body forward and disassembly of adhesions and retraction of the rear cell's portion (WEBB; PARSONS; HORWITZ, 2002).

Cell migration requires continuous coordination of assembly and disassembly of several types of adhesions, including focal adhesions which have a central role in cell migration through dynamic regulation of extracellular matrix components and actin filaments. Focal adhesion disassembly must occur both at the leading edge and the cell's tail, and thus has a direct impact on the global speed of cell migration. The faster this process occurs, the faster the cell migrates. Dynamin 2 is a component of focal adhesions and has a key function in their disassembly by endocytosis (BRIÑAS et al., 2013). Besides its well-characterized role in endocytosis, dynamin 2 is also a known regulator of the actin cytoskeleton dynamics (LEE; DE CAMILLI, 2002; MOOREN et al., 2009; SCHAFER et al., 2002). Dynamin 2 binds to short actin filaments and then self-assembly around them, activating their catalytic activity. Following, dynamin 2 GTPase activity facilitates the elongation of actin filaments (GU et al., 2010).

Thus, in myoblasts bearing mutations in dynamin 2 gene the impairment in cell migration may arise from a reduced rate on focal adhesion disassembly and reduced actin polymerization. In the case of p.R465W, which is located in the middle domain, close to the actin-binding region, the interaction with actin was recently shown to be impaired and thus the start of actin polymerization (GONZÁLEZ-JAMETT et al., 2017), which is crucial for the extension of protrusion in migrating cells. Moreover, in focal adhesion disassembly during cell migration, β1-integrin is internalized via DNM2-dependent endocytosis (CHAO; KUNZ, 2009; EZRATTY et al., 2009), which we have shown to be impaired in our transferrin uptake assay, suggesting that migration may also be impaired by the defective endocytosis through an altered focal adhesion disassembly. The mutation p.E650K localizes to the GED domain, which is important to self-assembly and GTPase functions (SEVER; MUHLBERG; SCHMID, 1999), also necessary for actin filament elongation (GU et al., 2010). Thus, this mutation may also impair

migration by a similar mechanism, affecting the formation of actin filaments at the cell's protrusion.

R465W and E650K mutant myoblasts showed impaired migratory properties in our experiments, justified by dynamin 2 functions in actin network and focal adhesions. Furthermore, cell migration is a key step of myogenesis: myoblasts need to touch each other, change their morphology and fuse their membranes. Recently, DNM2 was shown to be required for myoblast fusion (LEIKINA et al., 2013; SHIN et al., 2014). The driving force that promotes myoblast fusion comes from the actin cytoskeleton (ABMAYR; PAVLATH, 2012), and a recent study revealed a structural function of DNM2 in invadosomes, where it acts in the formation of rigid actin bundles, cooperating for myoblast fusion (CHUANG et al., 2019). These functions of dynamin 2 and the limited myoblast fusion we verified in E650K myoblast are directly related, together with our findings on reduced satellite cell population and altered regeneration in CNM (Chapter 4 of this thesis), and can also have a participation in the pathophysiology of centronuclear myopathy.

Transferrin and EGF endocytosis

The classical function of dynamin 2 is to release nascent vesicle buds at the plasma membrane during clathrin-mediated endocytosis (CME) (FERGUSON; DE CAMILLI, 2012). The effects of mutations over this specific function of dynamin 2 have been a source of debate in the literature in the last years. In COS7 cells transfected with several DNM2 mutations, it was demonstrated a decrease in CME by transferrin uptake assay (BITOUN et al., 2009; KOUTSOPOULOS et al., 2011). In fibroblasts derived from AD-CNM patients with p.R465W mutation, the same decrease was also observed (ALI et al., 2019; BITOUN et al., 2009; TROCHET et al., 2018), although this was not confirmed by another study in which no alteration was observed in p.R465W and p.S619L fibroblasts (KOUTSOPOULOS et al., 2011). In contrast, in conditional *Dnm2* knock-out mouse fibroblasts, no alterations in transferrin were observed, but there was an impairment of clathrin-independent endocytosis of EGF receptor(LIU; LUKIYANCHUK; SCHMID, 2011). Whatever it is the case, the cellular models used in these studies were not the cell type affected in CNM, so to test this phenotype in myoblasts was still lacking.

We assessed transferrin and EGF uptake on mouse myoblasts with the most frequent mutation p.R465W located in the middle domain and on human myoblasts derived from a patient with p.E650K mutation located in the GED domain. At a first moment, we observed an increase in transferrin and EGF uptake by mouse myoblasts, in accordance to a study published while this present manuscript was in preparation (RABAI et al., 2019). Nevertheless, differently from Rabai and colleagues that measured transferrin uptake by a FACS approach, we used confocal images so we were able to visualize the size of the cell and we noticed that though they were obtained using the same technique, they have a significant difference in their surface area. Thus, we reasoned that this could have a direct impact on endocytosis capability, once a larger surface is an advantage. To compensate this difference, we normalized the fluorescence values by the cell area and we found that, in fact, transferrin uptake is decreased in p.R465W murine myoblasts.

The analysis of endocytosis on the p.E650K mutation showed a discrete reduction of transferrin uptake what could suggest that this mutation also alters clathrin-mediated endocytosis. However, the results for EGF uptake are discrepant, showing increased, decreased or equal endocytosis, depending on the control with they were compared to. Moreover, the four healthy human controls presented considerable variability among them. Thus, in view of the controversy in the literature and the variability of endocytosis measurement in the four control cell lines used in our study, our data are unable to conclude on the impact of the E650K mutation on clathrin-mediated endocytosis.

In conclusion, the p.R465W and p.E650K mutations have different impacts on fusion and expression of myogenic genes but with the same expected result which is a decrease in the myogenic capabilities. In addition, these mutations also alter cell migration, which is important to the formation and repair of muscle, probably via impairment of the actin network and potential defective endocytosis. Thus, our work provides important data for the comprehension of the muscle-specific impact of DNM2 mutations in centronuclear myopathies.

References

ABMAYR, S. M.; PAVLATH, G. K. Myoblast fusion: lessons from flies and mice. **Development**, v. 139, n. 4, p. 641–656, 2012.

ALI, T. et al. Correlative SICM-FCM reveals changes in morphology and kinetics of endocytic pits induced by disease-associated mutations in dynamin. **The FASEB Journal**, 2019.

BEAUCHAMP, J. R. et al. Expression of CD34 and Myf5 defines the majority of quiescent adult skeletal muscle satellite cells. **Journal of Cell Biology**, v. 151, n. 6, p. 1221–1233, 2000.

BITOUN, M. et al. Mutations in dynamin 2 cause dominant centronuclear myopathy. **Nature Genetics**, v. 37, n. 11, p. 1207–1209, 2005.

BITOUN, M. et al. Dynamin 2 mutations associated with human diseases impair clathrin-mediated receptor endocytosis. **Human Mutation**, v. 30, n. 10, p. 1419–1427, 2009.

BRIÑAS, L. et al. Role of dynamin 2 in the disassembly of focal adhesions. **Journal of Molecular Medicine**, v. 91, n. 7, p. 803–809, 2013.

CADOT, B.; GACHE, V.; GOMES, E. R. Fast, multi-dimensional and Simultaneous Kymograph-like Particle Dynamics (SkyPad) analysis. **PLoS ONE**, v. 9, n. 2, p. e89073, 2014.

CHAO, W. T.; KUNZ, J. Focal adhesion disassembly requires clathrin-dependent endocytosis of integrins. **FEBS Letters**, v. 583, n. 8, p. 1337–1343, 2009.

CHEN, Y.-J. et al. The stalk region of dynamin drives the constriction of dynamin tubes. **Nature Structural & Molecular Biology**, v. 11, n. 6, p. 574–575, 2004.

CHIN, Y. H. et al. Dynamin-2 mutations associated with centronuclear myopathy are hypermorphic and lead to T-tubule fragmentation. **Human Molecular Genetics**, v. 24, n. 19, p. 5542–5554, 2015.

CHUANG, M. C. et al. Tks5 and Dynamin-2 enhance actin bundle rigidity in invadosomes to promote myoblast fusion. **Journal of Cell Biology**, 2019.

COWLING, B. S. et al. Increased expression of wild-type or a centronuclear myopathy mutant of dynamin 2 in skeletal muscle of adult mice leads to structural defects and muscle weakness. **American Journal of Pathology**, v. 178, n. 5, p. 2224–2235, 2011.

DOWLING, J. J. et al. Myotubular myopathy and the neuromuscular junction: a novel therapeutic approach from mouse models. **Disease Models & Mechanisms**, v. 5, n. 6, p. 852–859, 1 nov. 2012.

DURIEUX, A. C. et al. A centronuclear myopathy-dynamin 2 mutation impairs skeletal muscle structure and function in mice. **Human Molecular Genetics**, v. 19, n. 24, p. 4820–4836, 2010.

ECHANIZ-LAGUNA, A. et al. Subtle central and peripheral nervous system abnormalities in a family with centronuclear myopathy and a novel dynamin 2 gene mutation. **Neuromuscular Disorders**, v. 17, n. 11–12, p. 955–959, 2007.

EZRATTY, E. J. et al. Clathrin mediates integrin endocytosis for focal adhesion disassembly in

migrating cells. **Journal of Cell Biology**, v. 187, n. 5, p. 733–747, 2009.

FERGUSON, S. M.; DE CAMILLI, P. Dynamin, a membrane-remodelling GTPase. **Nature Reviews Molecular Cell Biology**, v. 13, n. 2, p. 75–88, 2012.

FONGY, A. et al. Nuclear defects in skeletal muscle from a Dynamin 2-linked centronuclear myopathy mouse model. **Scientific Reports**, v. 9, 2019.

FRANCK, A. et al. Clathrin plaques and associated actin anchor intermediate filaments in skeletal muscle. **Molecular Biology of the Cell**, v. 30, n. 5, p. 579–590, 2019.

FRAYSSE, B.; GUICHENEY, P.; BITOUN, M. Calcium homeostasis alterations in a mouse model of the Dynamin 2-related centronuclear myopathy. **Biology Open**, v. 5, n. 11, p. 1691–1696, 2016.

GAYRAUD-MOREL, B. et al. Myf5 haploinsufficiency reveals distinct cell fate potentials for adult skeletal muscle stem cells. **Journal of Cell Science**, v. 125, n. 24, p. 6198–6198, 2013.

GIBBS, E. M. et al. Neuromuscular junction abnormalities in DNM2-related centronuclear myopathy. **Journal of Molecular Medicine**, v. 91, n. 6, p. 727–737, 2013.

GONZÁLEZ-JAMETT, A. M. et al. Dynamin-2 mutations linked to Centronuclear Myopathy impair actin-dependent trafficking in muscle cells. **Scientific Reports**, v. 7, n. 1, p. 4580, 4 dez. 2017.

GU, C. et al. Direct dynaming-actin interactions regulate the actin cytoskeleton. **EMBO Journal**, v. 29, n. 21, p. 3593–3606, 2010.

HEYMANN, J. A. W.; HINSHAW, J. E. Dynamins at a glance. **Journal of Cell Science**, v. 122, n. 19, p. 3427–3431, 2009.

HNIA, K. et al. Myotubularin controls desmin intermediate filament architecture and mitochondrial dynamics in human and mouse skeletal muscle. **Journal of Clinical Investigation**, v. 121, n. 1, p. 70–85, 2011.

JAMES, N. G. et al. A mutation associated with centronuclear myopathy enhances the size and stability of dynamin 2 complexes in cells. **Biochimica et Biophysica Acta - General Subjects**, v. 1840, n. 1, p. 315–321, 2014.

KENNISTON, J. A.; LEMMON, M. A. Dynamin GTPase regulation is altered by PH domain mutations found in centronuclear myopathy patients. **EMBO Journal**, v. 29, n. 18, p. 3054–3067, 2010.

KIERDASZUK, B. et al. A novel mutation in the DNM2 gene impairs dynamin 2 localization in skeletal muscle of a patient with late onset centronuclear myopathy. **Neuromuscular Disorders**, v. 23, n. 3, p. 219–228, 2013.

KITZMANN, M. et al. The muscle regulatory factors MyoD and Myf-5 undergo distinct cell cycle-specific expression in muscle cells. **Journal of Cell Biology**, v. 142, n. 6, p. 1447–1459, 1998.

KLEIN, D. E. et al. The pleckstrin homology domains of dynamin isoforms require

oligomerization for high affinity phosphoinositide binding. **Journal of Biological Chemistry**, v. 273, n. 42, p. 27725–27733, 1998.

KOUTSOPOULOS, O. S. et al. Mild functional differences of dynamin 2 mutations associated to centronuclear myopathy and charcot-marie-tooth peripheral neuropathy. **PLoS ONE**, v. 6, n. 11, 2011.

KOUTSOPOULOS, O. S. et al. Dynamin 2 homozygous mutation in humans with a lethal congenital syndrome. **European Journal of Human Genetics**, v. 21, n. 6, p. 637–642, 2013.

KUTCHUKIAN, C. et al. Impaired excitation–contraction coupling in muscle fibres from the dynamin2R465W mouse model of centronuclear myopathy. **Journal of Physiology**, v. 595, n. 24, p. 7369–7382, 2017.

LEE, E.; DE CAMILLI, P. Dynamin at actin tails. **Proceedings of the National Academy of Sciences**, v. 99, n. 1, p. 161–166, 2002.

LEIKINA, E. et al. Extracellular annexins and dynamin are important for sequential steps in myoblast fusion. **Journal of Cell Biology**, v. 200, n. 1, p. 109–123, 2013.

LIU, Y. W.; LUKIYANCHUK, V.; SCHMID, S. L. Common membrane trafficking defects of disease-associated dynamin 2 mutations. **Traffic**, v. 12, n. 11, p. 1620–1633, 2011.

MAMCHAOUI, K. et al. Immortalized pathological human myoblasts: Towards a universal tool for the study of neuromuscular disorders. **Skeletal Muscle**, v. 1, n. 34, 2011.

MOOREN, O. L. et al. Dynamin2 GTPase and cortactin remodel actin filaments. **Journal of Biological Chemistry**, v. 284, n. 36, p. 23995–24005, 2009.

RABAI, A. et al. Allele-specific CRISPR/Cas9 correction of a heterozygous DNM2 mutation rescues centronuclear myopathy cell phenotypes. **Molecular Therapy - Nucleic Acids**, 2019.

RAMACHANDRAN, R.; SCHMID, S. L. The dynamin superfamily. **Current Biology**, v. 28, n. 8, p. PR411-R416, 2018.

ROBB, S. A. et al. Impaired neuromuscular transmission and response to acetylcholinesterase inhibitors in centronuclear myopathies. **Neuromuscular Disorders**, v. 21, n. 6, p. 379–386, 2011.

ROMERO, N. B.; BITOUN, M. Centronuclear myopathies. **Seminars in Pediatric Neurology**, v. 18, p. 250–256, 2011.

RUDNICKI, M. A. et al. Inactivation of MyoD in mice leads to up-regulation of the myogenic HLH gene Myf-5 and results in apparently normal muscle development. **Cell**, v. 71, n. 3, p. 383–390, out. 1992.

SCHAFER, D. A. et al. Dynamin2 and cortactin regulate actin assembly and filament organization. **Current Biology**, v. 12, n. 21, p. 1852–1857, 2002.

SCHMITTGEN, T. D.; LIVAK, K. J. Analyzing real-time PCR data by the comparative CTmethod. **Nature Protocols**, v. 3, n. 6, p. 1101–1108, 2008.

SEVER, S.; MUHLBERG, A. B.; SCHMID, S. L. Impairment of dynamin's GAP domain stimulates receptor-mediated endocytosis receptor-mediated endocytosis. **Nature**, v. 398, n. 6727, p. 481–486, 1999.

SHIN, N. Y. et al. Dynamin and endocytosis are required for the fusion of osteoclasts and myoblasts. **Journal of Cell Biology**, v. 207, n. 1, p. 73–89, 2014.

SMIRNOVA, E. et al. A model for dynamin self-assembly based on binding between three different protein domains. **Journal of Biological Chemistry**, v. 274, n. 21, p. 14942–14947, 1999.

TINELLI, E.; PEREIRA, J. A.; SUTER, U. Muscle-specific function of the centronuclear myopathy and charcot-marie-tooth neuropathy associated dynamin 2 is required for proper lipid metabolism, mitochondria, muscle fibers, neuromuscular junctions and peripheral nerves. **Human Molecular Genetics**, v. 22, n. 21, p. 4417–4429, 2013.

TROCHET, D. et al. Allele-specific silencing therapy for Dynamin 2-related dominant centronuclear myopathy. **EMBO molecular medicine**, v. 10, p. 239–253, 2018.

VALDEZ, M. R. et al. Failure of Myf5 to support myogenic differentiation without myogenin, MyoD, and MRF4. **Developmental Biology**, v. 219, n. 2, p. 287–298, 2000.

WANG, L. et al. Dynamin 2 mutants linked to centronuclear myopathies form abnormally stable polymers. **Journal of Biological Chemistry**, v. 285, n. 30, p. 22753–22757, 2010.

WEBB, D. J.; PARSONS, J. T.; HORWITZ, A. F. Adhesion assembly, disassembly and turnover in migrating cells - Over and over and over again. **Nature Cell Biology**, v. 4, p. E97–E100, 2002.

YOSHIDA, N. et al. Cell heterogeneity upon myogenic differentiation: down-regulation of MyoD and Myf-5 generates "reserve cells". **Journal of cell science**, v. 111, n. Pt6, p. 769–779, 1998.

ZAMMIT, P. S. Pax7 and myogenic progression in skeletal muscle satellite cells. **Journal of Cell Science**, v. 119, n. 9, p. 1824–1832, 2006.

Supplementary information

Table 3 Sequences of primers

Gene	Forward	Reverse	Amplicon length (bp)
Csnk2a	CCATATTTCTACCCGGTGGTGA	GATTCCCCAGGCTTCATCGT	100
Myf5	CTGTCTGGTCCCGAAGAAC	GACGTGATCCGATCCACAATG	130
Myod	TACAGTGGCGACTCAGATGC	TAGTAGGCGGTGTCGTAGCC	116
Myog	CTGCACTCCCTTACGTCCAT	CCCAGCCTGACAGACAATCT	103
Pax7	GAGTTCGATTAGCCGAGTGC	GTGTTTGGCTTTCTTCTCGC	100
Tgfb	CCCCACTGATACGCCTGAGT	AGCCCTGTATTCCGTCTCCTT	86
MYOD	TGCCACAACGGACGACTTC	CGGGTCCAGGTCTTCGAA	76
MYF5	CTCAGCAGGATGGACGTGAT	TATGCAGGAGCCGTCGTA	72
MYOG	CAGTGCCATCCAGTACATCG	AAGTTGTGGGCATCTGTAGG	225
RPLPO	GGATTACACCTTCCCACTTGCT	GCCACAAAGGCAGATGGATCA	66

VII. Chapter 7 - Final discussion and conclusions

In the present work, we investigated the regenerative potential and myogenic properties, as well as the functional aspects in the context of DNM2-related centronuclear myopathy.

The muscle regenerative potential is one of the most outstanding characteristics of this tissue. This process has been the subject of many works for many decades and there is still a lot to be unveiled in healthy and disease conditions. One important used approach to study muscle regeneration is by causing acute injury and flowing the subsequent cellular and molecular events. Acute lesions can be provoked either by chemicals, toxins or physical methods. Important differences have been revealed between them, highlighting the importance to carefully choose one method over the other, although the outcome can seem similar (HARDY et al., 2016).

Studies on gene therapy showed that the electroporation employed to DNA delivery on muscles have as a side effect an important muscle lesion (BALIGAND et al., 2012). Based on this, in Chapter 4, we presented the protocol we standardized to take benefit of this to induce muscle injury to the study of the regeneration events in muscle systems in which this mechanism is not activated. Our protocol showed to be simple to execute and efficient to provoke muscle degeneration and regeneration. With this system, we offer another alternative into the hall of injury methodologies that exclude the use of chemical compounds or toxins that may have off-target effects.

Dynamin 2 protein is expressed in all tissues, exerting diverse functions primarily related to membrane remodeling, especially on endocytosis, intracellular trafficking of membranes, and cytoskeleton dynamics. Mutations in the *DNM2* gene are linked to autosomal dominant centronuclear myopathy (AD-CNM), a disease that causes muscle weakness and mispositioning of nuclei in muscle fibers. Although many studies have already been published on the pathophysiological mechanisms of this disease, there is still lacking a comprehensive explanation for the muscle-specific impact of the mutations.

Defects in satellite cells population are an important component of several neuromuscular disorders. In the group of centronuclear myopathies, alterations in the biology

of satellite cells were found in X-linked myotubular myopathy, both in the animal model and muscle from human patients (LAWLOR et al., 2012). In a recent publication, it was found that the number of satellite cells is reduced in the tibialis anterior muscle of the KI-*Dnm2*^{R465W} mouse, the animal model for AD-CNM. But the functional consequences were not further explored.

In chapter 5, based on these observations, we sought the explore whether the regenerative capacity of KI-*Dnm2*^{R465W} mouse is compromised. For this, we used our protocol of muscle injury by electroporation and cardiotoxin injection to provoke muscle degeneration in the gastrocnemius muscle of KI-*Dnm2*^{R465W} (HTZ). We assessed histological parameters and the expression of genes important for muscle development and satellite cells function.

First, we saw that muscle mass after the lesion was reduced in HTZ and did not recover to normal values like in WT. In addition, the size and density of muscle fibers are decreased and not equivalent to healthy muscles. As a consequence, part of the muscle was replaced by fibrotic tissue, as evidenced by collagen deposition quantification. The number of new regenerating myofibers was also decreased in HTZ muscle, verified by the quantification of fibers expressing developmental myosin heavy chain.

We also quantified *Pax7* mRNA in the gastrocnemius muscles of KI-*Dnm2*^{R465W} mice and we found a reduction of 70% in its relative expression, as a result of the decreased number of satellite cells that we also quantified in muscle sections. Next, we measured the expression of the myogenic regulatory factors in injured muscles and we found that in HTZ animals they are all downregulated, suggesting that the regeneration in these mice is compromised. Moreover, the expression of *Spry1*, a regulator of quiescence, is upregulated in HTZ mice, suggesting that besides the reduced number of satellite cells, the muscle regeneration may also be impaired by a mechanism to maintain quiescence of its muscle stem cells. Taken together, our data provide evidence that dynamin 2 mutation also impacts on satellite cells and this impairs muscle regeneration, thus adding satellite cells defects as a pathophysiological component of AD-CNM.

In Chapter 6, we presented the functional consequences of two *DNM2* mutations on the myogenic potential of myoblasts *in vitro* system. For this, we used immortalized myoblasts obtained from the HTZ mouse, bearing the p.R465W mutation, and from a human patient

carrying the mutation p.E650K. First, the expression analysis of genes related to the myogenic program showed that, despite an apparently normal fusion, p.R465W myoblasts have an altered expression of *Pax7, Myf5, Myod,* and *Myog* genes as compared to WT cells, suggesting that the differentiation is somehow disturbed. Differently, p.E650K myoblasts showed, in general, a normal expression of myogenesis markers. However, we verified that they fused less, forming smaller myotubes.

Cell migration is an important step for myoblast fusion. So, we hypothesized that this property could be impaired in the mutated myoblasts. Indeed, we found that these cells developed a reduced speed and consequent coursed shorter distances in our migration assay. This was an additional phenotype that may be contributing to the reduced myogenic potential, given the role of dynamin 2 on actin dynamics and focal adhesion disassembly through endocytosis.

Finally, we tested the endocytosis capability on the mutant myoblasts, since this analysis has been made mostly on fibroblasts or other cell types and data from myoblasts was lacking. In the p.R465W myoblasts, we found a reduced endocytosis rate as compared to normal cells, in opposition to a recent publication in which it was described increased endocytosis (RABAI et al., 2019). Here, we used a different assay to measure the internalization of membrane receptors, but we also considered the size of the cells, which can account to the discrepancies between both studies. In p.E650K myoblasts, we verified a great variability among control cells, leading to the interpretation that significant alteration in the endocytosis process under the effect of this mutation could not be considered. Thus, the effect on endocytosis could be mutation-dependent, probably due to the different functions of the domains on which they localize. In the literature, there is a lot of controversy about the effects of DNM2 mutations in endocytosis, with some studies pointing to increased, normal or reduced endocytosis. The debate may persist for a while, but regarding the myogenic potential of the cells, our results can also be indirect evidence that an alteration in endocytosis is affecting cell migration, through an altered focal adhesion disassembly.

Collectively, our data support our hypothesis that dynamin 2 has a muscle-specific role, with important participation on satellite cells and myoblast differentiation, and these functions are impaired by mutations in centronuclear myopathies, contributing to the

development of the disease. Further studies are necessary to better explore the cellular and molecular mechanisms by which dynamin 2 participates on satellite cells biology.

VIII. References[2]

AGRAWAL, P. B. et al. SPEG interacts with myotubularin, and its deficiency causes centronuclear myopathy with dilated cardiomyopathy. **American Journal of Human Genetics**, v. 95, n. 2, p. 218–226, 2014.

AL-QUSAIRI, L. et al. T-tubule disorganization and defective excitation-contraction coupling in muscle fibers lacking myotubularin lipid phosphatase. **Proceedings of the National Academy of Sciences**, v. 106, n. 44, p. 18763–18768, 2009.

AL-QUSAIRI, L. et al. Lack of myotubularin (MTM1) leads to muscle hypotrophy through unbalanced regulation of the autophagy and ubiquitin-proteasome pathways. **FASEB Journal**, v. 27, n. 8, p. 3384–3394, 2013.

ALLBROOK, D. B.; HAN, M. F.; HELLMUTH, A. E. Population of Muscle Satellite Cells in Relation to Age and Mitotic Activity. **Pathology**, v. 3, n. 3, p. 233–243, 2007.

ALMEIDA, C. F. et al. Muscle satellite cells: Exploring the basic biology to rule them. **Stem Cells International**, v. 2016, 2016.

ANDRESEN, B. T. et al. The role of phosphatidic acid in the regulation of the Ras/MEK/Erk signaling cascade. **FEBS Letters**, v. 531, n. 1, p. 65–68, 2002.

ANTONNY, B. et al. Membrane fission by dynamin: what we know and what we need to know. **The EMBO Journal**, v. 34, n. 1, p. 81–86, 2016.

ASFOUR, H. A.; ALLOUH, M. Z.; SAID, R. S. Myogenic regulatory factors: The orchestrators of myogenesis after 30 years of discovery. **Experimental Biology and Medicine**, v. 243, n. 2, p. 118–128, 2018.

BALIGAND, C. et al. Multiparametric functional nuclear magnetic resonance imaging shows alterations associated with plasmid electrotransfer in mouse skeletal muscle. **Journal of Gene Medicine**, 2012.

BANKHEAD, P. et al. QuPath: Open source software for digital pathology image analysis. **Scientific Reports**, v. 7, n. 1, 2017.

BERKES, C. A.; TAPSCOTT, S. J. MyoD and the transcriptional control of myogenesis. **Seminars in Cell and Developmental Biology**, v. 16, n. 4–5, p. 585–595, 2005.

BEVILACQUA, J. A. et al. Recessive RYR1 mutations cause unusual congenital myopathy with prominent nuclear internalization and large areas of myofibrillar disorganization. **Neuropathology and Applied Neurobiology**, v. 37, n. 3, p. 271–284, 2011.

BIANCALANA, V. et al. Characterisation of mutations in 77 patients with X-linked myotubular myopathy, including a family with a very mild phenotype. **Human genetics**, v. 112, n. 2, p. 135–142, 2003.

BIGOT, A. et al. Age-Associated Methylation Suppresses SPRY1, Leading to a Failure of Re-quiescence and Loss of the Reserve Stem Cell Pool in Elderly Muscle. **Cell Reports**, v. 13, n. 6,

[2] In accordance to Associação Brasileira de Normas Técnicas (ABNT NBR 6023).

p. 1172–1182, 2015.

BISCHOFF, R.; HEINTZ, C. Enhancement of skeletal muscle regeneration. **Developmental Dynamics**, v. 201, n. 1, p. 41–54, 1994.

BITOUN, M. et al. Mutations in dynamin 2 cause dominant centronuclear myopathy. **Nature Genetics**, v. 37, n. 11, p. 1207–1209, 2005.

BITOUN, M. et al. Dynamin 2 mutations cause sporadic centronuclear myopathy with neonatal onset. **Annals of Neurology**, v. 62, n. 6, p. 666–670, 2007.

BITOUN, M. et al. Dynamin 2 mutations associated with human diseases impair clathrin-mediated receptor endocytosis. **Human Mutation**, v. 30, n. 10, p. 1419–1427, 2009.

BJORNSON, C. R. R. et al. Notch signaling is necessary to maintain quiescence in adult muscle stem cells. **Stem Cells**, v. 30, n. 2, p. 232–242, 2012.

BLONDEAU, F. et al. Myotubularin, a phosphatase deficient in myotubular myopathy, acts on phosphatidylinositol 3-kinase and phosphatidylinositol 3-phosphate pathway. **Human Molecular Genetics**, v. 9, n. 15, p. 2223–2229, 2000.

BÖHM, J. et al. Mutation spectrum in the large gtpase dynamin 2, and genotype-phenotype correlation in autosomal dominant centronuclear myopathy. **Human Mutation**, v. 33, n. 6, p. 949–959, 2012.

BÖHM, J. et al. Adult-onset autosomal dominant centronuclear myopathy due to BIN1 mutations. **Brain**, v. 137, n. 12, p. 3160–3170, 2014.

BRAUN, T. et al. Targeted inactivation of the muscle regulatory gene Myf-5 results in abnormal rib development and perinatal death. **Cell**, v. 71, n. 3, p. 369–382, 1992.

BRUNELLI, S.; ROVERE-QUERINI, P. The immune system and the repair of skeletal muscle. **Pharmacological Research**, v. 58, n. 2, p. 117–121, 2008.

BRUUSGAARD, J. C. et al. Number and spatial distribution of nuclei in the muscle fibres of normal mice studied in vivo. **Journal of Physiology**, v. 551, n. 2, p. 467–478, 2003.

BUAS, M. F.; KADESCH, T. Regulation of skeletal myogenesis by Notch. **Experimental Cell Research**, v. 316, n. 18, p. 3028–3033, 2010.

BUCKINGHAM, M. Gene regulatory networks and cell lineages that underlie the formation of skeletal muscle. **Proceedings of the National Academy of Sciences**, v. 114, n. 23, p. 5830–5837, 2017.

BUJ-BELLO, A. et al. The lipid phosphatase myotubularin is essential for skeletal muscle maintenance but not for myogenesis in mice. **Proceedings of the National Academy of Sciences**, v. 99, n. 23, p. 15060–15065, 2002.

CADOT, B.; GACHE, V.; GOMES, E. R. Moving and positioning the nucleus in skeletal muscle-one step at a time. **Nucleus**, v. 6, n. 5, p. 373–381, 2015.

CARMIGNAC, V. et al. C-terminal titin deletions cause a novel early-onset myopathy with fatal

cardiomyopathy. **Annals of Neurology**, v. 61, n. 4, p. 340–351, 2007.

CEYHAN-BIRSOY, O. et al. Recessive truncating titin gene, TTN, mutations presenting as centronuclear myopathy. **Neurology**, v. 81, n. 14, p. 1205–1214, 2013.

CHAL, J.; POURQUIÉ, O. Making muscle: skeletal myogenesis in vivo and in vitro. **Development**, v. 144, n. 12, p. 2104–2122, 2017.

CHARGÉ, S. B. P.; RUDNICKI, M. A. Cellular and Molecular Regulation of Muscle Regeneration. **Physiological Reviews**, v. 84, n. 1, p. 209–238, 2004.

CHEN, Y.-J. et al. The stalk region of dynamin drives the constriction of dynamin tubes. **Nature Structural & Molecular Biology**, v. 11, n. 6, p. 574–575, 2004.

CHIN, Y. H. et al. Dynamin-2 mutations associated with centronuclear myopathy are hypermorphic and lead to T-tubule fragmentation. **Human Molecular Genetics**, v. 24, n. 19, p. 5542–5554, 2015.

CLAEYS, K. G. et al. PHENOTYPE OF A PATIENT WITH RECESSIVE CENTRONUCLEAR MYOPATHY AND A NOVEL BIN1 MUTATION. **Neurology**, v. 74, n. 6, p. 519–521, 9 fev. 2010.

CLARK, K. A. et al. Striated Muscle Cytoarchitecture: An Intricate Web of Form and Function. **Annual Review of Cell and Developmental Biology**, v. 18, n. 1, p. 637–706, 2002.

CLARK, S. G. et al. A dynamin GTPase mutation causes a rapid and reversible temperature-inducible locomotion defect in C. elegans. **Proceedings of the National Academy of Sciences**, v. 94, n. 19, p. 10438–10443, 16 set. 1997.

CONBOY, I. M.; RANDO, T. A. The Regulation of Notch Signaling Controls Satellite Cell Activation and Cell Fate Determination in Postnatal Myogenesis. **Developmental Cell**, v. 3, n. 3, p. 397–409, set. 2002.

COWLING, B. S. et al. Increased expression of wild-type or a centronuclear myopathy mutant of dynamin 2 in skeletal muscle of adult mice leads to structural defects and muscle weakness. **American Journal of Pathology**, v. 178, n. 5, p. 2224–2235, 2011.

COWLING, B. S. et al. Defective membrane remodeling in neuromuscular diseases: Insights from animal models. **PLoS Genetics**, v. 8, n. 4, p. e1002595, 2012.

COWLING, B. S. et al. Reducing dynamin 2 expression rescues X-linked centronuclear myopathy. **Journal of Clinical Investigation**, v. 124, n. 3, p. 1350–1363, 2014.

COWLING, B. S. et al. Amphiphysin (BIN1) negatively regulates dynamin 2 for normal muscle maturation. **Journal of Clinical Investigation**, v. 127, n. 12, p. 4477–4487, 2017.

CRIST, C. G.; MONTARRAS, D.; BUCKINGHAM, M. Muscle satellite cells are primed for myogenesis but maintain quiescence with sequestration of Myf5 mRNA targeted by microRNA-31 in mRNP granules. **Cell Stem Cell**, v. 11, n. 1, p. 118–126, 2012.

DIATLOFF-ZITO, C. et al. Isolation of an ubiquitously expressed cDNA encoding human dynamin II, a member of the large GTP-binding protein family. **Gene**, v. 163, n. 2, p. 301–306, out. 1995.

DOWLING, J. J. et al. Loss of myotubularin function results in T-tubule disorganization in zebrafish and human myotubular myopathy. **PLoS Genetics**, v. 5, n. 2, 2009.

DOWLING, J. J. et al. Myotubular myopathy and the neuromuscular junction: a novel therapeutic approach from mouse models. **Disease Models & Mechanisms**, v. 5, n. 6, p. 852–859, 1 nov. 2012.

DUMONT, N. A. et al. Dystrophin expression in muscle stem cells regulates their polarity and asymmetric division. **Nature Medicine**, v. 21, n. 12, p. 1455–1463, 2015.

DURIEUX, A. C. et al. Dynamin 2 and human diseases. **Journal of Molecular Medicine**, v. 88, n. 4, p. 339–350, 2010a.

DURIEUX, A. C. et al. A centronuclear myopathy-dynamin 2 mutation impairs skeletal muscle structure and function in mice. **Human Molecular Genetics**, v. 19, n. 24, p. 4820–4836, 2010b.

DURIEUX, A. C. et al. A Centronuclear Myopathy - Dynamin 2 Mutation Impairs Autophagy in Mice. **Traffic**, v. 13, n. 6, p. 869–879, 2012.

DYE, D. E. et al. Novel slow-skeletal myosin (MYH7) mutation in the original myosin storage myopathy kindred. **Neuromuscular Disorders**, v. 16, n. 6, p. 357–360, jun. 2006.

ECHANIZ-LAGUNA, A. et al. Subtle central and peripheral nervous system abnormalities in a family with centronuclear myopathy and a novel dynamin 2 gene mutation. **Neuromuscular Disorders**, v. 17, n. 11–12, p. 955–959, 2007.

ERVASTI, J. M. A role for the dystrophin-glycoprotein complex as a transmembrane linker between laminin and actin. **The Journal of Cell Biology**, v. 122, n. 4, p. 809–823, 1 ago. 1993.

FERGUSON, S. et al. Coordinated Actions of Actin and BAR Proteins Upstream of Dynamin at Endocytic Clathrin-Coated Pits. **Developmental Cell**, v. 17, n. 6, p. 811–822, 2009.

FETALVERO, K. M. et al. Defective Autophagy and mTORC1 Signaling in Myotubularin Null Mice. **Molecular and Cellular Biology**, v. 33, n. 1, p. 98–110, 2013.

FISCHER, D. et al. Characterization of the muscle involvement in dynamin 2-related centronuclear myopathy. **Brain**, v. 129, n. 6, p. 1463–1469, 2006.

FONGY, A. et al. Nuclear defects in skeletal muscle from a Dynamin 2-linked centronuclear myopathy mouse model. **Scientific Reports**, v. 9, 2019.

FRANCK, A. et al. Clathrin plaques and associated actin anchor intermediate filaments in skeletal muscle. **Molecular Biology of the Cell**, v. 30, n. 5, p. 579–590, 2019.

FRAYSSE, B.; GUICHENEY, P.; BITOUN, M. Calcium homeostasis alterations in a mouse model of the Dynamin 2-related centronuclear myopathy. **Biology Open**, v. 5, n. 11, p. 1691–1696, 2016.

FRONTERA, W. R.; OCHALA, J. Skeletal Muscle: A Brief Review of Structure and Function. **Behavior Genetics**, v. 45, n. 2, p. 183–195, 2015.

FUKADA, S. et al. Molecular Signature of Quiescent Satellite Cells in Adult Skeletal Muscle.

Stem Cells, v. 25, n. 10, p. 2448–2459, 2007.

GARRY, G. A.; ANTONY, M. L.; GARRY, D. J. Cardiotoxin induced injury and skeletal muscle regeneration. **Methods in Molecular Biology**, v. 1460, p. 61–71, 2016.

GAYRAUD-MOREL, B. et al. A role for the myogenic determination gene Myf5 in adult regenerative myogenesis. **Developmental Biology**, v. 312, n. 1, p. 13–28, 2007.

GIBBS, E. M. et al. Neuromuscular junction abnormalities in DNM2-related centronuclear myopathy. **Journal of Molecular Medicine**, v. 91, n. 6, p. 727–737, 2013.

GIBBS, E. M. et al. The myopathy-causing mutation DNM2-S619L leads to defective tubulation in vitro and in developing zebrafish. **Disease Models & Mechanisms**, v. 7, n. 1, p. 157–161, 2014.

GONZÁLEZ-JAMETT, A. M. et al. Dynamin-2 mutations linked to Centronuclear Myopathy impair actin-dependent trafficking in muscle cells. **Scientific Reports**, v. 7, n. 1, p. 4580, 4 dez. 2017.

GOPINATH, S. D. et al. FOXO3 promotes quiescence in adult muscle stem cells during the process of self-renewal. **Stem Cell Reports**, v. 2, n. 4, p. 414–426, 2014.

GROUNDS, M. D. The need to more precisely define aspects of skeletal muscle regeneration. **International Journal of Biochemistry and Cell Biology**, v. 56, p. 56–65, 2014.

GU, C. et al. Direct dynaming-actin interactions regulate the actin cytoskeleton. **EMBO Journal**, v. 29, n. 21, p. 3593–3606, 2010.

GUREVICH, D. B. et al. Asymmetric division of clonal muscle stem cells coordinates muscle regeneration in vivo. **Science**, v. 353, n. 6295, p. aad9969-aad9969, 8 jul. 2016.

HALEVY, O. et al. Pattern of Pax7 expression during myogenesis in the posthatch chicken establishes a model for satellite cell differentiation and renewal. **Developmental Dynamics**, v. 231, n. 3, p. 489–502, nov. 2004.

HANISCH, F. et al. Phenotype variability and histopathological findings in centronuclear myopathy due to DNM2 mutations. **Journal of Neurology**, v. 258, n. 6, p. 1085–1090, 2011.

HARDY, D. et al. Comparative Study of Injury Models for Studying Muscle Regeneration in Mice. **PloS one**, v. 11, n. 1, p. e0147198, 2016.

HASTY, P. et al. Muscle deficiency and neonatal death in mice with a targeted mutation in the myogenin gene. **Nature**, v. 364, n. 6437, p. 501–506, 1993.

HAUSBURG, M. A. et al. Post-transcriptional regulation of satellite cell quiescence by TTP-mediated mRNA decay. **eLife**, v. 2015, n. 4, p. 1–18, 2015.

HERMAN, G. E. et al. Characterization of mutations in fifty North American patients with X-linked myotubular myopathy. **Human Mutation**, v. 19, n. 2, p. 114–121, fev. 2002.

HERNÁNDEZ-HERNÁNDEZ, J. M. et al. The myogenic regulatory factors, determinants of muscle development, cell identity and regeneration. **Seminars in Cell & Developmental**

Biology, v. 72, p. 10–18, dez. 2017.

HEYMANN, J. A. W.; HINSHAW, J. E. Dynamins at a glance. **Journal of Cell Science**, v. 122, n. 19, p. 3427–3431, 2009.

HNIA, K. et al. Myotubularin controls desmin intermediate filament architecture and mitochondrial dynamics in human and mouse skeletal muscle. **Journal of Clinical Investigation**, v. 121, n. 1, p. 70–85, 2011.

HORST, D. et al. Comparative expression analysis of Pax3 and Pax7 during mouse myogenesis. **The International Journal of Developmental Biology**, v. 50, n. 1, p. 47–54, 2006.

HUARD, J.; LI, Y.; FU, F. H. MUSCLE INJURIES AND REPAIR. **The Journal of Bone and Joint Surgery-American Volume**, v. 84, n. 5, p. 822–832, maio 2002.

HUTCHESON, D. A. et al. Embryonic and fetal limb myogenic cells are derived from developmentally distinct progenitors and have different requirements for -catenin. **Genes & Development**, v. 23, n. 8, p. 997–1013, 15 abr. 2009.

IBRAGHIMOV-BESKROVNAYA, O. et al. Primary structure of dystrophin-associated glycoproteins linking dystrophin to the extracellular matrix. **Nature**, v. 355, n. 6362, p. 696–702, fev. 1992.

IRINTCHEV, A.; WERNIG, A. Muscle damage and repair in voluntarily running mice: strain and muscle differences. **Cell and Tissue Research**, v. 249, n. 3, set. 1987.

JAMES, N. G. et al. A mutation associated with centronuclear myopathy enhances the size and stability of dynamin 2 complexes in cells. **Biochimica et Biophysica Acta - General Subjects**, v. 1840, n. 1, p. 315–321, 2014.

JEANNET, P.-Y. et al. Clinical and histologic findings in autosomal centronuclear myopathy. **Neurology**, v. 62, n. 9, p. 1484–1490, 11 maio 2004.

JIANG, C. et al. Notch signaling deficiency underlies age-dependent depletion of satellite cells in muscular dystrophy. **Disease Models & Mechanisms**, v. 7, n. 8, p. 997–1004, 1 ago. 2014.

JONES, N. C. et al. ERK1/2 is required for myoblast proliferation but is dispensable for muscle gene expression and cell fusion. **Journal of Cellular Physiology**, v. 186, n. 1, p. 104–115, jan. 2001.

JONES, N. C. et al. The p38α/β MAPK functions as a molecular switch to activate the quiescent satellite cell. **The Journal of Cell Biology**, v. 169, n. 1, p. 105–116, 11 abr. 2005.

JOUBERT, R. et al. Site-specific Mtm1 mutagenesis by an AAV-Cre vector reveals that myotubularin is essential in adult muscle. **Human Molecular Genetics**, v. 22, n. 9, p. 1856–1866, 1 maio 2013.

JUNGBLUTH, H. et al. Centronuclear myopathy with cataracts due to a novel dynamin 2 (DNM2) mutation. **Neuromuscular Disorders**, v. 20, n. 1, p. 49–52, jan. 2010.

JUNGBLUTH, H.; WALLGREN-PETTERSSON, C.; LAPORTE, J. Centronuclear (myotubular) myopathy. **Orphanet Journal of Rare Diseases**, v. 3, n. 1, p. 1–13, 2008.

KASSAR-DUCHOSSOY, L. et al. Mrf4 determines skeletal muscle identity in Myf5:Myod double-mutant mice. **Nature**, v. 431, n. 7007, p. 466–471, set. 2004.

KAWABE, Y. et al. Carm1 Regulates Pax7 Transcriptional Activity through MLL1/2 Recruitment during Asymmetric Satellite Stem Cell Divisions. **Cell Stem Cell**, v. 11, n. 3, p. 333–345, set. 2012.

KEE, A. J.; GUNNING, P. W.; HARDEMAN, E. C. Diverse roles of the actin cytoskeleton in striated muscle. **Journal of Muscle Research and Cell Motility**, v. 30, n. 5–6, p. 187–197, 8 set. 2009.

KENNISTON, J. A.; LEMMON, M. A. Dynamin GTPase regulation is altered by PH domain mutations found in centronuclear myopathy patients. **EMBO Journal**, v. 29, n. 18, p. 3054–3067, 2010.

KHARRAZ, Y. et al. Macrophage Plasticity and the Role of Inflammation in Skeletal Muscle Repair. **Mediators of Inflammation**, v. 2013, p. 1–9, 2013.

KIERDASZUK, B. et al. A novel mutation in the DNM2 gene impairs dynamin 2 localization in skeletal muscle of a patient with late onset centronuclear myopathy. **Neuromuscular Disorders**, v. 23, n. 3, p. 219–228, 2013.

KISSIEDU, J.; PRAYSON, R. A. Congenital fiber type disproportion. **Journal of Clinical Neuroscience**, v. 26, p. 136–137, 1 abr. 2016.

KLEIN, D. E. et al. The pleckstrin homology domains of dynamin isoforms require oligomerization for high affinity phosphoinositide binding. **Journal of Biological Chemistry**, v. 273, n. 42, p. 27725–27733, 1998.

KOUTSOPOULOS, O. S. et al. Mild functional differences of dynamin 2 mutations associated to centronuclear myopathy and charcot-marie-tooth peripheral neuropathy. **PLoS ONE**, v. 6, n. 11, 2011.

KOUTSOPOULOS, O. S. et al. Dynamin 2 homozygous mutation in humans with a lethal congenital syndrome. **European Journal of Human Genetics**, v. 21, n. 6, p. 637–642, 2013.

KRANENBURG, O.; VERLAAN, I.; MOOLENAAR, W. H. Dynamin Is Required for the Activation of Mitogen-activated Protein (MAP) Kinase by MAP Kinase Kinase. **Journal of Biological Chemistry**, v. 274, n. 50, p. 35301–35304, 10 dez. 1999.

KUANG, S. et al. Asymmetric Self-Renewal and Commitment of Satellite Stem Cells in Muscle. **Cell**, v. 129, n. 5, p. 999–1010, 2007.

KUTCHUKIAN, C. et al. Impaired excitation–contraction coupling in muscle fibres from the dynamin2R465W mouse model of centronuclear myopathy. **Journal of Physiology**, v. 595, n. 24, p. 7369–7382, 2017.

LAING, N. G. Genetics of neuromuscular disorders. **Critical Reviews in Clinical Laboratory Sciences**, v. 49, n. 2, p. 33–48, 2012.

LANDING, B.; DIXON, L.; WELLS, T. Studies on isolated human skeletal muscle fibersIncluding a proposed pattern of nuclear distribution and a concept of nuclear territories. **Human Pathology**, v. 5, n. 4, p. 441–461, jul. 1974.

LAPORTE, J. et al. A gene mutated in X-linked myotubular myopathy defines a new putative tyrosine phosphatase family conserved in yeast. **Nature Genetics**, v. 13, n. 2, p. 175–182, 1996.

LAPORTE, J. et al. MTM1 mutations in X-linked myotubular myopathy. **Human Mutation**, v. 15, n. 5, p. 393–409, maio 2000.

LAWLOR, M. W. et al. Myotubularin-deficient myoblasts display increased apoptosis, delayed proliferation, and poor cell engraftment. **American Journal of Pathology**, v. 181, n. 3, p. 961–968, 2012.

LE GRAND, F. et al. Wnt7a Activates the Planar Cell Polarity Pathway to Drive the Symmetric Expansion of Satellite Stem Cells. **Cell Stem Cell**, v. 4, n. 6, p. 535–547, jun. 2009.

LEE, E. Amphiphysin 2 (Bin1) and T-Tubule Biogenesis in Muscle. **Science**, v. 297, n. 5584, p. 1193–1196, 16 ago. 2002.

LEFAUCHEUR, J. P.; SÉBILLE, A. The cellular events of injured muscle regeneration depend on the nature of the injury. **Neuromuscular Disorders**, v. 5, n. 6, p. 501–509, nov. 1995.

LEIKINA, E. et al. Extracellular annexins and dynamin are important for sequential steps in myoblast fusion. **Journal of Cell Biology**, v. 200, n. 1, p. 109–123, 2013.

LEPPER, C.; PARTRIDGE, T. A.; FAN, C.-M. An absolute requirement for Pax7-positive satellite cells in acute injury-induced skeletal muscle regeneration. **Development**, v. 138, n. 17, p. 3639–3646, 2011.

LI, Y.-P. TNF-α is a mitogen in skeletal muscle. **American Journal of Physiology-Cell Physiology**, v. 285, n. 2, p. C370–C376, ago. 2003.

LIU, N. et al. Mice lacking microRNA 133a develop dynamin 2-dependent centronuclear myopathy. **Journal of Clinical Investigation**, v. 121, n. 8, p. 3258–3268, 2011.

LIU, Y. W.; LUKIYANCHUK, V.; SCHMID, S. L. Common membrane trafficking defects of disease-associated dynamin 2 mutations. **Traffic**, v. 12, n. 11, p. 1620–1633, 2011.

MAGLI, A. et al. Functional Dissection of Pax3 in Paraxial Mesoderm Development and Myogenesis. **STEM CELLS**, v. 31, n. 1, p. 59–70, jan. 2013.

MAJCZENKO, K. et al. Dominant Mutation of CCDC78 in a Unique Congenital Myopathy with Prominent Internal Nuclei and Atypical Cores. **The American Journal of Human Genetics**, v. 91, n. 2, p. 365–371, ago. 2012.

MAMCHAOUI, K. et al. Immortalized pathological human myoblasts: Towards a universal tool for the study of neuromuscular disorders. **Skeletal Muscle**, v. 1, n. 34, 2011.

MAURO, A. Satellite Cell of Skeletal Muscle Fibers. **The Journal of Cell Biology**, v. 9, n. 2, p. 493–495, 1961.

MCKINNELL, I. W. et al. Pax7 activates myogenic genes by recruitment of a histone methyltransferase complex. **Nature Cell Biology**, v. 10, n. 1, p. 77–84, 2008.

MELBERG, A. et al. Adult course in dynamin 2 dominant centronuclear myopathy with neonatal onset. **Neuromuscular Disorders**, v. 20, n. 1, p. 53–56, 2010.

MERLINI, L.; NISHINO, I. 201st ENMC International Workshop: Autophagy in muscular dystrophies - Translational approach, 1-3 November 2013, Bussum, The Netherlands. **Neuromuscular Disorders**, v. 24, n. 6, p. 546–561, 2014.

METTLEN, M. et al. Dissecting dynamin's role in clathrin-mediated endocytosis. **Biochemical Society Transactions**, v. 37, n. 5, p. 1022–1026, 1 out. 2009.

MITCHELL, C. A.; MCGEACHIE, J. K.; GROUNDS, M. D. Cellular differences in the regeneration of murine skeletal muscle: a quantitative histological study in SJL/J and BALB/c mice. **Cell and Tissue Research**, v. 269, n. 1, p. 159–166, jul. 1992.

MIZUSHIMA, N. Autophagy : process and function. **Genes Development**, p. 2861–2873, 2007.

MOOREN, O. L. et al. Dynamin2 GTPase and cortactin remodel actin filaments. **Journal of Biological Chemistry**, v. 284, n. 36, p. 23995–24005, 2009.

MORRIS, N. R. Nuclear positioning: the means is at the ends. **Current Opinion in Cell Biology**, v. 15, n. 1, p. 54–59, fev. 2003.

MOURIKIS, P. et al. A critical requirement for notch signaling in maintenance of the quiescent skeletal muscle stem cell state. **Stem Cells**, v. 30, n. 2, p. 243–252, 2012.

NABESHIMA, Y. et al. Myogenin gene disruption results in perinatal lethality because of severe muscle defect. **Nature**, v. 364, n. 6437, p. 532–535, ago. 1993.

NANCE, J. R. et al. Congenital myopathies: An update. **Current Neurology and Neuroscience Reports**, v. 12, n. 2, p. 165–174, 2012.

NICOT, A. S. et al. Mutations in amphiphysin 2 (BIN1) disrupt interaction with dynamin 2 and cause autosomal recessive centronuclear myopathy. **Nature Genetics**, v. 39, n. 9, p. 1134–1139, 2007.

NORTH, K. N. et al. Approach to the diagnosis of congenital myopathies. **Neuromuscular Disorders**, v. 24, n. 2, p. 97–116, 2014.

OLGUIN, H. C.; OLWIN, B. B. Pax-7 up-regulation inhibits myogenesis and cell cycle progression in satellite cells: A potential mechanism for self-renewal. **Developmental Biology**, v. 275, n. 2, p. 375–388, 2004.

OLSON, E. N. MyoD family: a paradigm for development? **Genes & Development**, v. 4, n. 9, p. 1454–1461, 1 set. 1990.

ONTELL, M.; KOZEKA, K. Organogenesis of the mouse extensor digitorum logus muscle: A quantitative study. **American Journal of Anatomy**, v. 171, n. 2, p. 149–161, out. 1984.

OTT, M. O. et al. Early expression of the myogenic regulatory gene, myf-5, in precursor cells of skeletal muscle in the mouse embryo. **Development (Cambridge, England)**, v. 111, n. 4, p. 1097–107, abr. 1991.

PAPPONEN, H. et al. Evidence for γ-actin as a Z disc component in skeletal myofibers. **Experimental Cell Research**, v. 315, n. 2, p. 218–225, jan. 2009.

PARKER, M. H.; SEALE, P.; RUDNICKI, M. A. Looking back to the embryo: Defining transcriptional networks in adult myogenesis. **Nature Reviews Genetics**, v. 4, n. 7, p. 497–507, 2003.

PATAPOUTIAN, A. et al. Disruption of the mouse MRF4 gene identifies multiple waves of myogenesis in the myotome. **Development (Cambridge, England)**, v. 121, n. 10, p. 3347–58, out. 1995.

PAVLATH, G. K. et al. Heterogeneity among muscle precursor cells in adult skeletal muscles with differing regenerative capacities. **Developmental Dynamics**, v. 212, n. 4, p. 495–508, ago. 1998.

RABAI, A. et al. Allele-specific CRISPR/Cas9 correction of a heterozygous DNM2 mutation rescues centronuclear myopathy cell phenotypes. **Molecular Therapy - Nucleic Acids**, 2019.

RAWLS, A. et al. Myogenin's Functions Do Not Overlap with Those of MyoD or Myf-5 during Mouse Embryogenesis. **Developmental Biology**, v. 172, n. 1, p. 37–50, nov. 1995.

RAZZAQ, A. Amphiphysin is necessary for organization of the excitation-contraction coupling machinery of muscles, but not for synaptic vesicle endocytosis in Drosophila. **Genes & Development**, v. 15, n. 22, p. 2967–2979, 15 nov. 2001.

REED, U. C. Doenças neuromusculares. **Jornal de Pediatria**, v. 78, p. S89–S103, ago. 2002.

ROBB, S. A. et al. Impaired neuromuscular transmission and response to acetylcholinesterase inhibitors in centronuclear myopathies. **Neuromuscular Disorders**, v. 21, n. 6, p. 379–386, 2011.

ROCHETEAU, P. et al. A subpopulation of adult skeletal muscle stem cells retains all template DNA strands after cell division. **Cell**, v. 148, n. 1–2, p. 112–125, 2012.

ROMERO, N. B. Centronuclear myopathies: A widening concept. **Neuromuscular Disorders**, v. 20, n. 4, p. 223–228, 2010.

ROMERO, N. B.; BITOUN, M. Centronuclear myopathies. **Seminars in Pediatric Neurology**, v. 18, p. 250–256, 2011.

RUDNICKI, M. A. et al. Inactivation of MyoD in mice leads to up-regulation of the myogenic HLH gene Myf-5 and results in apparently normal muscle development. **Cell**, v. 71, n. 3, p. 383–390, out. 1992.

RUDNICKI, M. A. et al. MyoD or Myf-5 is required for the formation of skeletal muscle. **Cell**, v. 75, n. 7, p. 1351–1359, dez. 1993.

RUDNICKI, M. A. et al. The molecular regulation of muscle stem cell function. **Cold Spring Harbor Symposia on Quantitative Biology**, v. 73, p. 323–331, 2008.

SAMBASIVAN, R. et al. Pax7-expressing satellite cells are indispensable for adult skeletal muscle regeneration. **Development**, v. 138, n. 17, p. 3647–3656, 2011.

SAMBUUGHIN, N. et al. Adult-onset autosomal dominant spastic paraplegia linked to a GTPase-effector domain mutation of dynamin 2. **BMC Neurology**, v. 15, n. 1, 2015.

SANDRI, M. et al. Misregulation of autophagy and protein degradation systems in myopathies and muscular dystrophies. **Journal of Cell Science**, v. 126, n. 23, p. 5325–5333, 2013.

SAVARESE, M. et al. Novel findings associated with MTM1 suggest a higher number of female symptomatic carriers. **Neuromuscular Disorders**, v. 26, n. 4–5, p. 292–299, 2016.

SCHMITTGEN, T. D.; LIVAK, K. J. Analyzing real-time PCR data by the comparative CTmethod. **Nature Protocols**, v. 3, n. 6, p. 1101–1108, 2008.

SEALE, P. et al. Pax7 is required for the specification of myogenic satellite cells. **Cell**, v. 102, n. 6, p. 777–786, 2000.

SEVER, S.; MUHLBERG, A. B.; SCHMID, S. L. Impairment of dynamin's GAP domain stimulates receptor-mediated endocytosis receptor-mediated endocytosis. **Nature**, v. 398, n. 6727, p. 481–486, 1999.

SEWRY, C. A.; WALLGREN-PETTERSSON, C. Myopathology in congenital myopathies. **Neuropathology and Applied Neurobiology**, v. 43, n. 1, p. 5–23, 2017.

SHEA, K. L. et al. Sprouty1 regulates reversible quiescence of a self-renewing adult muscle stem cell pool during regeneration. **Cell stem cell**, v. 6, n. 2, p. 117–29, 5 fev. 2010.

SHER, J. H. et al. Familial myotubular myopathy: a clinical, pathological, histochemical, and ultrastructural study. **Neuropatholy Experimental Neurology**, v. 6, p. 132–133, 1967.

SHIN, N. Y. et al. Dynamin and endocytosis are required for the fusion of osteoclasts and myoblasts. **Journal of Cell Biology**, v. 207, n. 1, p. 73–89, 2014.

SIDIROPOULOS, P. N. M. et al. Dynamin 2 mutations in Charcot-Marie-Tooth neuropathy highlight the importance of clathrin-mediated endocytosis in myelination. **Brain**, v. 135, n. 5, p. 1395–1411, 2012.

SMIRNOVA, E. et al. A model for dynamin self-assembly based on binding between three different protein domains. **Journal of Biological Chemistry**, v. 274, n. 21, p. 14942–14947, 1999.

SONNEMANN, K. J. et al. Cytoplasmic γ-Actin Is Not Required for Skeletal Muscle Development but Its Absence Leads to a Progressive Myopathy. **Developmental Cell**, v. 11, n. 3, p. 387–397, set. 2006.

SPIRO, A. J. Myotubular Myopathy. **Archives of Neurology**, v. 14, n. 1, p. 1, 1 jan. 1966.

SUSMAN, R. D. et al. Expanding the clinical, pathological and MRI phenotype of DNM2-related centronuclear myopathy. **Neuromuscular Disorders**, v. 20, n. 4, p. 229–237, 2010.

TASFAOUT, H. et al. Antisense oligonucleotide-mediated Dnm2 knockdown prevents and reverts myotubular myopathy in mice. **Nature communications**, v. 8, p. 15661, 7 jun. 2017.

TASFAOUT, H. et al. Single Intramuscular Injection of AAV-shRNA Reduces DNM2 and Prevents

Myotubular Myopathy in Mice. **Molecular Therapy**, v. 26, n. 4, p. 1082–1092, abr. 2018.

TATSUMI, R. et al. HGF/SF is present in normal adult skeletal muscle and is capable of activating satellite cells. **Developmental Biology**, v. 194, n. 1, p. 114–128, 1998.

TAYLOR, G. S.; MAEHAMA, T.; DIXON, J. E. Myotubularin, a protein tyrosine phosphatase mutated in myotubular myopathy, dephosphorylates the lipid second messenger, phosphatidylinositol 3-phosphate. **Proceedings of the National Academy of Sciences**, v. 97, n. 16, p. 8910–8915, 2002.

THOMAS, N.; WALLGREN-PETTERSSON, C. X-Linked myotubular myopathy 33rd ENMC international workshop Soest, The Netherlands, 9–11 June 1995. **Neuromuscular Disorders**, v. 6, n. 2, p. 129–132, mar. 1996.

THOMPSON, H. M. et al. Dynamin 2 binds γ-tubulin and participates in centrosome cohesion. **Nature Cell Biology**, v. 6, n. 4, p. 335–342, 14 abr. 2004.

TINELLI, E.; PEREIRA, J. A.; SUTER, U. Muscle-specific function of the centronuclear myopathy and charcot-marie-tooth neuropathy associated dynamin 2 is required for proper lipid metabolism, mitochondria, muscle fibers, neuromuscular junctions and peripheral nerves. **Human Molecular Genetics**, v. 22, n. 21, p. 4417–4429, 2013.

TOSCH, V. et al. A novel PtdIns3P and PtdIns(3,5)P2 phosphatase with an inactivating variant in centronuclear myopathy. **Human Molecular Genetics**, v. 15, n. 21, p. 3098–3106, 1 nov. 2006.

TOUSSAINT, A. et al. Defects in amphiphysin 2 (BIN1) and triads in several forms of centronuclear myopathies. **Acta Neuropathologica**, v. 121, n. 2, p. 253–266, 7 fev. 2011.

TROCHET, D. et al. Allele-specific silencing therapy for Dynamin 2-related dominant centronuclear myopathy. **EMBO molecular medicine**, v. 10, p. 239–253, 2018.

TSAI, T.-C. et al. Characterization of MTM1 mutations in 31 Japanese families with myotubular myopathy, including a patient carrying 240kb deletion in Xq28 without male hypogenitalism. **Neuromuscular Disorders**, v. 15, n. 3, p. 245–252, mar. 2005.

TSUJITA, K. et al. Myotubularin Regulates the Function of the Late Endosome through the GRAM Domain-Phosphatidylinositol 3,5-Bisphosphate Interaction. **Journal of Biological Chemistry**, v. 279, n. 14, p. 13817–13824, 2 abr. 2004.

TURNER, N. J.; BADYLAK, S. F. Regeneration of skeletal muscle. **Cell and Tissue Research**, v. 347, n. 3, p. 759–774, 11 mar. 2012.

VAN DER BLIEK, A. M.; MEYEROWRTZ, E. M. Dynamin-like protein encoded by the Drosophila shibire gene associated with vesicular traffic. **Nature**, v. 351, n. 6325, p. 411–414, maio 1991.

VANDERSMISSEN, I. et al. An integrated modelling methodology for estimating the prevalence of centronuclear myopathy. **Neuromuscular Disorders**, v. 28, n. 9, p. 766–777, set. 2018.

WANG, L. et al. Dynamin 2 mutants linked to centronuclear myopathies form abnormally stable polymers. **Journal of Biological Chemistry**, v. 285, n. 30, p. 22753–22757, 2010.

WANG, Y. X. et al. EGFR-Aurka Signaling Rescues Polarity and Regeneration Defects in Dystrophin-Deficient Muscle Stem Cells by Increasing Asymmetric Divisions. **Cell Stem Cell**, v. 24, n. 3, p. 419–432.e6, mar. 2019.

WEN, Y. et al. Constitutive Notch Activation Upregulates Pax7 and Promotes the Self-Renewal of Skeletal Muscle Satellite Cells. **Molecular and Cellular Biology**, v. 32, n. 12, p. 2300–2311, 2012.

WHITE, R. B. et al. Dynamics of muscle fibre growth during postnatal mouse development. **BMC Developmental Biology**, v. 10, n. 21, 2010.

WILMSHURST, J. M. et al. RYR1 mutations are a common cause of congenital myopathies with central nuclei. **Annals of Neurology**, v. 68, n. 5, p. 717–726, nov. 2010.

YABLONKA-REUVENI, Z.; SEGER, R.; RIVERA, A. J. Fibroblast growth factor promotes recruitment of skeletal muscle satellite cells in young and old rats. **Journal of Histochemistry and Cytochemistry**, v. 47, n. 1, p. 23–42, 1999.

YAMADA, H. et al. Stabilization of Actin Bundles by a Dynamin 1/Cortactin Ring Complex Is Necessary for Growth Cone Filopodia. **Journal of Neuroscience**, v. 33, n. 10, p. 4514–4526, 6 mar. 2013.

YENNEK, S. et al. Cell adhesion geometry regulates non-random DNA segregation and asymmetric cell fates in mouse skeletal muscle stem cells. **Cell Reports**, v. 7, n. 4, p. 961–970, 2014.

YOSHIDA, M.; OZAWA, E. Glycoprotein Complex Anchoring Dystrophin to Sarcolemma1. **The Journal of Biochemistry**, v. 108, n. 5, p. 748–752, nov. 1990.

YOSHIDA, N. et al. Cell heterogeneity upon myogenic differentiation: down-regulation of MyoD and Myf-5 generates “reserve cells”. **Journal of cell science**, v. 111, n. Pt6, p. 769–779, 1998.

ZAMMIT, P. S. et al. Muscle satellite cells adopt divergent fates. **The Journal of Cell Biology**, v. 166, n. 3, p. 347–357, 2 ago. 2004.

ZAMMIT, P. S. Function of the myogenic regulatory factors Myf5, MyoD, Myogenin and MRF4 in skeletal muscle, satellite cells and regenerative myogenesis. **Seminars in Cell & Developmental Biology**, v. 72, p. 19–32, dez. 2017.

ZHANG, W.; BEHRINGER, R. R.; OLSON, E. N. Inactivation of the myogenic bHLH gene MRF4 results in up-regulation of myogenin and rib anomalies. **Genes & Development**, v. 9, n. 11, p. 1388–1399, 1 jun. 1995.